AN ELECTROMAGNETIC FIELD MODEL FOR THE DESIGN OF RF REED RELAYS

by

ROBERT ANTHONY HARRISON

A thesis submitted to the University of Plymouth
in partial fulfilment for the degree of

DOCTOR OF PHILOSOPHY

Department of Marine and Mechanical Engineering
Faculty of Technology

In collaboration with
Crydom Magnetics Limited

October 2000

Abstract

A model of the electromechanical characteristics, electrostatic characteristics and coil eddy current losses of a reed relay was developed. These characteristics were returned from reed and coil dimensions. The model was intended as an aid to the design of reed relays for Radio Frequency (RF) and high voltage applications.

An electromechanical model of a reed switch and coil was developed using a combination of an axisymmetric finite element model and analytical methods. The characteristics returned from this model were operate, release and differential amp turns, contact gap and contact force. Inclusion of results for contact resistance against contact force yielded the contact resistance characteristics.

Electrostatic force between reed contacts was calculated and a criteria for contact arcing in a vacuum applied to allow prediction of breakdown voltage in an evacuated reed switch.

The above elements were incorporated in a "Reed Switch Design Program" in which operating, contact resistance and breakdown voltage characteristics were calculated from reed and coil dimensions. Results were found to be in agreement with measured values for three reed switch types.

Eddy current losses in relay coils were investigated through experimental measurement of losses occurring in coils mounted around a copper conductor carrying a high frequency current. The losses occurring in the coil were found to present an effective resistance to the current in the conductor. The influence of coil dimensions and the magnetic properties of the conductor on losses were observed. An analytical model of eddy current losses was derived from first principals results and were found concordant with those measured.

An "RF Reed Relay Design Program" embodying the eddy current loss model and preceding work was created to demonstrate how relay performance (and efficiency) can be enhanced by tuning reed and coil dimensions. An example of its successful application to product development at Crydom Magnetics Ltd is presented.

Proposals for future work are included.

Acknowledgements

I would like to thank the following for the valuable assistance given to this project.

All staff at Crydom Magnetics Ltd

Dr. D. Grieve of the University of Plymouth

Mr. C. F. Hamer of the University of Plymouth

Mr. J. Walker of Racal Defence Electronics

Mr G. W. Cullen (now enjoying retirement)

Mr J. Miles (as above)

Declaration

I declare that this thesis is the result of my investigations only and is not submitted in candidature for any other degree. At no time during the registration for the degree of Doctor of Philosophy has the author been registered for any other university award.

This study was financed with the aid of and carried out in collaboration with Crydom Magnetics Ltd where the author was initially employed as a Teaching Company Associate.

During the research programme a course of advanced studies was undertaken. This included a course on the use of ANSYS finite element software and courses held as part of the Teaching Company Programme.

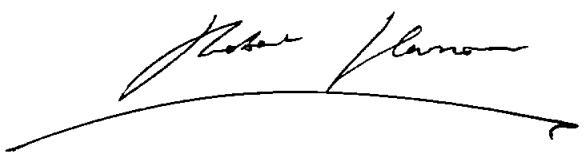

Glossary

As this thesis spans the areas of mechanical engineering, electrical engineering and physics some of the nomenclature has been changed from that used normally. The following nomenclature is used unless specified otherwise. SI units are used throughout.

V = electromotive force

I = current

I_{RF} = RF current

I_{eddy} = eddy current

R = resistance

R_1 = initial resistance

R_2 = final resistance

R_{eddy} = resistance to eddy current

mmf = magnetomotive force

mmf_g = magnetomotive force at contact gap

OAT = magnetomotive force required to operate reed switch (operate amp turns)

RAT = magnetomotive force at which reed switch releases (release amp turns)

Φ= magnetic flux

Φg = magnetic flux at contact gap

S = reluctance

S_{return} = return reluctance

$S_{return(g=0)}$ = return reluctance at zero contact gap

S_g = contact gap reluctance

C = capacitance

P = permeance

ε= permitivity of free space

μ= permeability of free space

w = length, defined fig 2.2

c = length, defined fig 2.2

b = contact breadth

d = contact overlap

g = contact gap

t = contact thickness

X = length, defined figs 2.5, 2.7

r = radius

r_1, r_2, r_3, r_4 = radii

l = length

A = contact area

A_{eddy} = cross sectional area through which eddy current flows

A_{coil} = cross sectional area of coil winding

OD = outside diameter of coil winding

ID = inside diameter of coil winding

F = magnetic force at reed contact

F_e = electrostatic force at reed contact

F_s = mechanical spring force at reed contact

E = Young's modulus

M = second moment of area

Q = quality factor of a resonant circuit

f = frequency

f_0 = resonant frequency

f_u = upper frequency (-3dB point)

f_l = lower frequency (-3dB point)

T = temperature

T_1 = initial temperature

T_2 = final temperature

W = power

W_{RF} = RF power

W_{DC} = DC power

H = magnetic field strength

δ = skin depth

σ = conductivity

ρ = resistivity

J = current density

J_0 = current density at the surface of a conductor

k = term defined with regard to skin depth

z = depth

N = no. of turns of coil winding

dia_w = diameter of winding wire

MTL = mean turn length of coil winding

F_{wire} = factor of eddy current self cancelling in winding wire

F_{loss} = loss factor

F_{pack} = packing factor of wire in coil winding

F_{cu} = proportion of winding wire cross sectional area which is copper

Contents

1. INTRODUCTION

1.1 The Reed Relay

1.1.1 Principle of Operation

A reed switch consists of two overlapping ferromagnetic "reeds" within a sealed glass tube . The reeds are cantilevered from the glass to metal seal. In the presence of a magnetic field the reeds are attracted together thereby closing the switch. A reed relay is simply a coil mounted around a reed switch with the basic arrangement as shown in figure 1.1. When a current is passed through the coil a magnetic field (measured in amp-turns) is generated and the switch operated. The geometry of the switch and coil will affect their electromechanical efficiency and operating characteristics .

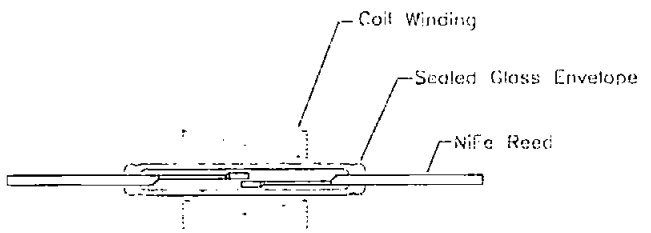

Figure 1.1 - Cross Section Through a Reed Switch and Coil

1.1.2 Reed Relays Manufactured by Crydom Magnetics

Crydom Magnetics manufacture RF (radio frequency) reed relays for use in HF (high frequency) radio equipment for both civil and military markets. In particular the relays are used in antenna tuning units (ATUs) where they are used to switch reactive components in order to tune the radio output to a particular frequency. They are used to switch in either capacitors or inductors in order to make the circuit resonate at the frequency of transmission. The resonant nature of this application gives rise to the following requirements:

i) High carry current (e.g. up to 20A at 30MHz)

ii) High isolation voltage (e.g. 8kV peak)

iii) Low loss (i.e. low resistance at HF/RF)

Additional requirements are :

iv) Low dc power consumption

v) Wide operating temperature range (typically –40 to +85°C)

vi) Low cost (particularly for civil markets where there may be competition between HF radio and other technologies).

The reed relays for this application at Crydom had evolved from the design of conventional relays rather than having been designed as an RF device from first principals. The alterations made to accommodate RF requirements were :

a) Use of switches with copper plated reeds in order to extend carry current performance

b) Use of evacuated switches in order to obtain maximum isolation voltage

c) Use of various electrostatic screening arrangements to reduce RF losses (and relay heating)

Reed relays of this type have been found to provide a cost effective solution for ATU applications when compared to alternatives such as evacuated electromechanical relays and high voltage solid state devices. Evacuated electromechanical relays are considerably more expensive than reed relays and are usually also of greater size and weight. In addition their speed of operation is slower than that of an equivalent reed relay. High voltage solid state devices are also more expensive than reed relays and require control voltages of several hundred volts whereas reed relays can be operated via a simple 12V or 24V DC supply. Furthermore, the Achilles heel of the reed relay, its inability to switch high loads reliably, is not a disadvantage as switching in ATUs is undertaken prior to maximum power being applied.

Examples of RF reed relays manufactured by Crydom Magnetics are shown below.

Figure 1.2 – FRS42500 Series (3A @ 30MHz carry current, 3kV isolation)

Figure 1.3 – FRD13000 Series (6A @ 30MHz carry current, 8kV isolation)

Figure 1.4 – FRD32000 Series (20A @30MHz carry current, 6.5kV isolation)

One particular point from above is that of relay heating. RF heating due to losses within the relay (when carrying an RF current) can be substantial (e.g. an increase of 100°C in some

products) and this is exacerbated if a high isolation voltage is also required (a high breakdown voltage switch requires a large contact gap and therefore a more powerful coil to provide the necessary amp-turns to close it). Relay heating limits operating temperature range as they are generally powered from a voltage source. As the resistance of the coil increases with temperature (about 0.4%/°C for copper) the amp-turns it produces drops accordingly. This means that a condition can easily be reached with a high RF carry current, high dc power requirement and high ambient temperature where the coil can no longer provide a sufficient magnetomotive force to operate the switch.

From previous work and testing existing products it was known that the geometry of the reed switch and coil influence both the electromechanical efficiency of the device and its performance at RF. Also, although various electrostatic screening arrangements were in use their relative effectiveness was not well understood. In particular the possibility of altering relay geometry to improve RF performance (i.e. reduce heating) so that electrostatic screening (which adds considerably to the cost of manufacture) was no longer required had not been pursued.

From the above it was considered that if a means of predicting electromechanical and RF performance from relay geometry could be developed this could be used to improve the performance of RF reed relays designed at Crydom. This is the aim of the work presented in this thesis.

1.2 Terminology and Background Theory

1.2.1 Reed Relay Terminology

Frequently used terms relating to reed relays and their characteristics are :

Operate Amp Turns (OAT) - The number of amp turns at which the switch will operate

Release Amp Turns (RAT) - The number of amp turns at which the switch will open from the closed state

Differential - The difference between operate and release amp turns

Contact Resistance - The electrical resistance across the switch contacts when closed

Breakdown Voltage - The voltage at which arcing occurs between the contacts

1.2.2 Background Theory

The purpose of this section is to give an introduction to the basics of the magnetic theory used in this thesis so as to put the research subsequently described into context .

The basic relationship for a magnetic circuit is analogous to Ohm's law for an electrical circuit . Whereas Ohm's law is :

$$V = I \cdot R \qquad (1.1)$$

where : V=electromotive force (volts)

I=current (amps)

R=resistance (ohms)

the equivalent for a magnetic circuit is :

$$mmf = \Phi \cdot S \quad (1.2)$$

where : mmf=magnetomotive force (amp-turns)

Φ= magnetic flux (webers)

S=reluctance (amp-turns/weber)

In the case of a reed relay the magnetomotive force can be determined simply from a knowledge of the number of turns in the coil and the current applied to it. However, the flux in the circuit (which determines the force between the switch contacts) is clearly dependent upon its reluctance and this, in turn, depends upon the material properties and geometry of the circuit elements. This is the reason for the link between the geometry of the relay and its magnetic efficiency.

The reciprocal of reluctance is known as permeance. Both terms are used in the following text. It should be noted that permeance is analogous to capacitance as described by the relationship below :

$$\frac{C}{\varepsilon} = \frac{P}{\mu} \qquad (1.3)$$

where :

C= capacitance (farads)

ε = permitivity (farads/m)

P= permeance (webers/amp-turn)

μ = permeability (webers/amp-turn.m)

This means that the capacitance and permeance can be modelled using the same technique.

1.3 Existing Work and Scope of Research

Following its invention (first patented by Dr.W.B.Ellwood of Bell Telephone Laboratories in 1938) numerous papers have been written about reed switches and relays. The aspects covered include:

1.3.1 Magnetic Theory for Reed Switches

Papers covering the magnetic theory for reed switches and its application to their design include Peek (1), Kato (2), which cover both static and dynamic analysis, and Cullen (3), which deals with only static analysis. In addition, Handa, Hamahata and Iida (4) covers the application of Peek's work to the development of one particular reed switch. Rensch (5) is a more general paper on reed switch characteristics and Stickley (6) covers aspects of reed relay design and application (taking an empirical approach). All of the above consider switches and relays for conventional applications (i.e. not high voltage or Radio Frequency).

Cullen had previously been an employee at Crydom and the inclusion of his work into a computer based design aid had begun. The theory uses techniques advocated by Roters (7) which provide a convenient means of calculating an estimate of permeance for three dimensional structures. This was particularly important as to link physical proportion and magnetic performance was a primary aim of the present work.

1.3.2 Contact Material and Resistance

A considerable amount of information about contact materials and their characteristics has been published. These consider material choice (8,9,10,11,12), switching life (8,10,12,14,15), material processing (13,16) and chemical reaction with forming gases (8,11,17).

The ability to predict contact resistance characteristics for rhodium and ruthenium sputtered contacts would be a useful addition to a reed switch design tool. A theoretical model for constriction resistance is presented by Cullen(9). Constriction resistance occurs when current is forced to flow between two contacts via a number of small points on the surfaces of the contacts (because they are not perfectly smooth) rather than being distributed evenly over the whole surface of the contacts. However, more convenient information, consisting of measured values of contact resistance versus contact force for both materials, was contained in Sekiya, et al(8).

1.3.3 Voltage Breakdown in a Vacuum

A method of calculating the breakdown voltage of a switch from its contact gap (in a vacuum) was required. A great deal of research has been conducted into electrical breakdown in a vacuum and much of it is outside the scope of this requirement. However, relevant papers include Theophilus et al(18), who gives a relationship for breakdown voltage against gap for d.c., 60 Hz a.c. and impulse conditions, and Takamisawa(19) who gives an alternative relationship for calculating d.c. voltage breakdown. It is detailed in these works that breakdown voltage depends on the electric field distribution, discharge circuit and electrode material, geometry, temperature and conditioning of the electrode surface. Despite referring to two spherical electrodes of different radii, and constructed of stainless steel rather than rhodium or ruthenium, the relationship presented by Takamisawa(19) has been used in the present work and has been shown to give good results (d.c. breakdown).

Although Theophilus et al(18), show that breakdown voltage is dependent on the frequency of the applied voltage, it also shows that d.c. and a.c. breakdown voltages vary in proportion. This means that a.c. breakdown could be predicted if the d.c. breakdown voltage were known. Ideally a means of predicting voltage breakdown under both dc and high frequency conditions is required. Practical experiment at Crydom (undertaken at ~2MHz) has shown

that, despite the findings in (18), the peak voltage at high frequency and dc voltage are similar at breakdown for an evacuated reed switch. Voltage isolation tests made by Crydom during the manufacture of reed switches and relays are undertaken at d.c.. Given this, and as back to back comparisons are made much more easily at d.c. (high voltages at high frequency are difficult to calibrate accurately), the work presented in this thesis concentrates on predicting breakdown voltage at d.c..

Cullen's "Prediction of Electrostatic Attraction in Reed Switch" (20) presents a method of calculating the electrostatic force between reed switch blades which is appreciable when isolating a high voltage. This forms an important part of any voltage breakdown calculations.

1.3.4 High Current Effects in Reed Switches

Some work has been undertaken on the maximum current carrying capacity of reed switches, in particular by Hara, Tanaka and Kume (21) and Kaczmarek and Weirzba (22). In both cases the effect of the magnetic field created by the current flow is considered. Weirzba (22) also considers thermal processes within the reeds and links this with the choice of contact material. This allows the maximum d.c. current carrying capacity of a reed switch to be calculated with reasonable accuracy.

It is not, however, concerned with alternating currents and, particularly, high frequency currents where the "skin effect" (the tendency of a high frequency current to flow only near the surface of a conductor) must be accounted for. In addition, the effect of copper plating on the reed blades (as used on switches manufactured by Crydom) is not incorporated in either (21) or (22).

1.3.5 RF Characteristics of Relays

Research into the high frequency characteristics of reed relays seems, so far , to have been limited to experimental measurement (without providing any accompanying theory). A method of measuring contact resistance at high power and frequency is presented by Kulikjan(23) which complements the equivalent measurement at low power detailed in the internal report Mason(24). Standard RF performance parameters -insertion loss and isolation- are measured on a high power reed relay (similar to some of those manufactured by Crydom) in Zawislanski, et al(25) and the results, and implications to their application, are discussed. However, a link between the geometry of the relay and its performance is not made.

More detailed measurements of RF and TDR (Time Domain Reflectometry) characteristics of reed relays over the frequency range 100 to 1.1GHz are presented by Fullem and Bateman(26). The performance of several different relay designs are compared and the link between design and performance discussed (particularly with regard to matching the characteristic impedance of the relay with that of a 50Ω system). However, no mention is made of a coupling between switch and coil (it may not be noticed at low power) and no mathematical relationships are used in the design/performance discussion. Also, as the relays discussed are for low power applications in 50Ω circuits and over a much higher frequency range (from 100MHz to 1GHz), the results are not directly applicable to the products considered in this report which operate in high power systems over 1 to 30MHz and frequently in low impedance (e.g. 2Ω) circuits.

1.3.6 Scope of Research

As described in the previous section the purpose of the present research was to develop a means of predicting electromechanical and RF performance from relay geometry. Specifically the aims and scope of the research were:

(i) To predict electromechanical performance of the relay from its geometry (i.e. contact gap vs. OAT) and to use this to determine breakdown voltage (the use of an evacuated switch being assumed). This involved verifying the model proposed by Cullen and extending it to include predictions for operate amp turns (OAT), release amp turns (RAT), differential, contact force, contact gap, breakdown voltage and contact resistance. Cullen's model was verified using practical experiment to assess his modelling technique (advocated by Roters (7)), Finite Element Analysis of a simplified, axisymmetric, model of a reed switch and coil, and the measurement of completed reed switches. A method of calculating the breakdown voltage of an evacuated reed switch was constructed using the arcing criteria contained in Takamisawa (19) and the procedure for calculating electrostatic attraction contained in Cullen (20). Contact resistance characteristics were derived from experimental data presented by Sekiya , et al(8).

(ii) To predict RF losses from relay geometry. In fact, in order to limit the scale of the project, only the relationship between coil geometry and the losses occurring in the coil are considered in the following work. Clearly losses occur within the switch also. However, as coil heating is frequently the principal factor limiting relay performance, it was the losses occurring in the coil which were of most interest to the author. It was known through practical experiment at Crydom that these RF losses (i.e. heating) were:

- not as a result of a simple capacitive coupling between reed switch and coil
- vastly reduced by placing a complete electrostatic screen around the coil

As no previous work was found relating geometry to RF performance the investigation initially involved a series of measurements under high and low power (using the technique described by Mason (24)) conditions with coils of various geometries. Relationships were

subsequently formed and compared to experimental data for the loss associated with "unscreened" coils (i.e. not fitted with an electrostatic screen).

2. ELECTROMECHANICAL MODEL

Section 2 covers the verification and development of Cullen's model of the electromechanical aspects (magnetostatic only) of a reed relay. This includes the work undertaken to refine the model of the magnetic circuit of a reed switch and coil and the additions made to it (specifically contact resistance and voltage breakdown characteristics of the switch) to enhance its usefulness as a reed relay design tool. The link between switch and coil dimensions and the operating and DC electrical characteristics of the resulting relay was of prime interest in this work.

The characteristics of the relay when used for RF applications are not considered at this stage.

2.1 Experimental Analysis of Roters' Method through Capacitance Measurement

Introduction

A key aspect of the present work was to establish the link between the dimensions of a reed relay and its magnetic and electrical characteristics. In Cullen's "A Practical Theory for Reed Switches" the characteristics of the magnetic circuit are determined using the technique presented by Roters. Roters' technique is a means of calculating the permeance of a 3D magnetic field from its shape and dimensions. This involves breaking the field down into sections and applying approximate relationships (derived by Roters) to calculate the permeance for each section. The approximate direction of the flux paths must be known before the sections can be chosen. These permeances are then summed in series or parallel as appropriate. The aim of the following experiments was to examine the accuracy of these approximations when applied to the model of a reed switch and coil as proposed by Cullen.

2.1.1 Cullen's Model of the Magnetic Circuit of a Reed Relay

The model of the magnetic circuit of a reed switch and coil as proposed by Cullen is as follows:

i) Magnetic Circuit

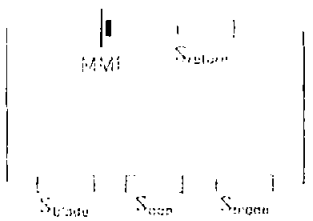

Figure 2.1 – Magnetic Circuit (Cullen)

ii) Return Path Reluctance

The return path was assumed to take the form of spherical shells as shown below. The shell which passes through the coil winding was assumed to have half the influence of that outside it. Relationships derived by Roters were then applied as below:

$$P = \mu \cdot (w + c/2) \qquad (2.1)$$

Figure 2.2 – Return Permeance (Cullen)

iii) Reed Reluctance

Reed reluctance is calculated from material properties (its BH characteristic) and cross sectional area. It is acknowledged that the flux density along the length of the reed varies. In order to allow for this an approximation is made whereby the drop in magnetomotive force along the length of the reed is taken as equal to that occurring with all the flux in the circuit flowing through half the length of each reed.

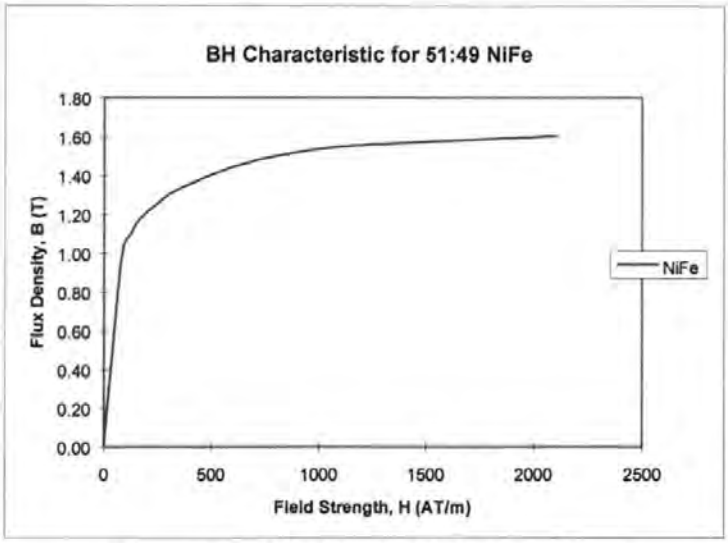

Figure 2.3 – BH Data for 51:49 Nickel Iron

iv) Contact Gap Reluctance

Contact gap reluctance was calculated by considering the permeance across the parallel contact faces and adding this to the permeance of each of the fringing paths as shown below. The permeance of each of these sections was calculated using approximate relationships derived by Roters.

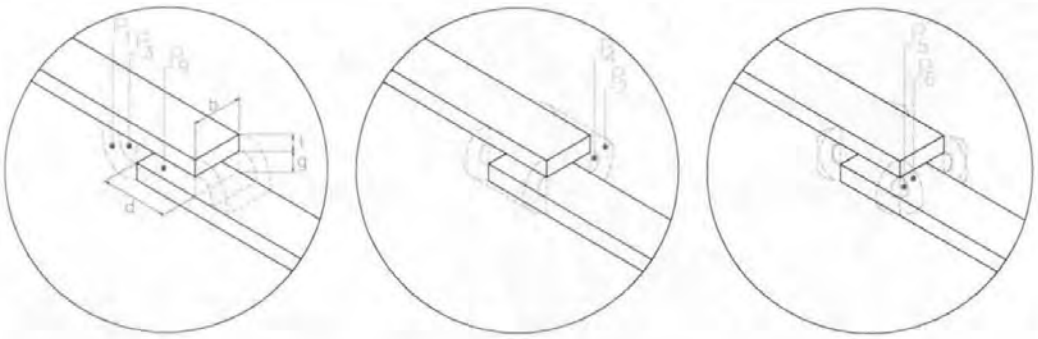

$$P_g = \mu \cdot \frac{b \cdot d}{g} \qquad P_2 = \mu \cdot \frac{2 \cdot d}{\pi} \cdot \ln\left(1 + \frac{2 \cdot t}{g}\right) \qquad P_5 = \mu \cdot 0.077 \cdot g$$

$$P_1 = \mu \cdot \frac{2 \cdot b}{\pi} \cdot \ln\left(1 + \frac{t}{g}\right) \qquad P_4 = \mu \cdot 0.26 \cdot d \qquad P_6 = \mu \cdot \frac{t}{4}$$

$$P_3 = \mu \cdot 0.52 \cdot b$$

$$P = P_r + 2 \cdot P_1 + 2 \cdot P_2 + 2 \cdot P_3 + 2 \cdot P_4 + 4 \cdot P_5 + 4 \cdot P_6 \qquad \textbf{(2.2)}$$

Figure 2.4 – Contact Permeance (Cullen)

2.1.2 Capacitance Measurements – Simplified Reed Switch (contacts open)

Introduction

As already noted, capacitance and permeance are linked as follows:

$$\frac{C}{\varepsilon} = \frac{P}{\mu} \qquad (1.3)$$

By measuring the capacitance of structures resembling a reed switch and coil the accuracy of Roters' method was tested. The structure tested initially was that of two wires placed end on end. This was essentially a simplified model of a switch with its contacts open and the form of the resulting electrostatic field was similar to the return path in Cullen's model of the magnetic circuit of a reed switch and coil.

Note that it is not possible to arrange a capacitance test which is equivalent to the complete magnetic circuit for an open reed switch and coil.

Theory

The structure in this instance was two lengths of wire placed end to end. The field produced is similar to that of the return path in the reed relay magnetic circuit already described. In order to calculate the capacitance between the two wires using Roters' technique the field was split into two sections as shown below:

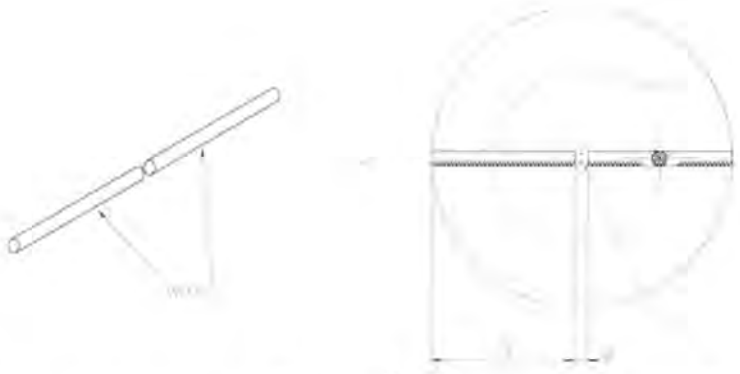

$$C_{sph} = \varepsilon \cdot x \qquad C_g = \varepsilon \cdot \frac{A}{g} \qquad C = C_{sph} + C_g \qquad (2.3)$$

Figure 2.5 – Capacitance Between Two Wires Mounted End on End

Method

The capacitance between two wires arranged as above was measured as the length of the wires (X) was altered. The gap between the wires was held constant and the wires were held clear of the work bench (which might have influenced results) by thin walled insulating posts. Measurements were taken using a Wayne Kerr LCR bridge measuring to 0.01pF at a frequency of 10kHz. Due to the sensitive nature of the measurements they were repeated 3 times and an average result taken.

Results

The measured and calculated results for capacitance between the two wires shown in figure 2.5, as their lengths (X) were altered, are shown below:

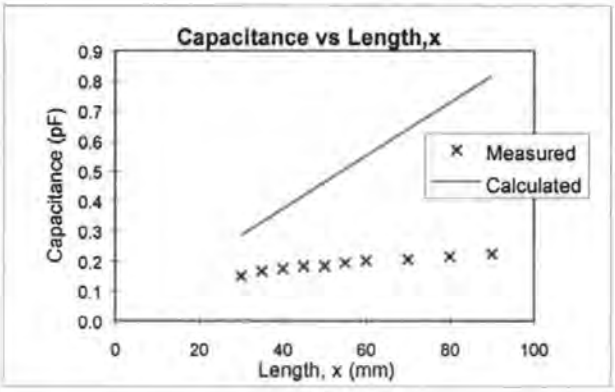

Figure 2.6 – Capacitance vs. Wire Length

Discussion

The results show that, as the length of the wire increases, the significance of the fringing field is over estimated by the spherical shell approximation and the calculated results diverge from those measured. The spherical shell approximation is important to Cullen's model as it is used to approximate the permeance of the return path between the reeds. This would indicate that there could be significant error in this model.

2.1.3 Capacitance Measurements – Simplified Reed Switch and Coil (contacts closed)

Introduction

Using the same reasoning as before the accuracy of Roters' technique in predicting the capacitance between a wire and tube (representing a simplified closed reed switch and coil) was measured. Predicted and measured results were compared.

Theory

This model comprised a length of wire (representing a closed switch) mounted within a thick walled tube (representing the coil). In order to calculate the capacitance between the wire and tube using Roters technique the field was split into sections as shown below:

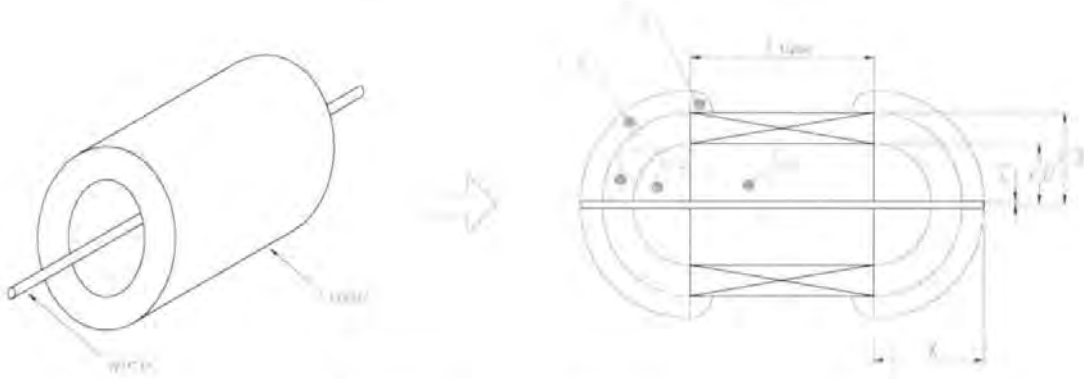

$$C_1 = \frac{2 \cdot \pi \cdot \varepsilon \cdot l_{tube}}{\ln\left(\frac{r_2}{r_1}\right)} \qquad C_2 = \frac{\frac{4}{3} \cdot \pi \cdot \varepsilon \cdot r_1}{\ln\left(\frac{r_2}{r_1}\right)} \qquad C_3 = \varepsilon \cdot (r_3 - r_2) \qquad C_4 = \varepsilon \cdot (X - r_3)$$

$$C_5 = \frac{3.3}{2} \cdot \varepsilon \cdot (X + r_3)$$

$$C = C_1 + 2 \cdot C_2 + 2 \cdot C_3 + 2 \cdot \left[\frac{1}{\frac{1}{C_4} + \frac{1}{C_5}} \right] \qquad (2.4)$$

Figure 2.7 – Capacitance Between a Concentric Wire and Tube

Method

The capacitance between the wire and tube was measured as the length of the wire protruding from the coil (X) was altered. Measurements were taken with three different tubes (coils). As before the test pieces were held clear of the work bench (which might have influenced results) by thin walled insulating posts. Measurements were taken using a Wayne Kerr LCR bridge measuring to 0.01pF at a frequency of 10kHz. Due to the sensitive nature of the measurements they were repeated and an average result taken.

Results

The measured and calculated results for capacitance between the wire and tubes, as the length of the wire was altered, are shown overleaf:

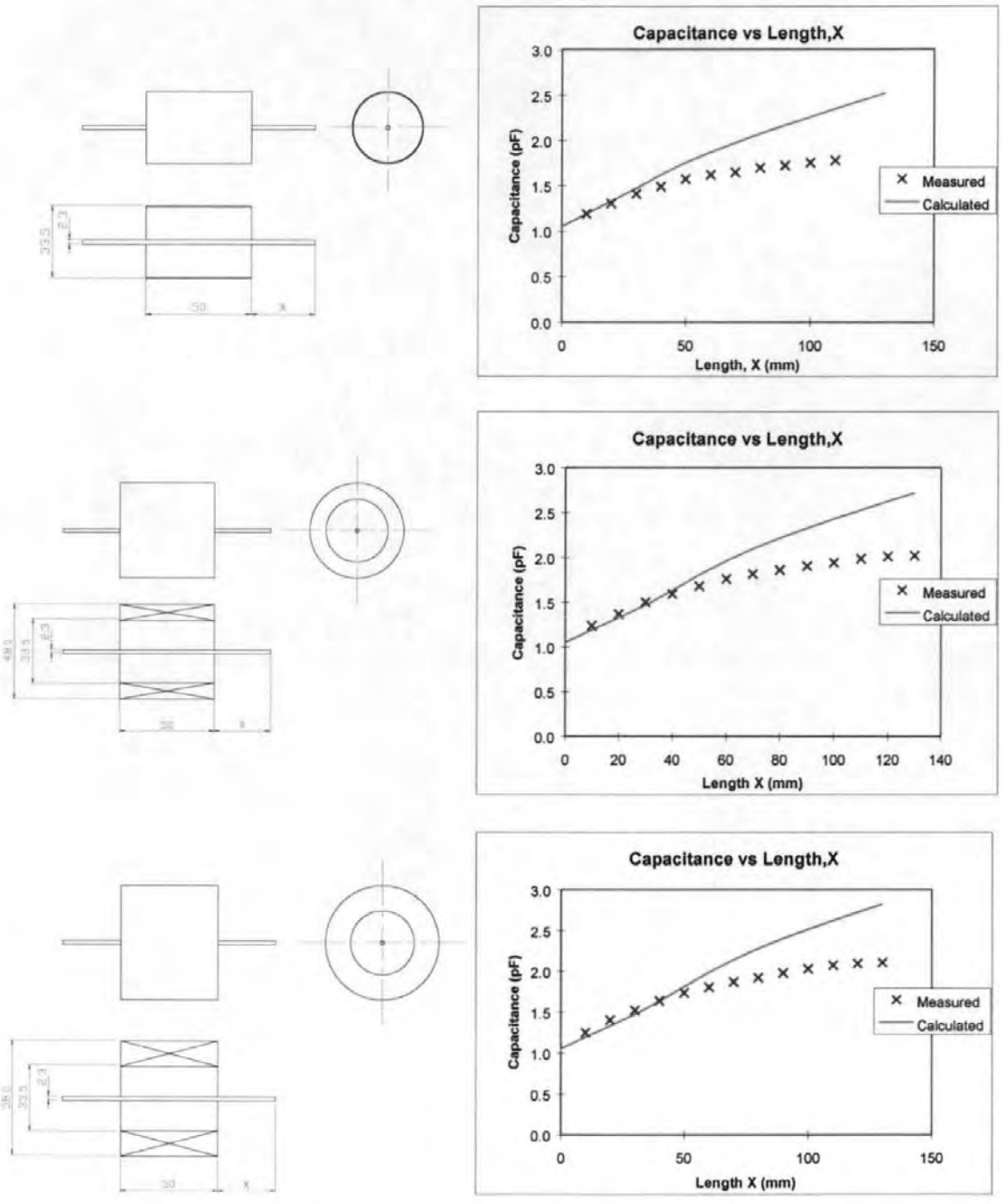

Figure 2.8 – Capacitance vs. Wire Length for Three Tube Assemblies

Discussion

The results show again that, as the length of the wire increases, the significance of the fringing field is over estimated by the spherical shell approximation and the calculated results diverge from those measured. It was concluded from the above experiments that Roters' method of approximating permeance must be applied with care and that the model proposed by Cullen, which uses this method, could contain significant error. The aim of subsequent finite element work was to investigate this.

2.2 Finite Element Analysis

In the previous section it was noted that the complete magnetic circuit for a reed relay could not be modelled by means of capacitance experiments. Conversely, finite element analysis does allow this and, additionally, is ideally suited to investigating the effect of coil and reed dimensions on the efficiency of the magnetic circuit. This is important given the aim of the present work of linking relay geometry to efficiency.

A 2D axisymmetric model representing a simplified reed switch and coil was constructed using the ANSYS finite element package and used to:

a) visualise the paths taken by the magnetic flux

b) calculate return path reluctance

c) calculate fringing (or leakage) reluctance

In each case above the variation of the properties examined with reed and coil dimensions was of prime interest. The findings were to be used to compare with and refine the model of the magnetic circuit of a reed switch and coil as proposed by Cullen.

2.2.1 The Finite Element Model

Introduction

As already mentioned the finite element model constructed was a 2D axisymmetric representation of a simplified reed switch and coil. This allowed the complete magnetic circuit of the reed switch and coil to be modelled. It should be noted that the geometry of the contact gap is not correctly reproduced - it appears as a simple parallel gap between the end faces of the two reeds rather than the correct overlapped arrangement. However, provided that the parallel gap is chosen so that it has a similar reluctance to that of the overlapped arrangement the effect of this approximation on the rest of the field will be minimal.

To accurately model the fields in the region of the contact gap a 3D model would be required. A full 3D model of the entire structure is, in theory, possible but has not been constructed as the (considerable) computing power required is not available to the author. Also, it was considered that useful results would be obtained and implemented much more rapidly with the simpler 2D model.

Software

The software package used to create the finite element model was the ANSYS program from Ansys Corporation(27). This was chosen as it was a well established finite element package (28) offering magnetic analysis in two and three dimensions for static, harmonic and transient problems. The problem described here covers only 2D static analysis. However, should more advanced analysis be required this could be carried out with the same software (and possibly the same model) if required.

Work undertaken by van Oss (29) using this package had reported good results and offered helpful tips as to its use.

Additionally a training course, run by Strucom (who were the distributors of ANSYS in the UK), was attended by the author.

Area Included in Finite Element Model

As indicated above a 2D axisymmetric representation of two ferromagnetic reed blades within a centrally located coil and volume of air was constructed using the ANSYS FEA package. The area covered by this model was as shown overleaf. Using suitable boundary conditions on the axes of symmetry only a quarter of this area need be meshed and analysed in the finite element model.

The overall dimensions of the finite element model were chosen to correspond with those of Crydom's smaller ranges (known internally as "S" and "T" sizes) of reed switches and relays. The reed blades for these switches are produced from 0.56mm diameter Nickel Iron wire and have a maximum length of 27.2mm (i.e. the maximum length of a completed switch is 54.4mm).

The range of possible coil dimensions was chosen to coincide with those which would be suitable for reed relays based around these switches. These were a maximum length of 20mm and maximum outside diameter of 16mm.

The outer dimensions of the volume of air in the model surrounding the reeds and coil were an overall length of 60mm and maximum diameter of 50mm.

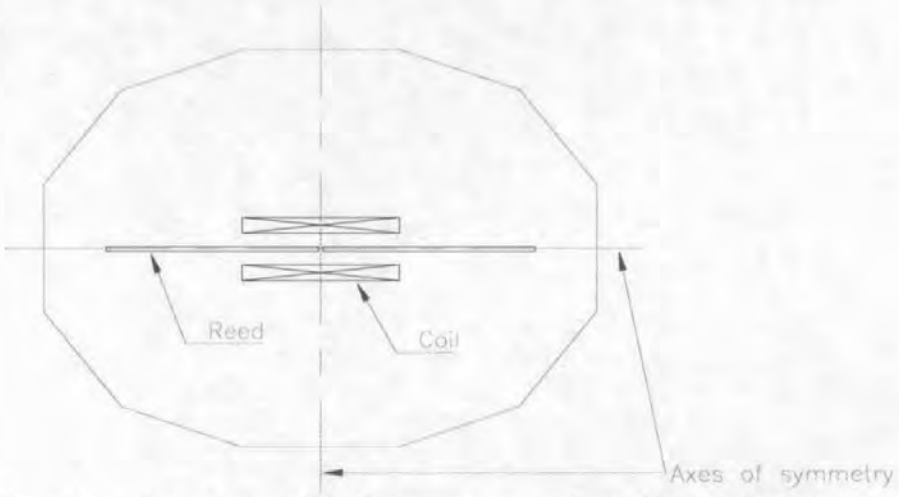

Figure 2.9 – Area Covered by 2D Axisymmetric Finite Element Model

Boundary Conditions

The boundary conditions are flux parallel along the line of axial symmetry and flux normal everywhere else. The flux normal constraint around the external edge of the model is not one which exists in the real case. However, as the boundary is shaped so as to minimise the interference of this constraint the effect on the flux flowing across the contacts (the most important aspect of the current analysis) will be minimal.

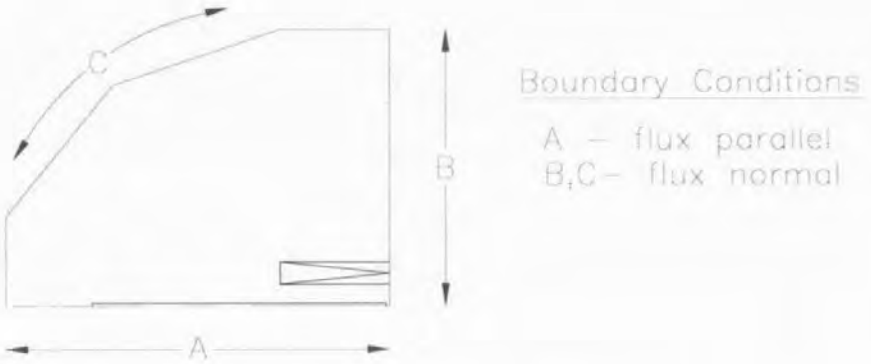

Figure 2.10 – Boundary Conditions

Material Properties

The material properties for the reed blades (i.e. their BH characteristic) was for Nickel Iron (51% Ni) as used Crydom (see figure 2.3 in section 2.1.1). The relative permeability of the coil winding and surrounding volume of air were taken as unity. The reason for

differentiating between the two was to simplify identification of the area covered by the coil and application of current density (to load the model).

Mesh

The model was constructed using a mixture of quadrilateral and triangular elements. For the reed, air surrounding the reed and contact gap a fine mesh of quadrilateral elements was used and care was taken to ensure that element aspect ratios were <8 in order to aid accuracy. A further benefit of using quadrilateral elements for the contact gap was that its size could be altered simply by altering the material properties of rows of these elements from NiFe to air or vice versa. Ten rows of elements were placed in the gap area each with an edge length of 0.01mm. Bearing in mind the axis of symmetry this gave an effective range of contact gaps of 0.04mm (four elements across the gap) to 0.2mm (20 elements across the gap).

A similar approach was taken in the area occupied by the coil. Again quadrilateral elements were used so that the dimensions of the coil could be altered by changing the material properties of selected elements from that of the coil to air. The desired current density could then be applied to the coil elements to load the model.

The area surrounding the coil was meshed with a combination of quadrilateral and triangular elements. This was to allow a variation in mesh density so that a relatively course mesh could be used close to the outer boundaries of the model, where great accuracy was not required, whilst still matching the fine mesh around the reed and contact gap.

The mesh of the completed model is shown below. Note that, in the figure below, a change in material is denoted by a change in colour. The coil is shown occupying the elements to give it maximum possible length (20mm) and outside diameter (16mm). In the vicinity of the reed,

however, the mesh is so dense as to obscure the exact location of the reed. The completed mesh contained approximately 1400 elements.

An example input data file is contained in Appendix 1.

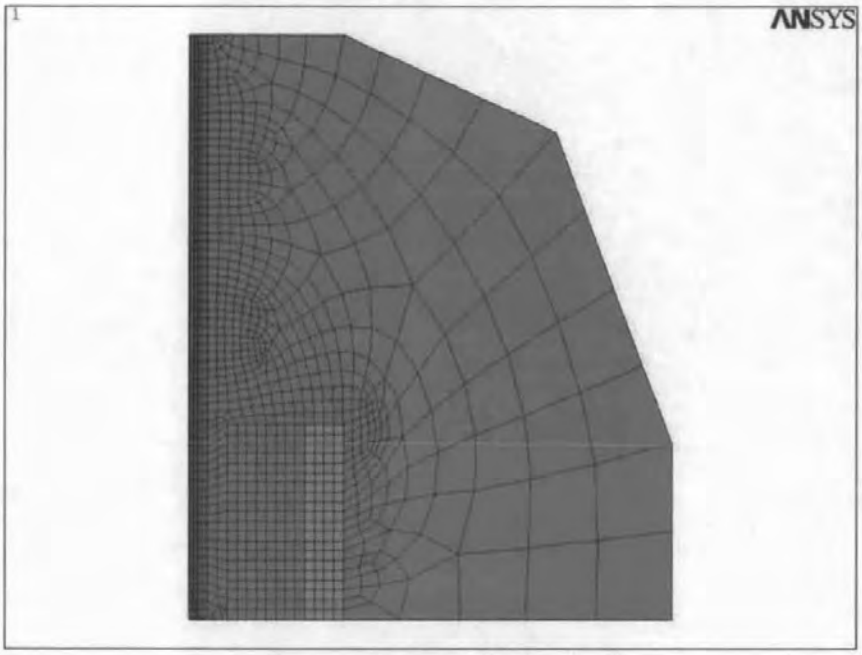

Figure 2.11 – Finite Element Mesh

2.2.2 Visualisation of flux paths

Introduction

Using Finite Element Analysis (FEA) allows the complete magnetic circuit for the reed switch and coil to be modelled. This is important as, if Roters method is to be subsequently applied, a knowledge of the geometry of the magnetic flux paths is required. In this instance the model which has been constructed is a 2-D axisymmetric simplification of a reed switch and coil. This means that the geometry of the contact gap is not correctly reproduced - it appears as a simple parallel gap between the end faces of the two reeds rather than the correct overlapped arrangement. However, provided that the parallel gap is chosen so that is has a similar reluctance to the real case the effect of this approximation on the form of the rest of the field should be minimal.

The primary area of interest at this stage is how the flux paths displayed compare with those inferred in Cullen's model.

Procedure

The model was run with a current density applied to the coil winding corresponding to 5AT in all cases. The low applied current ensured that the form of the field displayed would not be influenced by saturation of the reed blades. This was because, in a typical reed relay, saturation of the blades does not occur prior to operation of the switch. The characteristics of the field without saturation of the blades was therefore of most interest.

Results

Running the model produced the results shown in figures 2.12 to 2.15. In order to verify the model it was run first with a reed blade but no contact gap (i.e. a continuous NiFe reed). Figure 2.12 shows the resulting flux plot which displays the expected result.

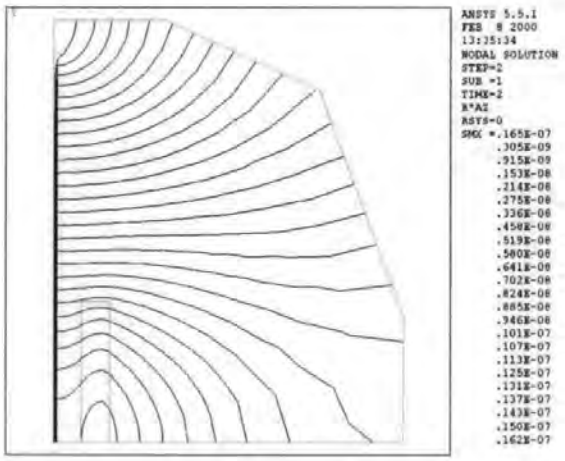

Figure 2.12 - Flux Plot with a continuous NiFe Reed

Note : In the above figure one quarter of the axisymmetric model is shown as indicated on Figure 2.9.

Figures 2.13,2.14 and 2.15, overleaf, show the flux paths as the coil length is varied from 8mm to 20mm whilst the contact gap remains constant (at 0.04mm). The contact gap was chosen in order to give a similar reluctance to that of a relatively similarly sized reed switch.

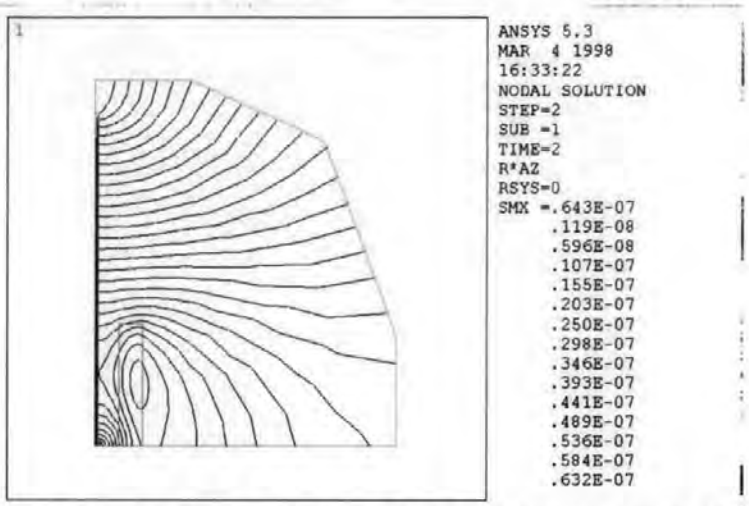

Figure 2.13 - Flux Plot with 20mm Coil and 0.04mm Contact Gap

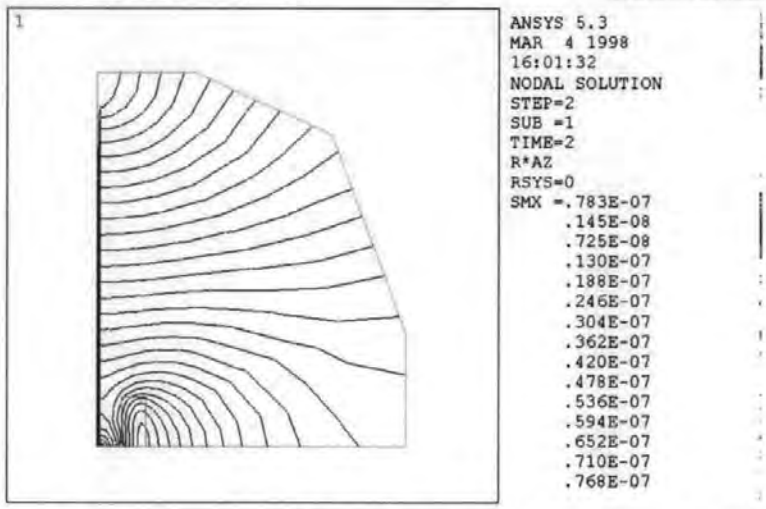

Figure 2.14 - Flux Plot with 8mm Coil and 0.04mm Contact Gap

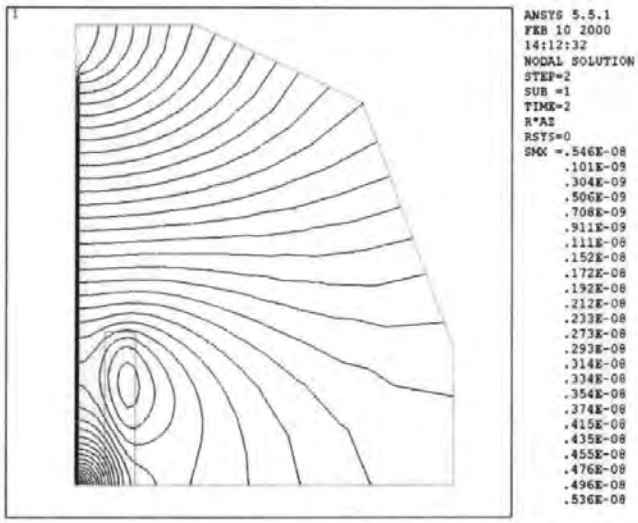

Figure 2.15 - Flux Plot with 20mm Coil and 0.2mm Contact Gap

Discussion of Results

The primary area of interest is how the flux paths compare to those assumed by Cullen. The return path around the outside of the coil is similar in all three cases. However, the paths within the coil are somewhat different. In particular there is an area of fringing around the contact gap. The size of this fringing region is larger than expected and varies with coil length. The presence of this fringing path is significant as it provides an alternative path for flux which would otherwise flow directly across the contacts and develop a force between them. This indicates that shorter coils are likely to be more efficient (in converting coil energy to a mechanical force at the contacts) than longer ones.

It is also interesting to note the circular paths which flow directly around the coil cross section. For the 8mm coil this is a single loop but, as coil length increases to 20mm, it splits into two. This is a further indication of the extent of the fringing field around the contacts and its variation with coil length.

Figure 2.15 shows the flux plot for a 20mm coil (as figure 2.13) but with the contact gap increased from 0.04mm to 0.2mm. Comparing the two it can be seen, as might be expected, that the fringing path around the contacts expands as the contact gap increases. This indicates that the reluctance of the fringing path reduces as contact gap is increased. When considered in isolation the attractive force across the contact gap, for parallel gap faces, will diminish according to the inverse of the square of the gap. The variation in fringing reluctance noted will make this decay more rapid and, in a reed switch, will limit the maximum contact gap which can be closed.

Conclusions

The visualisation of the magnetic flux paths afforded by the finite element model shows that they are similar in arrangement to those assumed by Cullen. However, as it has already been

shown that the use of Roters' method to estimate permeance can lead to significant error, the aim of the following section was to use the finite element model to determine the values of permeance for parts of the magnetic circuit and compare the results.

2.2.3 Calculation of Return Path Reluctance (No contact gap present)

Introduction

The 2D axisymmetric finite element model does not model the real contact geometry correctly. However, the return path between the reeds (which runs outside the coil) is faithfully reproduced. This is because a reed switch mounted centrally within a coil of circular cross section is an axisymmetric structure with the exception of the contact area. Assuming a magnetic circuit of the form in the figure below the aim of the following work was to use the 2D FEA model to estimate the value of return path reluctance and how it altered with changes in reed and coil dimensions. This could then be compared to the approximation used in Cullen's model.

Initially the case with no contact gap (i.e. a continuous NiFe reed passing through the coil) was considered.

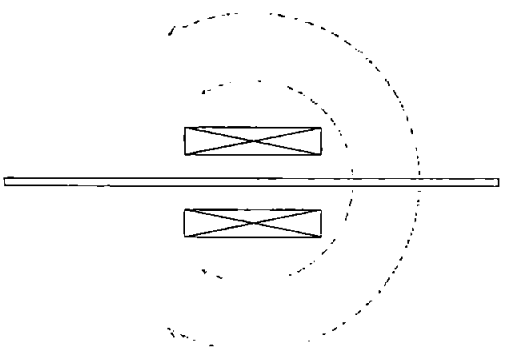

Figure 2.16 – Return Path

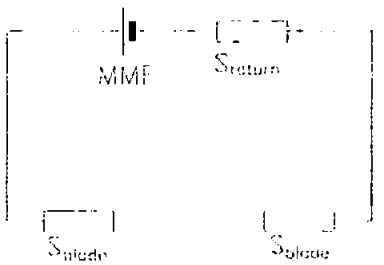

Figure 2.17 – Magnetic Circuit

Method

It was not possible to obtain a value of return path reluctance directly from the finite element model. Instead the finite element model was run with a known AT applied to the coil and the maximum flux density in the reed recorded. The AT applied to the coil was chosen so that the flux density in the reed was well below that at which saturation occurred. This being the case the reluctance of the reed could be assumed negligible. In a typical reed relay the reed blades

do not become saturated prior to operation of the switch and so the reluctance of the return path without saturation of the reeds was of interest. Referring to figures 2.13 to 2.15 it can be seen that flux enters the reed along its length where it protrudes from the coil. Inside the coil and in the vicinity of the contacts flux is seen to be leaving the reed. Between the two is the point at which the flux density in the reed is at a maximum. The total flux in the magnetic circuit is then the flux density at this point multiplied by the cross sectional area of the reed. The return path reluctance could then be determined from:

$$S_{return} = \frac{mmf}{\Phi} \qquad (2.5)$$

This was repeated for a range of coil and reed geometries as below.

Geometry

The range of coil and reed geometries investigated were relevant to the "S" and "T" series reed switches (and their respective relays) manufactured by Crydom. Reed diameter was fixed at 0.56mm and their length varied in four steps from 27.2 mm (standard length as manufactured) to 7mm. Note that the two reeds are effectively joined to form one of twice these lengths. Coil length was varied from 20mm to 8mm in four steps and its outside diameter from 8mm to 16mm in three steps.

Results

The return path reluctance values derived from the finite element model for a coil and reed combination as reed length, coil length and coil outside diameter are varied in turn are shown below compared to those calculated using the method suggested by Cullen. In each of the figures shown below the starting point is a coil of 20mm length, 8mm outside diameter with each reed of 27.2mm length and each of these parameters is varied individually. Further results for other coil and reed dimensions are shown in appendix 2.

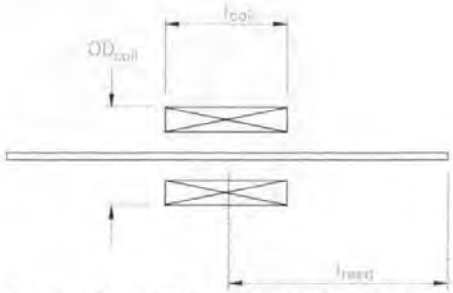

Figure 18 – Coil and Reed Dimensions

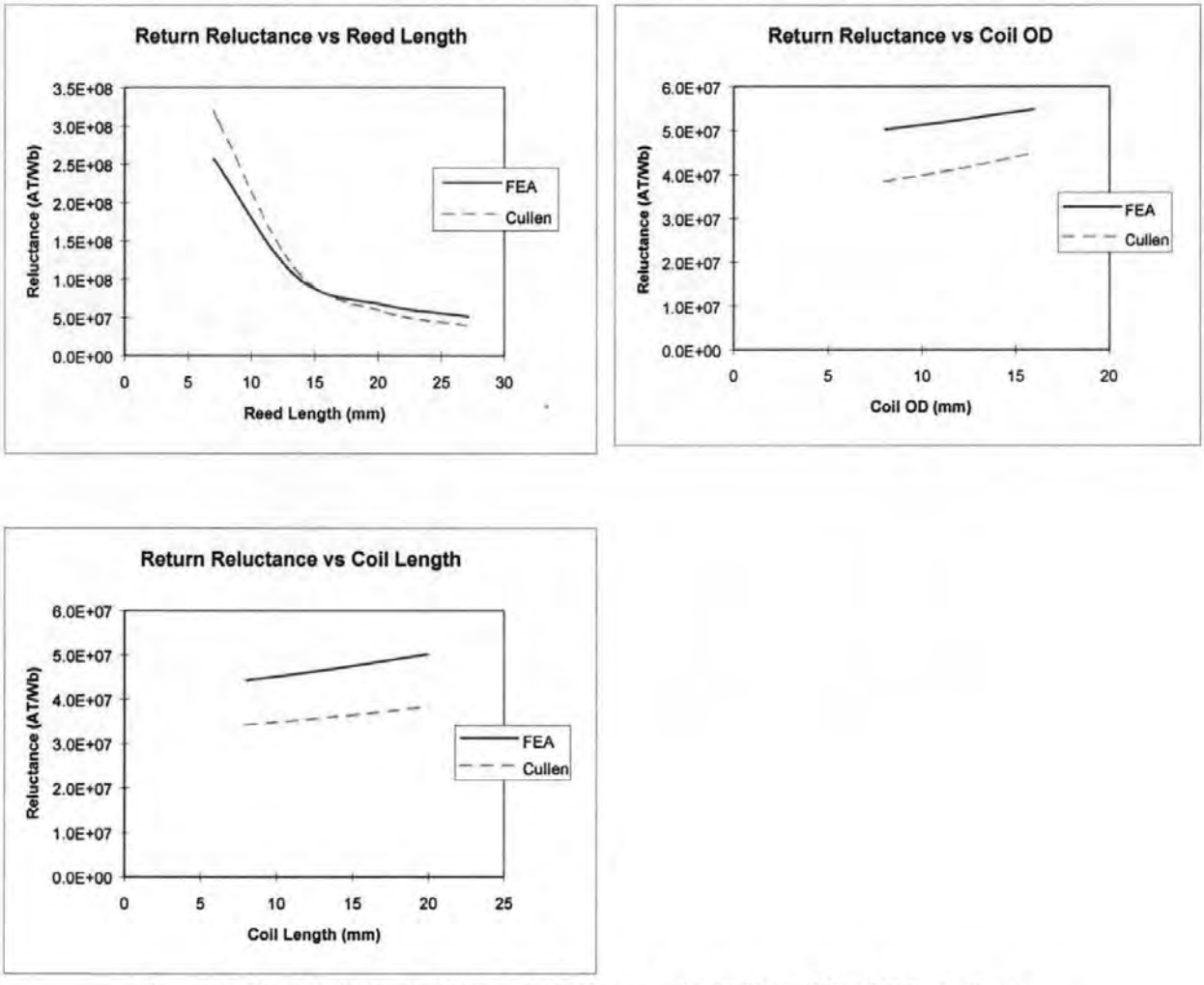

Figure 2.19 – Variation in Return Reluctance with Coil and Reed Dimensions

Discussion of Results

The above results show that return path reluctance calculated from the finite element model was similar to results calculated using the method suggested by Cullen. Also, as a general note, the results show that, as would be expected from the flux plots shown in section 2.2.1, return path reluctance reduces with short coils wound closely around long reeds. However, there is a discrepancy between the two sets of calculated values of up to 25%. The reason for this discrepancy is most likely as a result of the difference in the form of the flux paths assumed in Cullen's model and those shown on the finite element model.

The experimental work in sections 2.1.2 and 2.1.3 indicated that a divergence between calculations based on Roters' technique and experimental measurements of 25% and above was possible. Accordingly the results from the finite element, rather than from Cullen's work, were incorporated into the reed switch design program using interpolation to allow the return path reluctance for any coil and reed combination to be calculated.

A further possibility, not accounted for by Cullen's model, was that return path reluctance was influenced by the presence of a gap in the reed, i.e. that the presence of a gap in the reed could alter the flux paths within the whole system sufficiently to change the reluctance of the return path. This was investigated in the following section.

2.2.4 Calculation of Return Path Reluctance (contact gap present)

Introduction

In the preceding section return path reluctance for the case where no contact gap was present in the reed was calculated from the finite element model. The following work was to determine whether this value was affected by the introduction of a gap in the reed.

Method

A selection of finite element models from 2.2.2 were re-run with a parallel faced gap introduced in the centre of the reed as shown in the figure below.

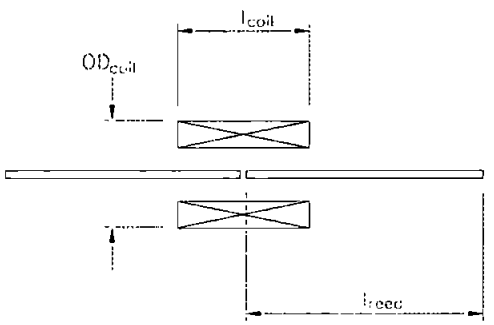

Figure 2.20 – Axisymmetric Model with Contact Gap

The magnetic circuit then becomes:

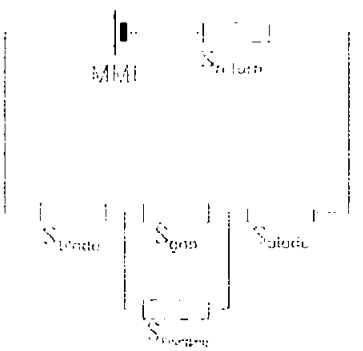

Figure 2.21 – Magnetic Circuit with Contact Gap

The size of the gap was varied over a range from 0.04mm to 0.2mm. In each case the maximum flux density in the reed and the flux density at the contact gap face was recorded.

Again the applied AT was chosen so that saturation would not occur in the reed and, consequently, its reluctance could be assumed negligible.

The form of the contact gap is that of two parallel surfaces and its reluctance (excluding fringing) can be calculated from

$$S_g = \frac{g}{\mu \cdot A} \qquad (2.6)$$

As the flux density at the contact gap and its area are known the AT drop across it is

$$mmf_g = \Phi_g \cdot S_g \qquad (2.7)$$

The return path reluctance is then given by

$$S_{return} = \frac{mmf - mmf_g}{\Phi} \qquad (2.8)$$

Results

The results for return path reluctance against gap reluctance are shown below for various coil and reed geometries.

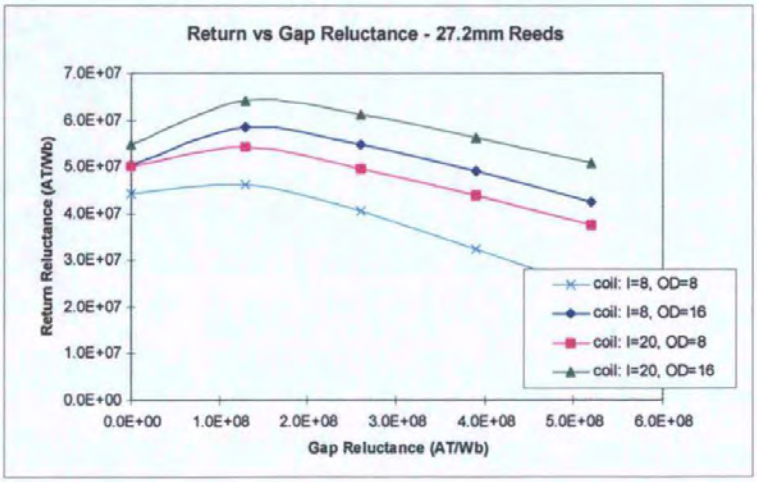

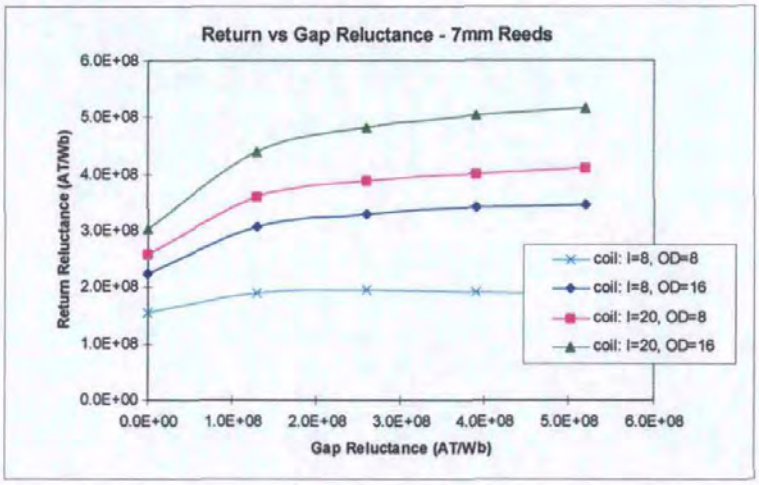

Figure 2.22 – Return Reluctance vs. Gap Reluctance

Analysis of Results

It can be seen in each of the above cases that there is a variation in return path reluctance with gap reluctance which, for most geometries, is significant. A likely reason for this is that the presence of the fringing field distorts the return path and increases its reluctance as a result. A simple means of incorporating this characteristic into the reed switch design program was therefore sought. Although one possibility was to interpolate between the finite element results, as in the preceding section, inspection revealed that the characteristic could be approximated with a quadratic function. Reforming the results so that each characteristic was shown as the ratio

$$ratio = \frac{S_{return}}{S_{return(g=0)}} \qquad (2.9)$$

demonstrated, as shown in the figures below, that the curvature, i.e. the squared term, was very similar for all cases considered. The linear coefficient is seen to vary primarily with reed length and the intercept is obviously one. The linear coefficient also varies, to a much smaller degree, with coil outside diameter. There is little variation in the characteristics with coil length. Accordingly a function was devised by the author for use in the reed switch design program with the following form :

$$f = a \cdot S_g^{\,2} + b \cdot S_g + c \qquad (2.10)$$

where

$$a = -4.5^{-18}$$

$$b = \frac{1}{l_{reed} + 13.2} \cdot (0.275 \cdot OD_{coil} + 2.6) \cdot 10^{-8}$$

$$c = 1$$

The coefficients of the function were determined by experimentation until a good match between the function and the finite element results was obtained. This function is shown overleaf with the reformed results from the finite element model for comparison. It should be noted that the above coefficients are relevant only to the range of geometries considered in the finite element model and are not universal i.e. its application to a much bigger reed switch or one using a different diameter may not be appropriate.

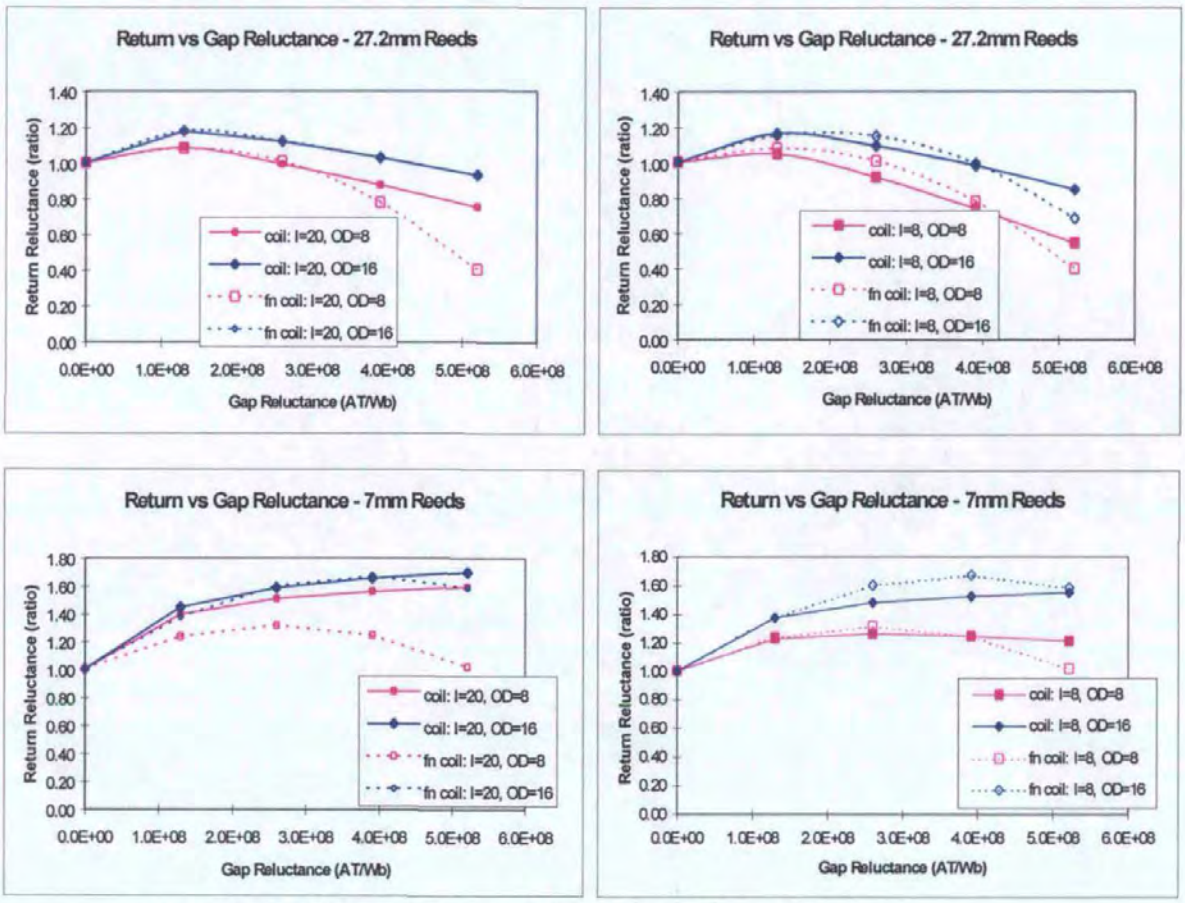

Figure 2.23 – Change in Return Reluctance with Gap Reluctance

In order to incorporate the above work into the reed switch design program the results for return path reluctance (with S_g=0 and over the range of coil and reed geometries as previously described) from the finite element model have been included in it and interpolation used to determine the value of return path reluctance for any given geometry (with S_g=0). The quadratic function above is then applied to give the variation in return path reluctance with gap reluctance.

2.2.5 Calculation of Fringing Reluctance

Introduction

Analysis of the output from the finite element model also allows the reluctance of the fringing path around the contact gap to be calculated. The reluctance of the fringing path has a strong influence on the force available at the contact gap. Its value and variation with coil and reed geometry was therefore of interest and was to be included in the reed switch design program. Fringing reluctance with a fixed contact gap (0.04mm) was determined over the same range of coil and reed geometries as return path reluctance. In addition the variation in fringing reluctance with contact gap was also investigated.

Method

As mentioned in the previous section the maximum flux in the reed and the flux at the contact gap are given in the finite element model. As the reluctance of the contact gap is known and if the drop in AT in the reed can again be neglected the reluctance of the fringing path is given by

$$S_{fr} = \frac{\Phi_g}{\Phi - \Phi_g} \cdot S_g \qquad (2.11)$$

Fringing reluctance was measured in this way over the same range of coil and reed geometries as return path reluctance. This was with reed diameter fixed at 0.56mm and its length varied in four steps from 27.2mm (standard length as manufactured) to 7mm. Coil length was varied from 20mm to 8mm in four steps and its outside diameter from 8mm to 16mm in three steps.

The variation in fringing reluctance with contact gap was also of interest. In this case a subset of the above range of geometries was chosen and fringing reluctance calculated using the same method as above as the contact gap was altered from 0.04mm to 0.2mm.

Results

The results for fringing reluctance against gap reluctance are shown below for the case of a 20mm long coil of 8mm outside diameter surrounding two 27.2mm long reeds with a 0.04mm gap between them as each of the principal dimensions is altered.

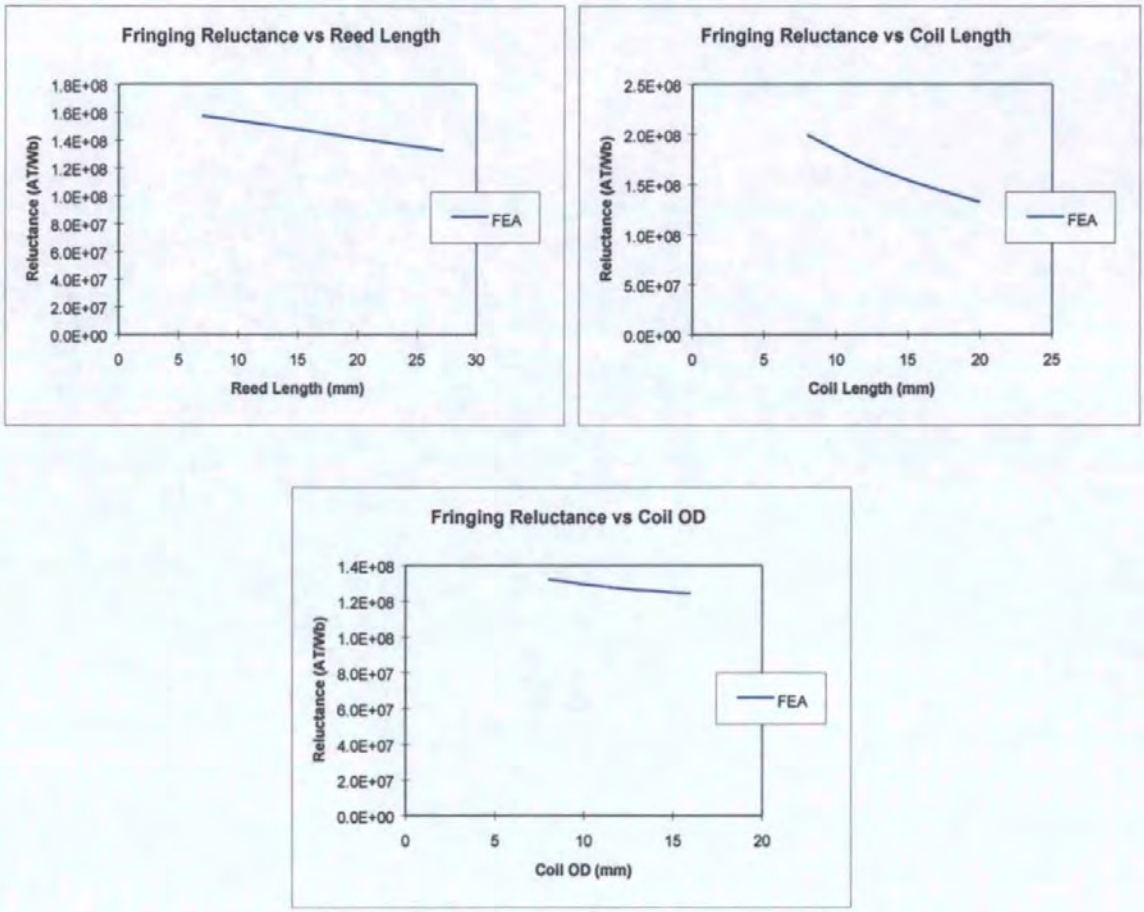

Figure 2.24 – Fringing Reluctance vs. Reed & Coil Geometry

The change in fringing reluctance with contact gap for the same coil and reeds are shown overleaf.

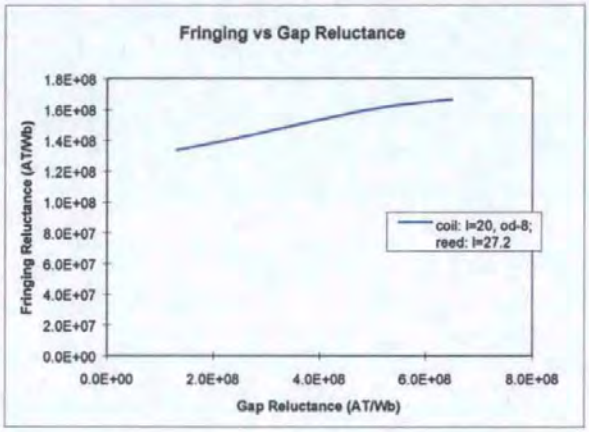

Figure 2.25 – Fringing Reluctance vs. Gap Reluctance

Discussion of Results

The results for the variation in fringing reluctance with coil and reed geometry show that the factor with the strongest influence is coil length. Returning to the flux plots in the visualisation section (2.2.2) this can be seen in that the length of reed over which fringing takes place is linked to coil length (the area which the fringing paths occupy shortens with coil length and the reluctance of the path therefore increases). A further important note stemming from the flux plots is that the area the fringing paths occupy is much greater than assumed by Cullen. They are therefore considered additional to the more local fringing paths shown in Cullen's model of contact gap permeance.

The results for fringing reluctance also show that its magnitude will have a significant effect on the force available at the contact gap. This is because the flux passing through the fringing path does not contribute to the force between the contacts and, instead, presents an alternative to the "working" path through the contact faces. In the example above fringing reluctance is similar to gap ("working") reluctance. The flux at the contact faces is therefore roughly halved and, as force is proportional to flux squared, force quartered by the presence of the fringing path.

The results for the variation in fringing path reluctance with contact gap show (in figure 2.25 and appendix 4) a linear characteristic in all cases with the value of fringing reluctance at the intercept approximately 90% of that with a gap of 0.04mm. The reluctance of the 0.04mm gap in the finite element model is $1.3 \cdot 10^8$. When expressed in terms of this gap reluctance this gives the following empirical function, derived by the author, for fringing reluctance:

$$S_{fr} = m \cdot S_g + c \qquad (2.12)$$

where

$$m = \frac{S_{fr(S_g = 1.3 \cdot 10^8)}}{1.3 \cdot 10^8} \cdot 0.1$$

$$c = S_{fr(S_g = 1.3 \cdot 10^8)} \cdot 0.9$$

To incorporate the above work into the reed switch design program the results for fringing reluctance (with $S_g = 1.3 \cdot 10^8$ and over the range of coil and reed geometries as previously described) from the finite element model have been included in it and interpolation used to determine the value of fringing reluctance for any given geometry (with $S_g = 1.3 \cdot 10^8$). The linear function above is then applied to give the variation in fringing reluctance with gap reluctance.

Further results for the variation of fringing reluctance with coil and reed dimensions and the variation of fringing reluctance with contact gap are shown in appendix 3 and appendix 4 respectively.

2.3 Contact Gap Permeance

Introduction

The 2D axisymmetric finite element model already described cannot be used to precisely model the real contact geometry and, as previously discussed, a full 3D model of the reeds and coil was not considered practical. As a result it is not possible to compare directly results for contact gap permeance from Cullen's model to any derived from the finite element model. Instead results were compared against those derived from other researchers' models. These were from Peek(1) and Kato(2). Peek's model was formed from an empirical relationship applied to experimental results whereas Kato's model was mathematically derived.

Method

In order to compare the three models the permeance against gap characteristic was calculated for each using the dimensions of a Crydom "S" type reed switch contact. In addition the force against gap characteristic was also calculated for a nominal 100AT applied across the gap. Force is given by the relationship below which can be obtained from any text covering magnetic theory:

$$F = \frac{1}{2} \cdot mmf^2 \cdot \frac{dP_g}{dg} \qquad (2.13)$$

It should be noted that the magnetomotive force in this instance is applied directly across the contact gap and not to the complete magnetic circuit for a reed switch and coil. The forces calculated are therefore greater than would occur with 100AT applied to a coil around a reed switch.

Results

The results for permeance against gap and force against gap are shown overleaf.

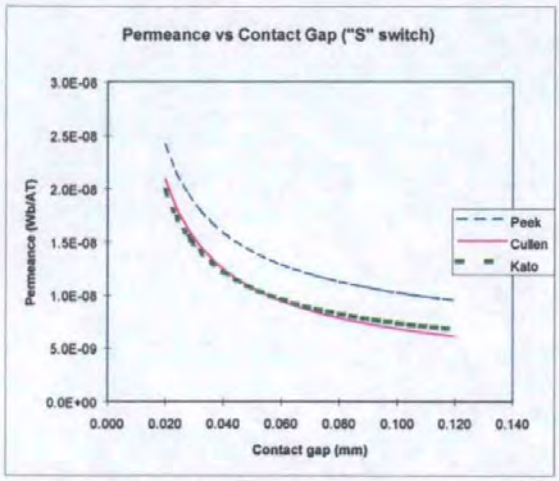

Figure 2.26 – Contact Permeance vs. Gap

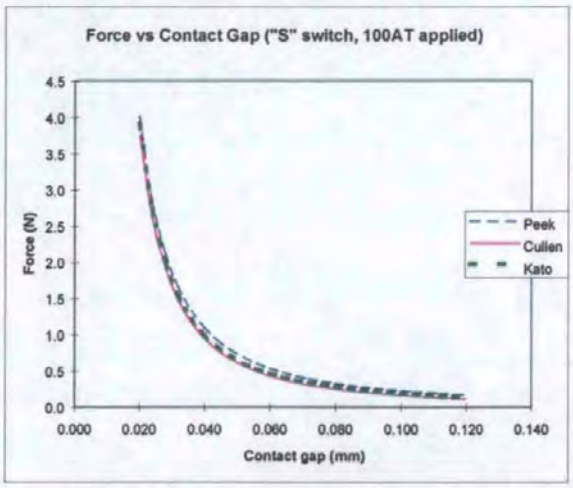

Figure 2.27 – Contact Force vs. Gap

Discussion of Results

From the permeance against gap characteristics it can be seen that the models developed by Cullen and Kato give virtually identical results. The model presented by Peek gives a somewhat greater permeance for a given contact gap and, as this was derived from experimental results, this cannot be ignored.

Comparing the force against gap characteristics shows that all three models give very similar results. This indicates that the discrepancy between the results for permeance between Peeks model and those of Cullen and Kato must be due to fringing effects (flux flowing in the fringing path will not create any significant contact force).

It should be noted that in this instance, to simplify the comparison, the magnetomotive force is applied directly across the contact gap and not to the complete magnetic circuit for a reed relay. Therefore, the effect of the fringing path is simply to permit more flux to flow between the contacts with a negligible effect on contact force. The flux flowing between the contacts is restricted only by the permeance between the contacts. This is in contrast to the real case, with a complete magnetic circuit, where the flux in the circuit is restricted also by return path reluctance. In this instance flux flowing in the fringing path essentially detracts from that

which would otherwise flow in the "working" path between the contacts and therefore has a strong (adverse) influence on contact force.

As Peek's model is derived from experimental measurement this would suggest that more fringing exists in practise than is predicted by Kato or Cullen. However the analysis of fringing reluctance in the finite element model (section 2.2.5) showed that it varies with coil and reed geometry. The dimensions of the coil and reed used in Peek's experiments were, unfortunately, different to those considered in the present work. The measurements undertaken by Peek involved recording the force between two reeds mounted inside a coil with a range of contact gaps. A "search coil" was fitted within this coil from which the flux in the reeds was determined. As the means of determining the flux in the reeds from the search coil was not apparent to the author a similar experiment with a suitably sized coil and reeds was not attempted.

In order to incorporate the results from the finite element model the approach taken for the gap permeance (including fringing) calculations was to assume that the permeance of the area immediately adjacent to the gap could be calculated as per Cullen or Kato. As it covers the area outside that immediately adjacent to the gap the fringing permeance calculated from the finite element model was considered additional to this. Force could be calculated using either Cullen's or Kato's model for the derivative of gap permeance with respect to gap.

2.4 Contact Resistance Characteristics

The characteristic of contact resistance against contact force was presented by Sekiya, et al for Rhodium and Ruthenium contacts. The measurements were made using reed switch blades of a similar size to Crydom "S" type switches mounted in apparatus incorporating a strain gauge. This allowed contact force and contact resistance to be measured simultaneously and their results are shown below:

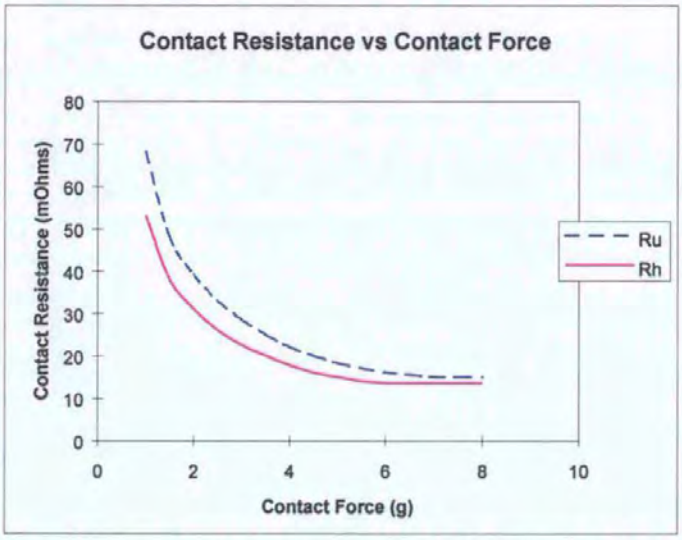

Figure 2.28 – Contact Resistance vs. Force for Rhodium & Ruthenium

The above information was incorporated into the reed switch design program directly. It should be noted that an important design consideration for reed switches is that they should not be expected to carry a significant current at the point where contact resistance increases steeply with a small decrease in contact force. This is particularly relevant to "latching" (bistable) reed relays where the amp turns applied to hold the switch closed are less than that required to operate the switch. The above therefore forms a useful addition to the program.

2.5 Calculation of Breakdown Voltage

A key aspect of reed relay and reed switch performance is the voltage which can be applied across the contacts before arcing (breakdown) occurs. Clearly a means of predicting breakdown voltage for a reed switch with a particular contact gap or operate amp turn rating would be an important addition to any design tool. Vacuum switches are the only type considered here.

There are two mechanisms in operation when breakdown voltage is reached. These are :

i) Electrostatic attraction between the reed blades (which reduces the contact gap)

ii) The voltage/contact gap condition at which arcing occurs

2.5.1 Electrostatic Attraction between Reed Blades

When reed switches are evacuated the voltage which can exist between the contacts before arcing occurs will be of the order of several thousand volts. Under these conditions the electrostatic force present between the blades is appreciable and can be great enough to close the contacts. Electrostatic force can be calculated according to the following relationship, which can be found in many texts, as applied by Cullen (20):

$$F_e = \frac{1}{2} \cdot V^2 \cdot \frac{dC_R}{dg} \qquad (2.14)$$

2.5.2 Contact Arcing

There is a large quantity of published information concerning voltage breakdown in a vacuum. The relationship used in the present work is that formulated by Takamisawa (19). This was developed to describe voltage breakdown between spheres of different sizes but, as

demonstrated by the results shown in section 2.5.4, was found by the author to give good results when applied to reed switch contacts.

$$V = 13.4 \cdot 10^{-3} \cdot \frac{1}{\sqrt{C_g \cdot 10^{-3}}} \cdot g^{0.641} \qquad (2.15)$$

2.5.3 Calculation of Breakdown Voltage

In order to calculate the breakdown voltage of a given reed switch from its contact gap both of the above mechanisms need to be taken into account. To do this in the reed switch design program the procedure as described below was developed by the author and used:

i) a range of gaps from 0 to the natural contact gap is defined.

ii) the voltage at which $F_e = F_s$ is calculated for each of the above gaps (where F_s is the spring force from the mechanical bending of the blades).

iii) the derivative dF_e/dg is calculated for the above voltage (ii) for each of the above gaps. If dF_e/dg is greater than the spring rate of the reed blades failure caused by electrostatic attraction is inferred.

iv) the voltage at which arcing occurs for each of the above gaps is calculated. If the voltage at which arcing occurs is less than that in (ii) then failure through contact arcing is inferred.

v) the largest gap at which one of the failure mechanisms occurs gives the breakdown voltage.

2.5.4 Comparison of Measured and Calculated Results

The breakdown voltage of Crydom "TDA832" and "SRA830" vacuum reed switches were calculated for various contact gaps using the method described in 2.5.3. A comparison between these and measured results is made in figures 2.29 and 2.30. Breakdown voltage and contact gap were measured using a MEGGER FT6/12 Mk2 isolation tester and travelling microscope respectively. The results, presented below, show a good correlation. Also, it is interesting to note that, when the results were interrogated, the dominant mode of failure was found to be from switch closure due to electrostatic attraction. In the only cases where the arcing criteria was reached (TDA832, >60AT) it was at a voltage only slightly lower than that for closure due to electrostatic attraction. A simplified breakdown voltage calculation considering only the effects of electrostatic attraction would therefore still give good results for the small switches considered.

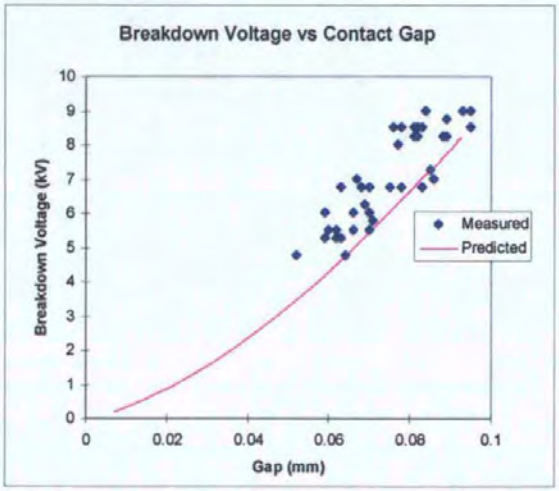

Figure 2.29 – Breakdown Voltage vs. Gap (SRA830)

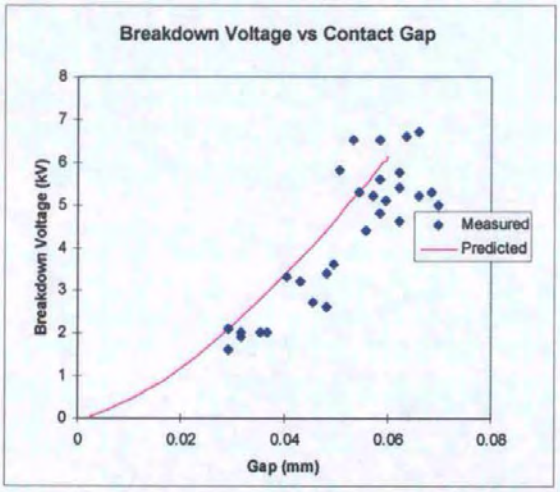

Figure 2.30 – Breakdown Voltage vs. Gap (TDA832)

2.6 Reed Switch Design Program

Introduction

The aim of the reed switch design program was to combine the preceding work into a single program, in this case written using Mathcad software, which can be used to predict the performance of a reed switch from its physical dimensions and material properties. This is ultimately intended to be used as part of a design aid which will demonstrate how the proportions of a reed relay can be altered to enhance its electrical performance.

The model used in the program is essentially a development of that presented by Cullen and incorporates the findings of the finite element analysis, contact resistance and voltage breakdown calculations as described in the preceding sections. The following characteristics are predicted :

Contact gap vs. Operate Amp-Turns (OAT)

Differential and Release Amp-Turns (RAT) vs. OAT

Breakdown Voltage vs. OAT

Contact Resistance for given OAT switches vs. Applied AT

The program has been verified against reed switches based around 0.56mm NiFe wire as used on the "S" and "T" type switches manufactured by Crydom. The influence of wire size on return and fringing reluctance, etc, has not yet been investigated.

2.6.1 Structure

The calculations in the program are split into four main sections covering the mechanical stiffness of the blades, the magnetic circuit, contact resistance calculations and voltage breakdown calculations as described below.

Blade Stiffness

The blade is modelled as a cantilevered beam. The relationship for the stiffness of such a beam can be found in any structural engineering text and is given by the equation

$$stiffness = \frac{F}{deflection} = \frac{3 \cdot E \cdot M}{l^3} \qquad (2.16)$$

Two changes in section are catered for in the program as reed switches frequently have a different blade thickness at the contact area than over the main section of the blade. An example of this is the "New TDA832" reed switch described in section 2.6.4. Also, it should be noted that the stiffness which the magnetic force must act against is that of the two blades in series as follows:

$$stiffness = \frac{1}{\left(1/stiffness_1 + 1/stiffness_2\right)} \qquad (2.17)$$

Magnetic Circuit

The magnetic circuit used is as shown in the diagram below:

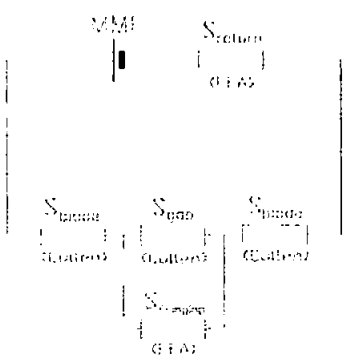

Figure 2.31 – Magnetic Circuit

The reluctance of each part of the circuit is calculated based on the findings of the previous sections.

Return path reluctance is calculated by interpolating between the results for return path reluctance with no contact gap obtained from the finite element model for the coil and reed dimensions chosen. A quadratic function, dependent upon reed length, is then applied to give the variation in return path reluctance with gap reluctance.

Reed reluctance is calculated from the BH characteristic of the NiFe used, the cross sectional area of the reed and the approximation that all the flux flows through half of each reed (as in Cullen(3)).

Contact gap reluctance is calculated using the method presented by Cullen. That presented by Kato was also be used but, as this is considerably more complex to implement, Cullen's method has been chosen over it.

The value of fringing reluctance, which acts in parallel to that of the contact gap, is obtained from the finite element model by interpolating between the results for fringing reluctance with a nominal "working" gap reluctance (i.e. that of the parallel faces alone) of $1.3 \cdot 10^8\ AT/Wb$ for the coil and reed dimensions chosen. The value of $1.3 \cdot 10^8\ AT/Wb$ arises as this was the "working" gap reluctance of the 0.04mm gap in the finite element model from which the data was taken. A linear function is then applied to give the variation in fringing reluctance with "working" gap reluctance. This is described in greater detail in section 2.2.5.

The above circuit allows the magnetic force at the contacts to be calculated for a given applied AT. In order to verify its correct functioning a model was built to represent the 2D axisymmetric model used in the finite element analysis. The forces and flux densities

produced for the appropriate applied AT as coil and reed dimensions were altered were calculated using the model and compared against the data from the finite element work. A match was obtained in all cases.

The aspects of reed switch performance which can be determined from the magnetic circuit and blade stiffness include RAT, differential AT, contact gap and contact force for a given OAT reed switch.

Contact Resistance

Contact resistance is calculated from contact force using the relationship from Sekiya, et al (13) in section 2.5. Results are presented for the variation of contact resistance with applied AT for a given OAT switch.

Voltage Breakdown

Breakdown voltage is calculated using the method presented in 2.6. This includes the calculation of electrostatic attraction between the blades from Cullen (20) and the arcing criteria from Takamisawa (19).

A listing of the reed switch design program is presented in appendix 5.

2.6.2 Variation in Operate Amp Turns with Coil and Reed Geometry

Introduction

As the data from the finite element work, in which coil and reed dimensions were altered, was included in the reed switch design program it was hoped that it would accurately predict the change in reed switch operate characteristics with reed and coil geometry. In order to test this a trial was run in which the operate amp turns (OAT) of a Crydom "S" type switch was measured in coils of lengths from 4.5 to 18.3mm and with the switch uncropped at ~54mm overall length and then progressively shortened to ~24mm. The results were compared from those derived from the reed switch design program.

Method

For the experimental work a set of 8 coils of lengths varying from 4.5 to 18.3mm was produced. The inside and outside diameters of the coils were constant at 3.5 and 8.5mm respectively. Operate amp-turns were measured with the switch uncropped at 54mm overall length (27mm reed length) and with 10 progressive reductions in length to 24mm (12mm reed length). As the "S" type switch has a glass length of approximately 20mm a reduction in overall length below 24mm would risk damaging the glass to metal seals. This set the lower limit for reed length. It should be noted that this trial involved only one reed switch and so parameters such as contact gap remained constant.

In order to produce the predicted results a reference OAT was taken, in this case the experimental result with the switch uncropped and with the longest coil, and the AT against gap characteristic from the program was interpolated to give the contact gap corresponding to this OAT. The program was then re-run, with the reed and coil dimensions altered as required, and the AT against gap characteristic interpolated to find the new OAT

corresponding to the above gap. Results which could be compared directly to those obtained by experiment were thereby produced.

Results

The results for the change in OAT with coil length are shown below:

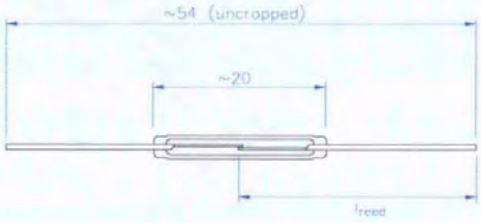

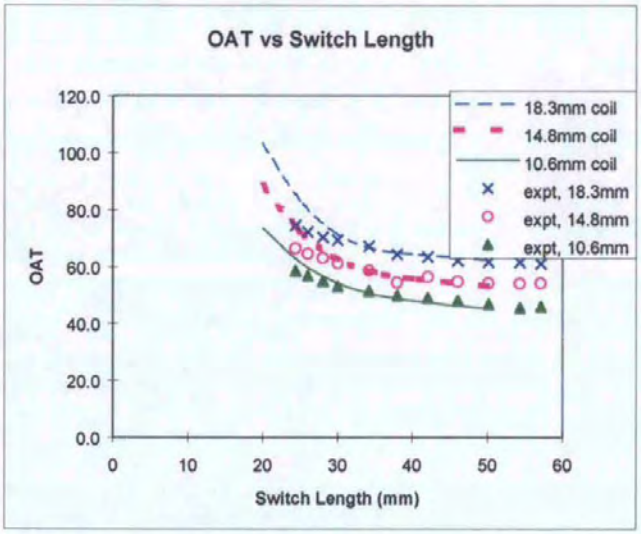

Figure 2.31 – Variation in OAT with Switch Length

The results for the change in OAT with reed length are shown below:

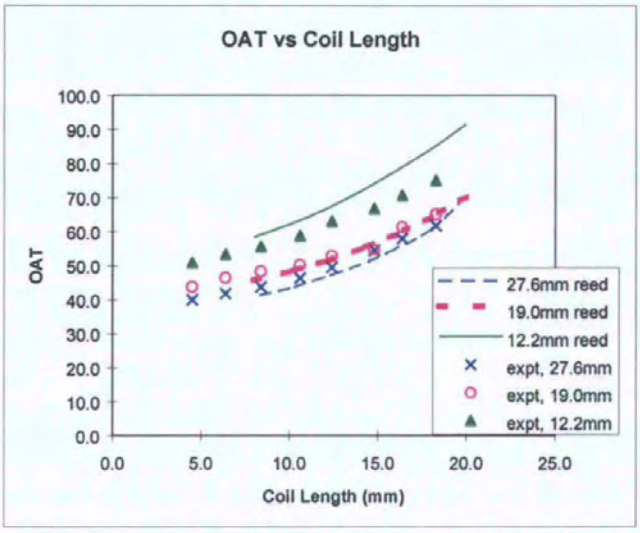

Figure 2.32 – Variation in OAT with Coil Length

Discussion of Results

Both of the above figures show a good match between experiment and theory. This would indicate that the effort involved in incorporating the finite element work into the reed switch design program has not been wasted and that it is sufficiently accurate to be used as a design tool. Also, an important aim of the present research was to determine the link between relay geometry and its performance characteristics. The above represents a significant step towards that aim.

2.6.3 Reed Switch Characteristics with Test Coil (SRA830 & SRA831)

Introduction

Within Crydom switches are graded according to their operate amp turns in a particular test coil. In the following work the operating and voltage isolation characteristics of two batches of "S" type switches (one of "SRA830" and the other of "SRA831") were measured using the appropriate test coil.

Method

The operate and release amp turns of the two batches of switches (40 in each) were measured using the appropriate "RSC09" test coil as shown below:

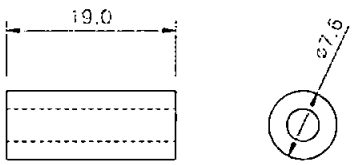

Figure 2.33 - RSC09 Test Coil

The breakdown voltage, contact gap and overlap were also measured for each switch using a MEGGER FT6/12 Mk2 voltage isolation tester and travelling microscope respectively.

The experimental data was compared directly with the output from the reed switch design program.

Results

The results for the SRA830 switches are shown below:

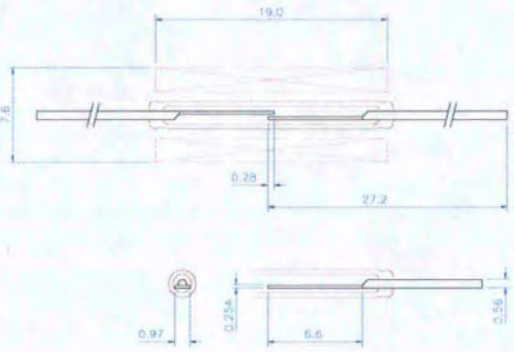

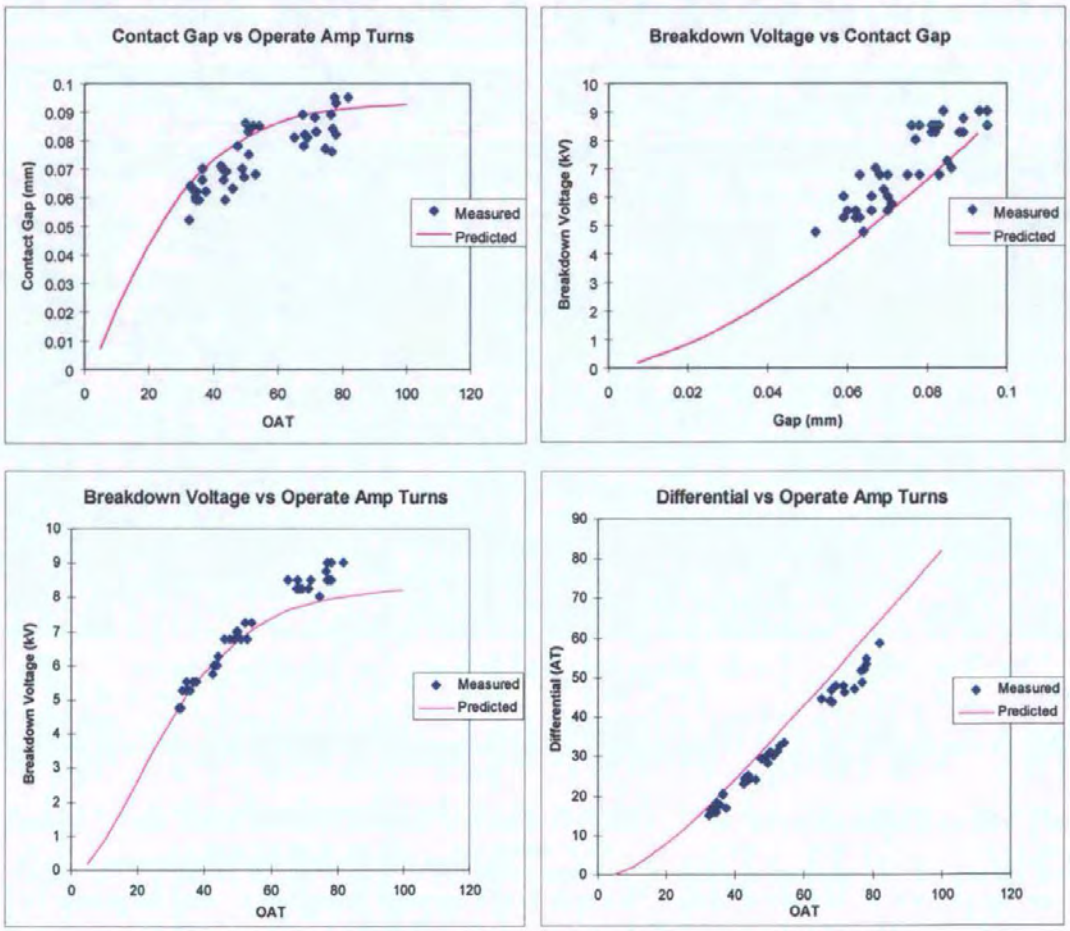

Figure 2.34 – Predicted and Measured Characteristics of SRA830

The results for the SRA831 switches are shown below. It should be noted that the principal difference between the two types of switches is that the SRA831 switch has thicker contact plating (~6μm thick on each contact instead of ~3μm). The two types are, otherwise, mechanically identical. The significance of the plating arrangements on the intended application of SRA830 and SRA831 switches is discussed in section 3.2.4.2. For the purposes of the present analysis the subtle difference between the switch types makes an interesting comparison both between each other and between predicted and measured results.

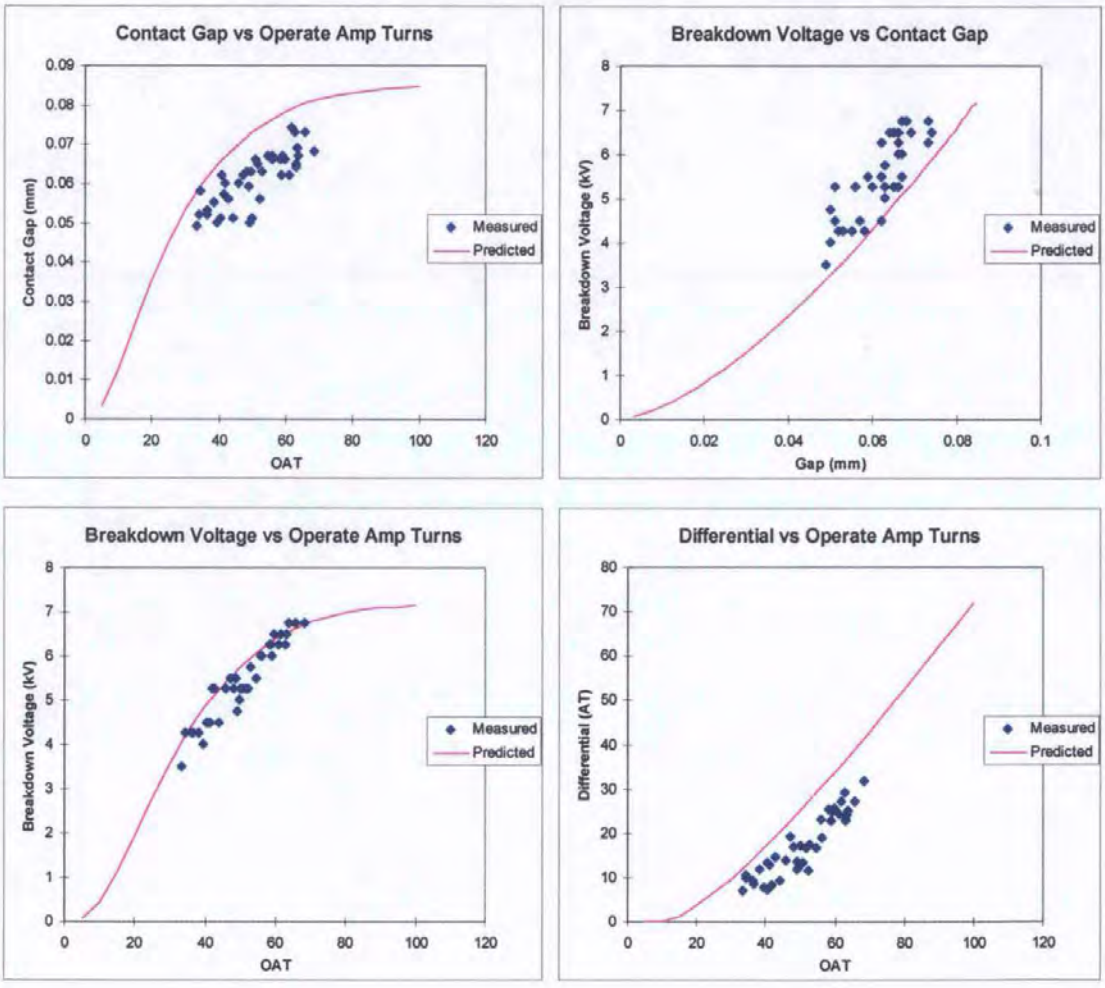

Figure 2.35 – Predicted and Measured Characteristics of SRA831

Discussion of Results

In general, the above figures show a good match between predicted and measured results. In particular the results for contact gap against operate amp turns are well matched as are those for differential against operate amp turns. This would suggest that the magnetic circuit is modelled with reasonable accuracy.

In both cases (SRA830 and SRA831) the differential measured is slightly lower than that predicted. A possible explanation for this is that, in practise, the reed switch contacts will not mate perfectly and so this effectively adds to the magnetic gap when in the closed state. An increase in magnetic gap when closed will, of course, lead to a reduction in contact force and differential. This is also seen when the characteristics for the SRA830 and SRA831 are compared - the differential for an SRA831 (which has thicker contact plating) is ~10AT lower than that for an equivalent SRA830.

The predicted characteristic for breakdown voltage against contact gap is close to that measured although, in both instances, gives values which are slightly lower than those measured. Possible explanations for this are that the electrostatic force of attraction between the reed contacts is slightly lower in practise than that calculated or that the arcing criteria is not absolutely accurate when applied to reed switch contacts. However, when it is borne in mind that reed switch design program is intended to be used as a design aid this slight conservatism is perhaps not a disadvantage.

The slight underestimation of breakdown voltage for a given contact gap is also seen in the results for breakdown voltage against contact gap. The effect is most pronounced with high OAT switches.

2.6.4 Reed Switch Characteristics with Test Coil (TDA832)

Introduction

During the period in which the program was being developed a trial was run involving the production of a batch of "T" size (company terminology for the smallest reed switch they produce) switches with a new blade design. The aim of the exercise was to use the program to design a new blade which would give a higher breakdown voltage (for a given OAT) and which would help alleviate problems with high contact resistance by increasing contact force.

It should be noted that, at this time, the design and prediction work was undertaken with a previous incarnation of the reed switch design program which did not benefit from the finite element analysis described in section 2.2 (it used Cullen's model of the magnetic circuit without modification). As a result a result the improvement in performance expected was not realised.

However, the exercise of comparing batches of "old" and "new" switches has provided a substantial amount of experimental data which is shown here to demonstrate the current reed switch design program as described in the preceding sections.

Method

As with the preceding trials operating characteristics were measured using an "RSC09" test coil, contact dimensions were measured using a travelling microscope and breakdown voltage using a MEGGER FT6/12 Mk2 isolation tester. In addition, as contact resistance was an issue with the "T" switch, an example of the variation in contact resistance with applied AT is also shown. Contact resistance was measured using a Startronic M210 milli-ohmeter at a current of 5mA.

Results

The comparison of experimental and predicted data from the program in its current state is shown below for a batch of "old" TDA832 switches.

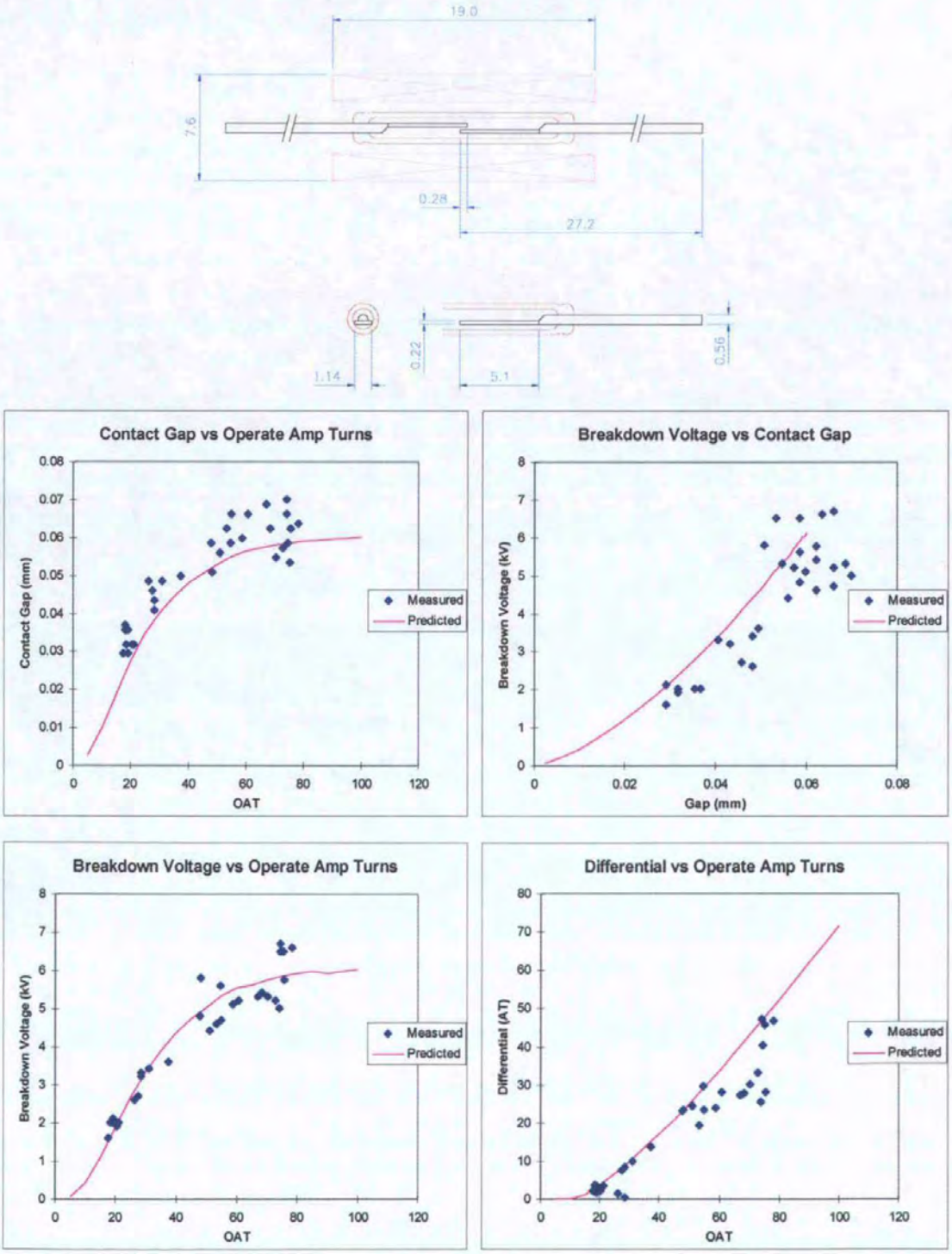

Figure 2.36 – Predicted and Measured Characteristics of TDA832

The comparison of experimental and predicted data from the program in its current state is shown overleaf for the batch of "new" TDA832 switches produced. As can be seen from the accompanying drawing the principal change in the design was the use of a "stepped" blade (that is a blade with two changes in section along its length – the blade is thicker and narrower at its tip than over the main section of the blade). All other parameters, including contact plating, remained constant.

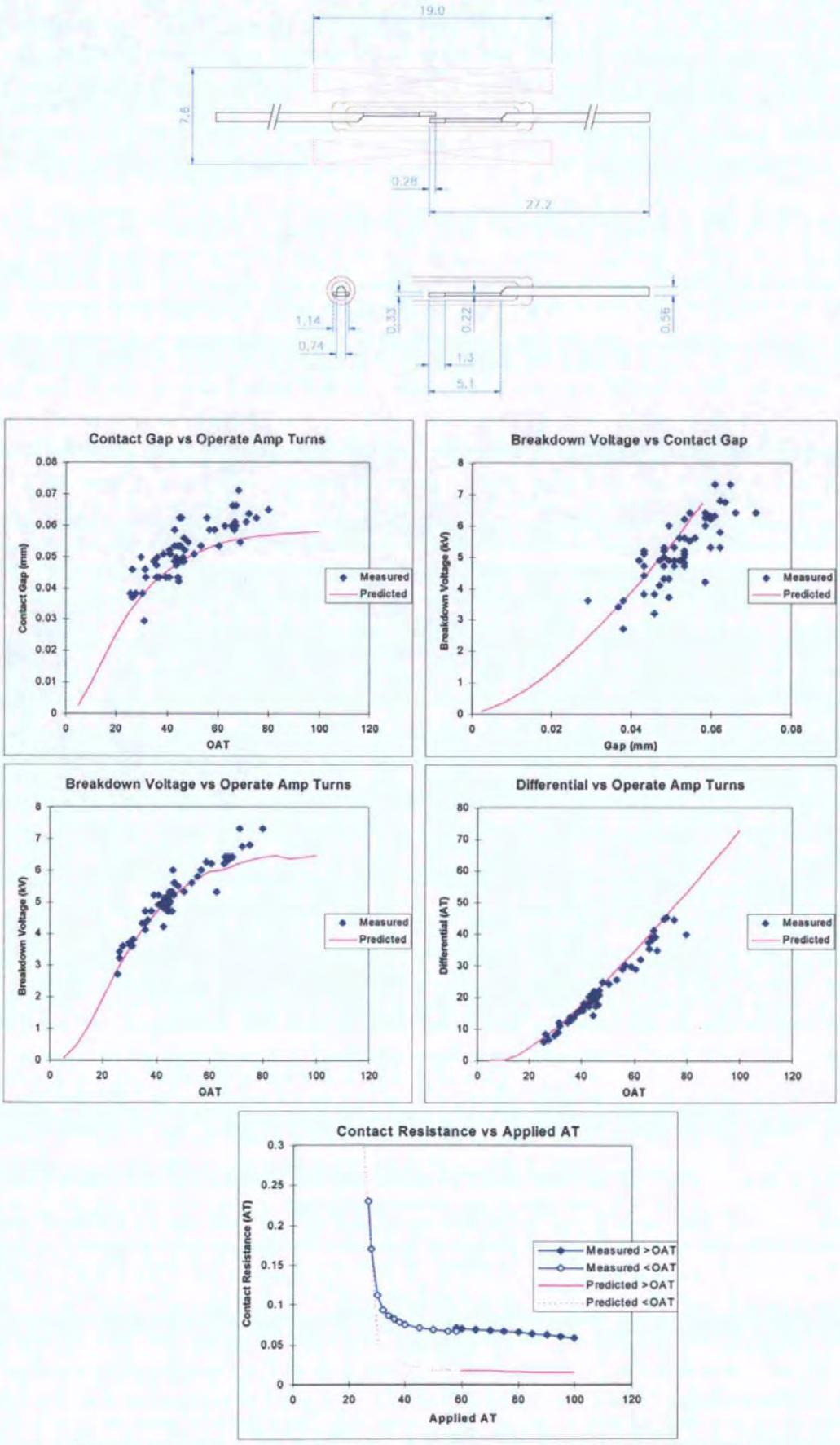

Figure 2.37 – Predicted and Measured Characteristics of "New" TDA832

Discussion of Results

The relationship between predicted and experimental results shown above is very similar to those in the trial with the "S" switches. Again a good match has been obtained for the contact gap against OAT and differential against OAT characteristics which gives further confidence in the accuracy of the model of the magnetic circuit. A good match is also obtained in the results for breakdown voltage against gap and breakdown voltage against OAT although, as in section 2.6.3, the breakdown voltage predicted for high OAT switches is slightly lower than that measured.

Also of note is that the contact resistance against applied AT characteristic showed a good correlation between predicted and measured results. In particular the form of the characteristic was reproduced well. This is useful when designing for "latching" (bistable) reed relays where the contact resistance characteristics below the operate point are of interest. In this instance it is important to ensure that, if the reed switch is expected to carry current, it is not at a point where a small change in contact force leads to a large change in contact resistance.

The above trial also showed that the change in geometry of the reed switch contacts had very little influence on switch performance.

2.6.5 Summary of Reed Switch Design Program

The results from the reed switch design program for the change in operate characteristics with coil and reed dimensions, when applied to an "S" type reed switch, showed good correlation with experimental results.

When used to predict the performance characteristics of SRA830, SRA831 and TDA832 switches in an RSC09 test coil good correlation between predicted and measured results was, again, obtained.

The aim of the present research work was to characterise the link between the geometry of a reed relay and its electrical performance. In the reed switch design program an important step towards this aim has been made.

3. RF LOSS MODEL

Section 3 covers the investigation of eddy current losses occurring in the coil of an RF reed relay. Experimental measurements of these losses were made and a theoretical relationship developed to describe them. This relationship linked coil dimensions, no. of turns and wire size with RF losses. The calculation of the RF losses in a reed relay coil when used in an RF application was then possible.

This information was intended to be used with the electromechanical model presented in the previous section in order to form a tool for the design of RF reed relays.

3.1 Experimental Measurements at RF of Coil Induced Losses at Low and High Power

Introduction

When a high frequency current is passed through the switch of a reed relay some of the energy from this current is dissipated in the coil of the relay. This is as a result of an electromagnetic coupling between the reed switch and coil and is clearly undesirable.

In order to investigate this effect the resistance imposed upon a copper wire (representing a reed switch) by a coil fitted around it was measured at both low and high powers. The frequency of the current in the copper wire was approximately 25.8MHz in both cases and the magnitude, in the high power case, 3.5A RMS. The frequency chosen so as to be close to the relays upper operating limit of 30MHz and, due to limitations of the low power test apparatus (described later), at which both low and high power measurements could be made. The measurements taken at low power allowed resistance to be measured directly. At high power resistance was determined from coil heating.

It was of interest to determine whether the resistance measured at low power was directly related to the temperature rise measured at high power. Also, measurements were taken with coils of different geometries, etc, in order to gain information on the effect of coil parameters on losses measured.

Theory - General

All experiments were undertaken with the reed switch replaced by a length of copper wire and the coils used were of the self bonding type (so that no supporting bobbin was required). This was to eliminate any spurious effects caused by variations in reed switch contacts, bobbin dielectric properties, etc. The ends of the coil winding were left "floating" (i.e. not electrically connected to any other part of the test circuit) as, in a typical application, the RF

and coil drive circuits would be completely separate. In order to gain an appreciation of the influence of coil geometry upon RF losses four "sets" of coils were wound as follows :

Set 1: 4 coils wound with the same sensitivity, wire size, inside diameter and outside diameter. Length, number of turns and resistance were varied.

Name	Length (mm)	ID (mm)	OD (mm)	Wire Size (mm)	No. of Turns	Resistance (Ohms)	Sensitivity (AT/V)
A1	10	6	14	0.1	2727	186	14.6
B1	15	6	14	0.1	4091	280	14.6
C1	20	6	14	0.1	5454	373	14.6
D1	25	6	14	0.1	6818	466	14.6

Set 2: 3 coils wound with the same length, inside and outside diameter. Resistance, number of turns, wire size and sensitivity were varied .

Name	Length (mm)	ID (mm)	OD (mm)	Wire Size (mm)	No. of Turns	Resistance (Ohms)	Sensitivity (AT/V)
A2	20	6	14	0.071	10227	1362	7.4
B2	20	6	14	0.1	5454	373	14.6
C2	20	6	14	0.16	2246	60	37.7

Set 3: 3 coils were wound with the same length, inside diameter and sensitivity. Outside diameter, number of turns, resistance and wire size were varied.

Name	Length (mm)	ID (mm)	OD (mm)	Wire Size (mm)	No. of Turns	Resistance (Ohms)	Sensitivity (AT/V)
A3	20	6	8.8	0.071	3636	365	10.0
B3	20	6	17.7	0.09	9636	962	10.0
C3	20	6	23.2	0.01	11735	1171	10.0

Set 4: 5 coils were wound with the same length, inside diameter and number of turns. Outside diameter, resistance, sensitivity and wire size were varied.

Name	Length (mm)	ID (mm)	OD (mm)	Wire Size (mm)	No. of Turns	Resistance (Ohms)	Sensitivity (AT/V)
A4	20	6	7.2	0.071	4000	415	9.7
B4	20	6	9.2	0.09	4000	284	14.1
C4	20	6	10.8	0.1	4000	240	16.4
D4	20	6	11.8	0.112	4000	210	19.1
E4	20	6	20.2	0.16	4000	140	28.3

Note that the coils were all representative of those which might be fitted to a typical reed relay i.e. they all comprised of many turns of a relatively fine wire.

Theory - Measurements at Low Power

The principal of the measurements taken at low power is to determine the resistive component present in a resonant series LC circuit by looking at the "sharpness" (or "Q") of

its frequency response at resonance. The "sharper" the response (higher "Q") the lower the resistance present in the circuit.

"Q" is measured as :

$$Q = \frac{f_o}{f_u - f_l} \qquad (3.1)$$

where

f_0= resonant frequency

f_u= upper frequency at which the response has half the amplitude of that at resonance

f_l= lower frequency at which the response has half the amplitude of that at resonance

The resistance present in the circuit is given by :

$$R = \frac{1}{2\pi f_o CQ} \qquad (3.2)$$

where

f_0= resonant frequency

C= value of capacitor C

Q= Q from above

The above relationships for Q and R can be found in any electrical engineering text. The resistance of interest is that created by the presence of the coil. As a component of resistance is present in all the elements of the LC circuit used measurements were taken with and without the coil fitted so that the components which were not of interest could be eliminated.

Apparatus – Low Power Measurements

For the experimental measurements a series LC circuit with "loosely coupled" input (from a Marconi 2031 signal generator) and output (to a Boonton 92E RF millivoltmeter) was constructed (see figure 3.1 below). Care was taken in the selection of the components and

design of the circuit board in order to maximise its "Q". As the inductor (L) is fixed the frequency at which measurements are taken is set by changing the capacitor (C). The inductor was mounted at 90° to the test coil in order to eliminate any coupling between them.

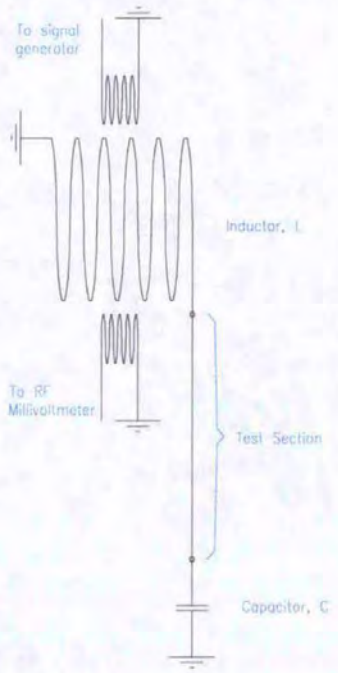

Figure 3.1 – Circuit for Low Power Measurements

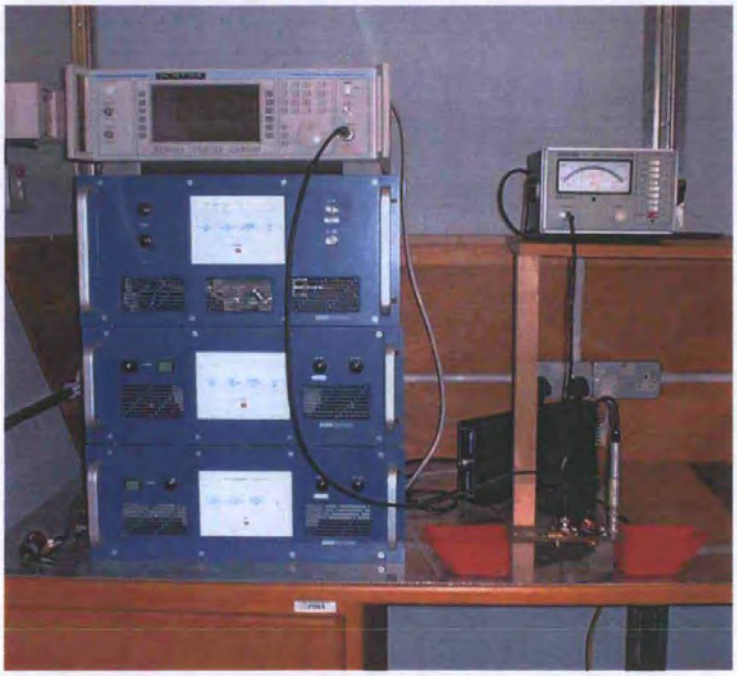

Figure 3.2 – Signal Generator, RF Millivoltmeter and Test Fixture

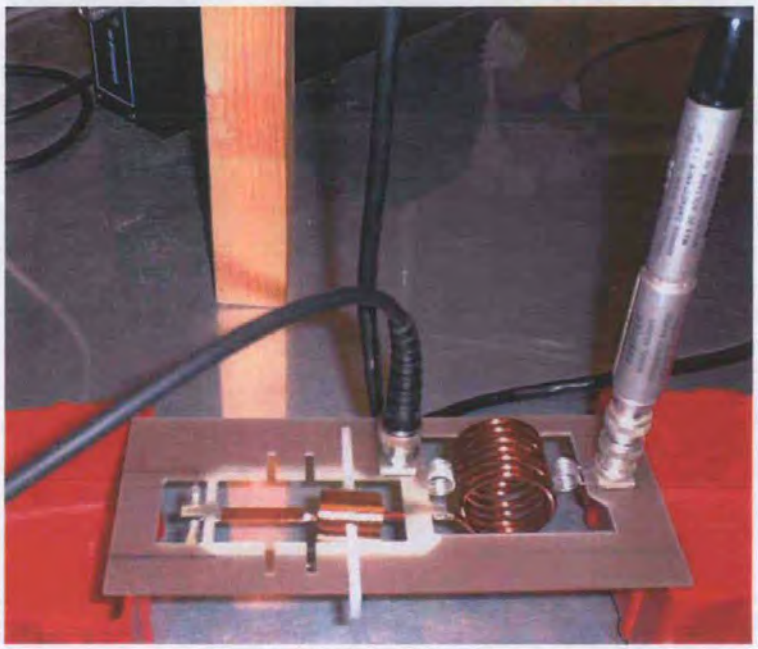

Figure 3.3 – Test Fixture

Figures 3.2 and 3.3 show photographs of the general arrangement of the test apparatus and detail of the test fixture respectively. Of note in figure 3.2 is that the test fixture is mounted above the ground plane on the bench. The power amplifier on which the signal generator is siting is not used in this experiment. In figure 3.3 the "loosely coupled" and main inductor coils can be seen to be at 90° to that of the coil under test. The coil under test is supported on its outside diameter using insulating "V" shaped mounts. The coil is of the "self bonding" type and no supporting bobbin is present.

Procedure – Low Power Measurements

Initially measurements were taken at approximately 5MHz, 10MHz and 25MHz. In these cases the resonant frequency of the circuit was altered by changing the value of the capacitor only. However, as the resistance measured was found to rise with frequency (so that experimental error would be proportionally smaller) and as the high power test equipment available was tuned to frequencies close to 30MHz all subsequent measurements were taken at the highest frequency (actually 25.8MHz). This made it possible to take high and low power measurements at the same frequency.

Each measurement was repeated three times to improve the accuracy of the readings.

Theory - Measurements at High Power

The principal behind the high power measurements was simply to measure the heating of the coils with an RF current in a conductor passing through them and relate this to the power dissipated in the coil. From this power and the magnitude of the current the effective resistance presented by the coil to the current flowing in the conductor could be calculated from

$$R = \frac{P}{I^2} \qquad (3.3)$$

where P = power dissipated in the coil

I = RF current in the conductor

The resistivity of copper changes with temperature. Using this characteristic coil heating was determined from its change in resistance according to the following relationship

$$T_2 = \frac{R_2}{R_1}(234.5 + T_1) - 234.5 \qquad (3.4)$$

where :

T_2= final temperature (°C)

T_1= initial temperature (°C)

R_2= final resistance (Ω)

R_1= initial resistance (Ω)

This relationship is a standard used in the coil winding industry and may be found in (30) amongst others. To relate coil heating to the power dissipated in it requires the power vs. temperature characteristic for each of the coils to be known. This was determined by applying a range of DC voltages to them and measuring the steady state current drawn in

each case. The coil resistance, and therefore heating (using the relationship above), was determined directly from Ohm's law.

Apparatus – High Power Measurements

Measurements at high power were undertaken at the same frequency as the low power measurements above (25.8MHz) using a Marconi 2031 signal generator, BNOS RF power amplifier and 36:1 transformer. Figure 3.4 below shows the general arrangement.

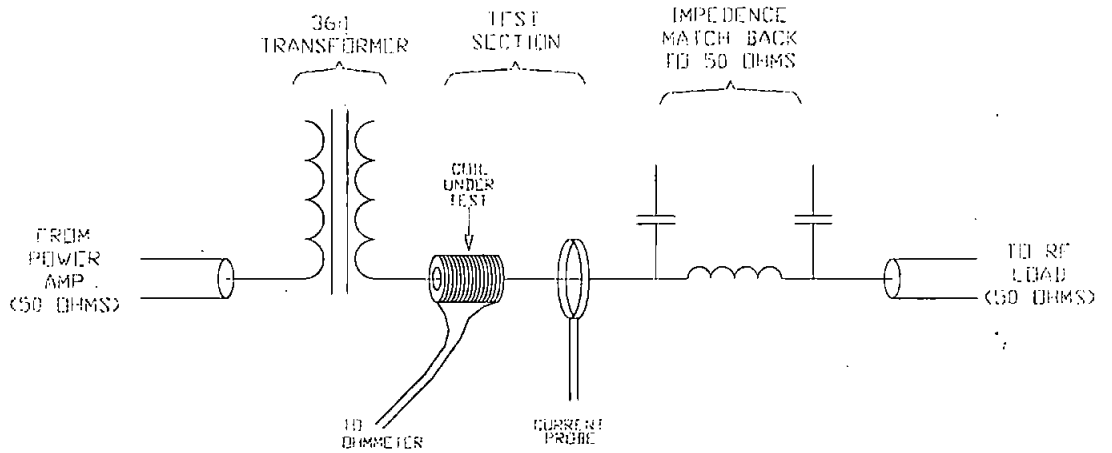

Figure 3.4 – Circuit for High Power Measurements

The current in the test section was measured using a Tektronix P6021 current probe and 60MHz Hameg oscilloscope. Coil resistance and ambient temperature were measured using a Racal-Dana 4008 digital multimeter and RS components digital thermometer respectively.

Figures 3.5 and 3.6 show the general arrangement of the high power test apparatus and detail of the test fixture (which includes the current transformer and impedance matching components) respectively.

Figure 3.5 – Apparatus for High Power Measurements

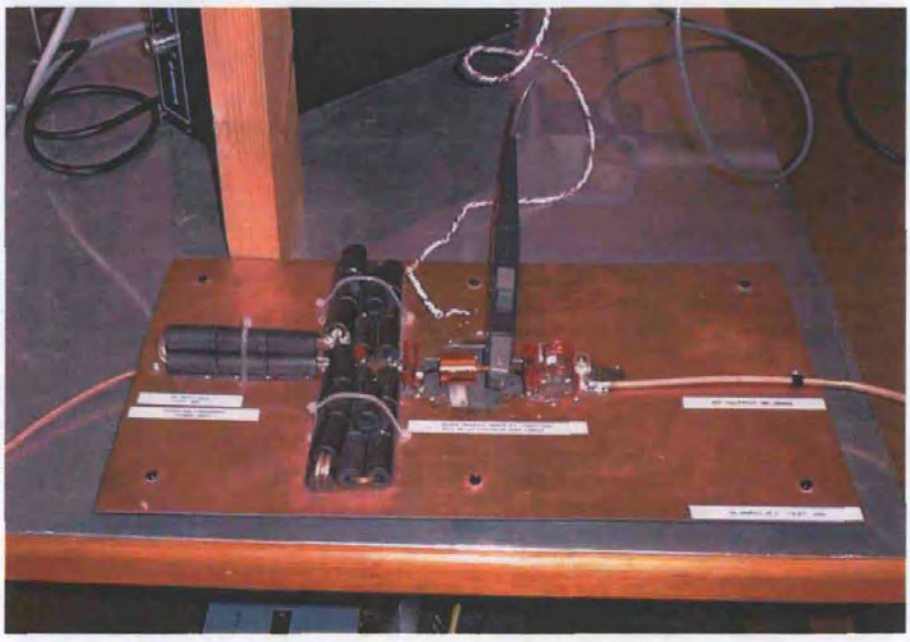

Figure 3.6 – Current Transformer used in High Power Measurements

Procedure – High Power Measurements

In order to measure RF heating the resistance of the coil under test was measured as the RF current in the test section was varied from 0-3.5A RMS. A delay of at least 15 minutes between measurements was made to allow for the coil to reach a steady state temperature.

Ambient temperature was recorded on each occasion so that only RF heating was recorded (i.e. any change in ambient temperature over the duration of the test was not allowed to influence the results).

In a separate test the power against heating characteristic was determined for each of the coils by applying a range of DC voltages across their terminals and measuring the steady state current drawn. Again a delay of at least 15 minutes was made between each measurement and the ambient temperature recorded in each instance so that the influence of any change over the test period could be eliminated. A cubic spline was fitted to the experimental data in order to give the power against heating characteristic for each coil.

The effective resistance presented to the RF current in the conductor was then calculated from the RF heating and the power vs. heating characteristic for that coil.

Results

The increase in RF resistance of a conductor caused by the presence of the coil placed around it (measured at low and high powers) were as in the figures below for each of the four sets of coils.

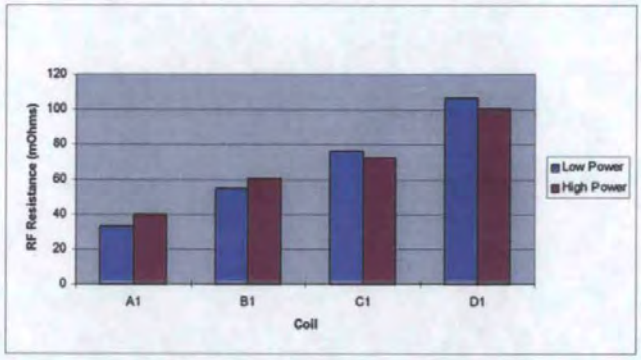

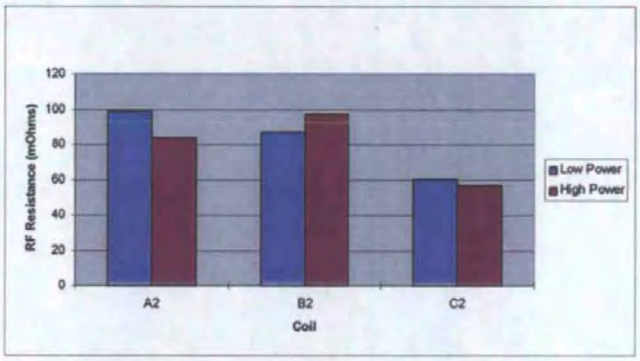

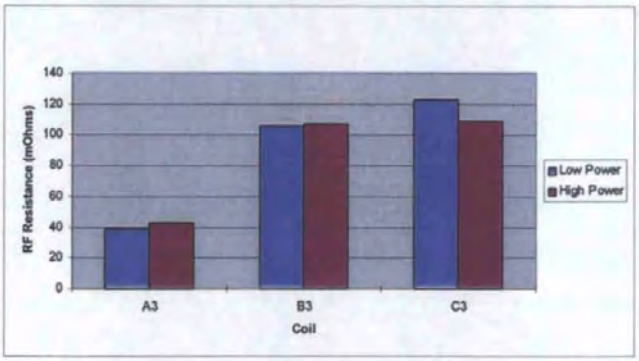

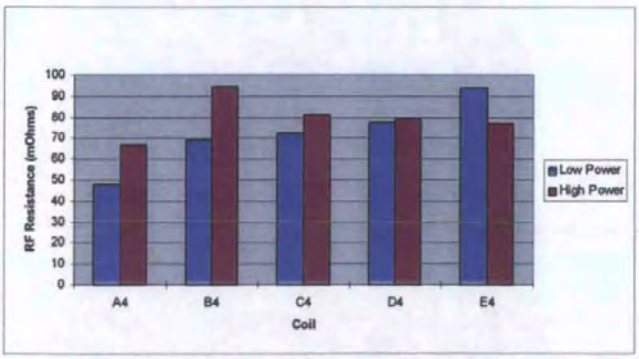

Figure 3.7 – RF Resistance Measured at Low and High Power for Coil Sets 1-4

For the measurements undertaken at high power the power dissipated in the coil was found to be roughly proportional to RF current squared in each case (as would be expected if there was little change in the RF resistance as current was increased). An example of this is shown below :

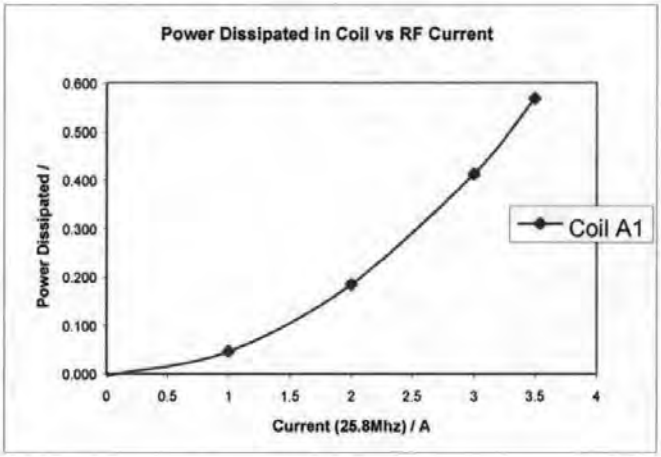

Figure 3.8 – Power Dissipated vs. RF Current for Coil A1

Errors – Low Power Measurements

Experimental errors arising from the electronic equipment used in the low power measurements are minimal as it is relative measurements which were taken – the only source of error in this instance is in the linearity of the RF millivoltmeter and signal generator. The RF millivoltmeter was calibrated to an accuracy of ±1% full scale deflection and a reading error would be additional to this. There was no reading error associated with the signal generator as it is equipped with a digital read-out.

As the readings with each coil were repeated three times (without dismantling the circuit in between) the reading error, combined with any thermal "settling" of the circuit (inevitable as test components were soldered in), is shown in the variation in these readings. The maximum variation in these readings was 10% (for the coil presenting the lowest resistance to the current in the conductor) and <5% was typical. This good repeatability is in part due to the high "Q" of the circuit ("Q" of between 330 and 400 was obtained depending upon the coil

under test). A high "Q" gives a "sharp" response around resonance so that the RF voltage measured on the output of the test circuit changes rapidly with frequency. This makes it easy to identify the frequency at the required test points.

However, when measurements were repeated and the test circuit was dismantled between readings greater variations were observed. Possible reasons for this include a change in capacitor characteristic with the heat of soldering (it was mounted very close to a joint which was re-made every time the coil under test was changed), the effect of the proximity of miscellaneous items to the test circuit (it was noted that, despite the test circuit being mounted at a fixed height above a ground plane, a hand held over it could change the output reading considerably) and changes in ambient temperature (which was not recorded for these measurements). The true extent of these errors is difficult to determine. The maximum variation between repeated RF resistance measurements of this type corresponded to 14%. In this instance the reading/settling error as discussed above was 5% and 2% for the two measurements. The ambient temperature could have varied anywhere between 20°C and 30°C. If the change in resistance with temperature for the circuit is assumed to be due to the copper components in it this corresponds to a maximum 4% error. This leaves at least 3% of the 14% noted above unaccounted for. It is thought that, in reality, the unaccounted error is greater than this and an overall error of 30% (±15%) on the RF resistance measured is suggested as a realistic worst case.

Errors – High Power Measurements

The errors involved in the measurement of RF coil heating stem principally from the oscilloscope (±5%) and current probe (±3%). As it has been shown that RF heating is proportional to RF current squared this results in a ±16% error in RF heating measured.

In addition to this are errors in coil resistance and ambient temperature measurement. The multimeter used was accurate to ±1% and the thermometer to ±0.1°C. In reality, to account for the fact that temperature was not measured at the exact location of the coil, a true accuracy of temperature of ±1°C is more likely. Relative to absolute zero this gives an error of approximately ±0.3%.

The overall error for the RF heating measured for a given RF current is then ±17.3%.

When determining the power vs. heating relationship for the coils under test current and voltage were both measured to an accuracy of ±1%. This gives a potential ±2% error on the power and resistance (from which heating was determined) calculated. As before an error on the ambient temperature of ±0.3% was considered reasonable. This gives a combined error of ±4.3%.

The overall error limits on the RF resistance calculated from RF heating is then ±20.6%. However, looking at results where measurements had been re-taken, very good repeatability (within 5%) was obtained. It is surmised from this that, although the potential errors are quite large, they remain largely fixed and therefore allow accurate repetition. This is in contrast to the low power measurements where, although the accounted error is relatively small, accurate repetition is difficult.

Discussion of Results

The good correlation between the above results suggests that the RF resistance measured at low power is directly related to the temperature rise of the coil measured at high power. Also, the power dissipated in the coil is roughly proportional to RF current squared indicating no significant change in resistance as current was increased (in fact, a relationship slightly steeper than a pure square law is observed as the resistance of the loss inducing elements will

increase with temperature). This lends further support to the argument that there is a direct relationship between the losses measured using the low and high power techniques. Furthermore, RF losses (whether expressed as an effective resistance or heating) are dependent upon the dimensions and details of the coil winding. This is an important point given the overall research aim of finding a link between relay performance and relay geometry.

It should be noted that experimental error in the experiments (as discussed above) was appreciable and more than accounts for the discrepancy between low and high power results.

It was found that the high power measurements were much less susceptible to outside interference and were more easily repeated. For this reason further measurements in the following sections were taken using the high power technique.

Conclusion

A coil fitted around a conductor carrying a high frequency current was found to increase the resistance of the conductor. This resistance, measured at low power, was found to correspond to the resistance deduced from coil heating measured at high power. Coil geometry and other parameters (winding wire diameter, etc) were found to influence this resistance.

The link between coil geometry and RF losses is key to the thrust of the present research (to create a design tool to allow the proportions of RF reed relays to be optimised for minimum losses) and the aim of the following section was to find a relationship between the two.

3.2 Eddy Current Analysis

3.2.1 Initial Analysis

Introduction

In the previous section the RF resistance imposed on a conductor by a coil wound around it was measured with coils of various geometries, wire sizes, etc. This showed that there was a link between coil geometry and RF resistance and therefore that RF losses in a reed relay were influenced by the geometry of its coil. This was clearly important to the present work and a relationship to describe the link was sought as below.

Analysis

From the outset an electromagnetic coupling between conductor and coil was assumed. The magnetic field strength at a distance, r, from a long, straight conductor is given by:

$$H = \frac{I_{RF}}{2 \cdot \pi \cdot r} \quad \text{(A/m)} \quad (3.5)$$

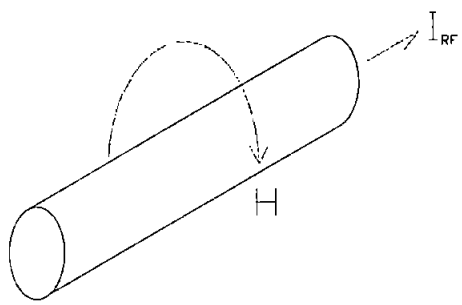

Figure 3.9 – Magnetic Field Around a Conductor

The eddy current occurring in a single turn of wire, of circumferential length l and winding radius r, around the central conductor is then:

$$I_{eddy} = H \cdot l$$

$$I_{eddy} = \frac{I_{RF}}{2 \cdot \pi \cdot r} \cdot 2 \cdot \pi \cdot r = I_{RF} \quad (3.6)$$

The eddy current induced on the surface of the wire is therefore equal to the RF current in the conductor. The resistance presented to the eddy current is effectively a resistance presented to the RF current in the conductor.

Losses occurring due to the eddy current are dependent upon the resistance presented to it. The eddy current will naturally have the same frequency as the RF current and can be considered to flow within the skin depth, δ. Skin depth can be calculated from the following relationship which can be found in any electrical engineering text.

$$\delta = \frac{1}{\sqrt{\pi \cdot f \cdot \mu \cdot \sigma}} \qquad (3.7)$$

where

f=frequency

μ=permeability

σ=conductivity

For a single turn of wire, of radius r, around the conductor the eddy current will flow in the area indicated in the diagram below:

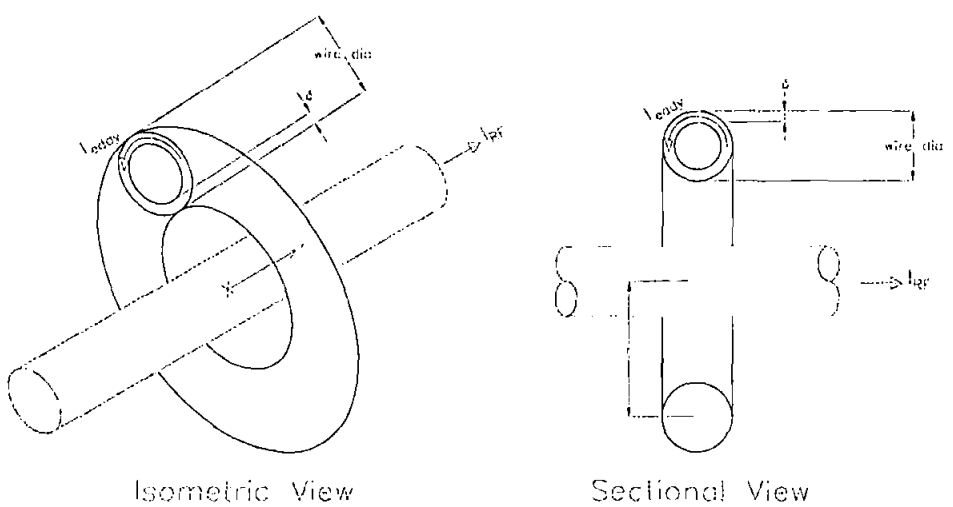

Figure 3.10 – Eddy Current Skin Depth in a Single Turn Around a Conductor

The cross sectional area of this is :

$$A_{eddy} = 2 \cdot \pi \cdot r \cdot \delta \qquad (3.8)$$

The resistance presented to the eddy current is then :

$$R_{eddy} = \frac{\rho}{A_{eddy}} \cdot l = \frac{\rho}{2 \cdot \pi \cdot r \cdot \delta} \cdot \pi \cdot dia_{wire} = \frac{\rho}{2 \cdot r \cdot \delta} \cdot dia_{wire} \qquad (3.9)$$

For a cylindrical coil around a conductor with N turns :

$$R_{eddy} = \frac{\rho}{2 \cdot \delta} \cdot dia_{wire} \cdot N \cdot \overline{\left(\frac{1}{r}\right)} \qquad (3.10)$$

where $\overline{\left(\frac{1}{r}\right)} = \frac{1}{r_2 - r_1} \cdot \ln\left(\frac{r_2}{r_1}\right)$ (3.11)

which is the mean value of $\frac{1}{r}$ for the turns in the coil. The derivation of this relationship may be found in appendix 9.

3.2.2 Influence of Coil Winding Wire Diameter on RF Losses

Introduction

The above relationship (equation 3.9) yielded a good match with the experimental results in section 3.1. However, further experimental work related to a product development project at Crydom (involving measuring RF losses in coils filling the same cross sectional area but with different winding wire diameters) showed a discrepancy between predicted and measured results for coils with small winding wire diameters (0.05mm and below).

Revisiting the above relationship showed that, at the frequency of interest (30MHz) the skin depth was not greatly smaller than the diameter of the winding wire. This prompted a more thorough analysis of the eddy current in the winding wire as below.

Analysis

In a normal conductor high frequency currents are modelled as flowing entirely within a skin depth, delta. This is a convenient approximation but, in fact, re-course to any electrical engineering text will show that the current density, J, follows an exponential relationship with thickness in the conductor as follows:

$$J = J_0 \cdot e^{-k \cdot z} \quad (3.12)$$

where $k = \sqrt{\pi \cdot f \cdot \mu \cdot \sigma}$

z=depth

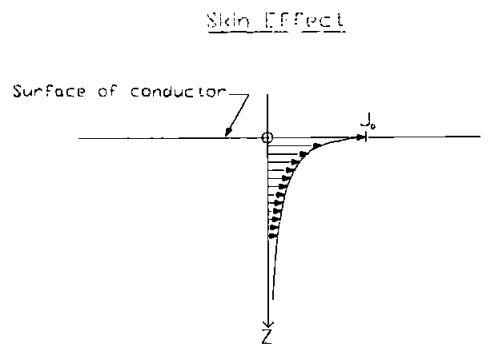

Figure 3.11 – Skin Effect in a Conductor

In the case of the eddy current in the winding wire the situation is as below :

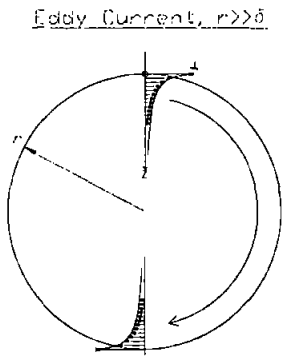

Figure 3.12 – Skin Depth of an Eddy Current in a Winding Wire

When the diameter of the winding wire, about which the eddy current is flowing, is small it is proposed that there is a tendency for the eddy current to be party self cancelling as indicated below:

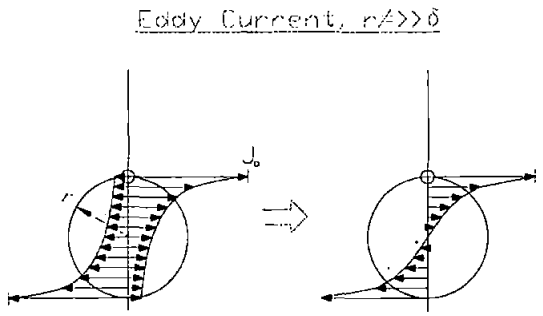

Figure 3.13 – Eddy Current "Self Cancelling" when Wire Diameter ≠<<Skin Depth

The resultant eddy current is then :

$$I = \frac{I_{eddy}}{\delta} \cdot \left(\frac{-2}{k} \cdot e^{-k \cdot r} + \frac{1 + e^{-2 \cdot k \cdot r}}{k} \right)$$

The effect on the apparent eddy current resistance is that it reduces in proportion to the change in current squared. It is convenient to express this as a factor applied to the result derived in 3.2. This factor, F_{wire}, is :

$$F_{wire} = \left[k \cdot \left(\frac{-2}{k} \cdot e^{-k \cdot r} + \frac{1 + e^{-2 \cdot k \cdot r}}{k} \right) \right]^2$$

This result, the derivation of which is shown in appendix 9, was applied to the experimental work described overleaf.

Experimental Procedure

A series of coils was wound on a common bobbin with a range of winding wire diameters from 0.032mm to 0.16mm such that the outside diameter and cross sectional area of the coils were constant. The dimensions of the coils were:

Inside diameter	4.8mm
Outside diameter	8.0mm
Length	8.4mm

Clearly the number of turns of wire was altered to achieve this. The table below shows the winding details for each:

Wire Diameter (mm)	No. of Turns	Resistance (Ohms)
0.032	8400	3600
0.036	6900	2330
0.04	5400	1470
0.045	4350	950
0.05	3500	620
0.056	2800	390
0.063	2200	240
0.071	1720	150
0.08	1400	96
0.09	1100	60
0.10	900	40
0.112	750	26
0.125	610	17
0.14	500	11
0.16	380	6.5

The RF resistance associated with each coil was measured using the "high power" technique described in 3.1. The coils were each mounted around a copper conductor through which 3A at 30MHz was passed. RF heating was measured via the change in coil resistance. A subsequent experiment to determine the coil temperature against power dissipated characteristic allowed the power associated with the RF heating to be calculated. This, divided by the square of the RF current, yielded the RF resistance.

Results

The following experimental results were obtained with the coils and "high power" measurement technique as described above. They are compared with the RF resistance calculated using the relationship described above (which takes into account the effect of eddy currents in small diameter winding wire) and, for illustrative purposes only, the relationship as described in 3.2.1 (which does not).

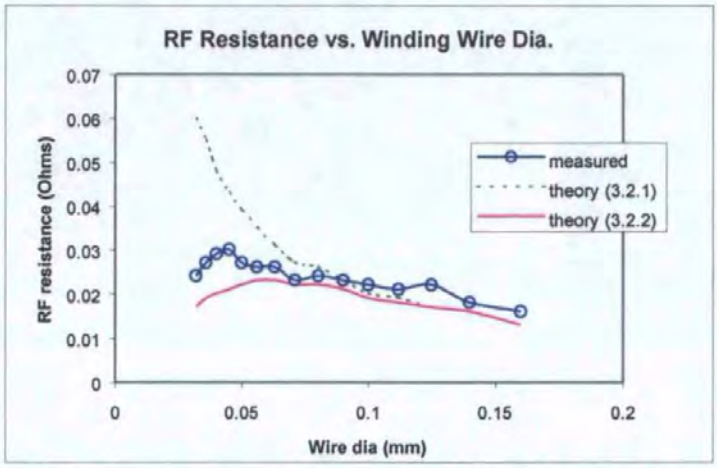

Figure 3.14 – RF Resistance vs. Winding Wire Dia with a Copper Conductor

Discussion of Results

The results show that the relationship derived above provides a more accurate means of predicting the losses induced in a coil from its winding and geometry when mounted around a conductor carrying a high frequency current.

The accuracy of the above relationship (equation 3.9 with the correction factor for winding wire diameter, equation 3.14, added), when applied to the four sets of coils used in section 3.1, is shown in appendix 6.

Experimental errors for the "high power" technique are as described in section 3.1.

3.2.3 The Influence of the Reed Switch on RF Losses

Introduction

It was noticed that in trials similar to 3.2.2, except with reed switches rather than a simple copper conductor, that the losses measured (i.e. coil heating) were greater than expected. Results from these trials are presented below.

Method

Using the set of coils as described in 3.2.2 (with the same dimensions but with winding wire diameters ranging from 0.032mm to 0.16mm) RF heating of the coils, when mounted around an SRA831 type switch carrying 3A at 30MHz, was measured for each coil by monitoring the change in their resistance.

Results

The results of the trial are shown below along with those for coil heating when mounted around a copper conductor.

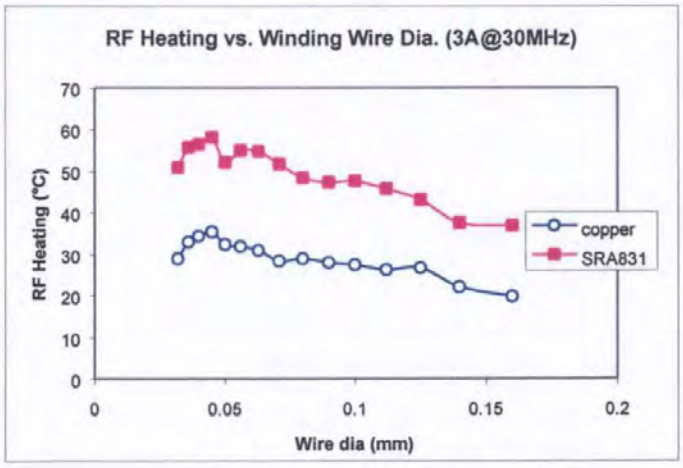

Figure 3.15 – RF Coil Heating vs. Winding Wire Dia for Copper and SRA831

Discussion of Results

Experimental errors are, again, as those for the "High Power" technique described in section 3.1. An illustration of the repeatability of the above measurements is shown in appendix 7.

The above results show a substantial increase in RF heating with the SRA831 switch, rather than a copper conductor, fitted. It should be noted that the SRA831 reed switch has copper plated reed blades to improve its current carrying performance. However, the thickness of this plating in the contact area is only 3μm (12μm elsewhere on the blade) and, as the skin depth at 30MHz is greater than this (12μm), it is almost certain that some current will flow in the NiFe part of the blades. Because of the ferromagnetic nature of the NiFe the "skin effect", and therefore resistive losses, will be much greater in the reed switch than in a solid copper conductor. This will result in the reeds becoming hotter than a solid copper conductor for a given carry current. It is possible that this heating of the reeds is transferred to the coil around it giving the results shown.

A further possibility was that heat could be transferred from the reeds to the coil by means of radiation from the contact point. Due to the small size of the reed contacts, and their being the most resistive part of the switch, high temperatures at the contact point are possible.

The above mechanisms were investigated in the following sections.

3.2.4 The Effect of a Ferromagnetic Conductor on RF Coil Heating

Introduction

As already described it was thought that the more resistive nature of a ferromagnetic conductor passing through a coil could influence the RF losses (heating) occurring in it. In order to investigate this two trials were undertaken.

In the first RF heating was measured with a coil fitted around a NiFe conductor, copper plated NiFe conductors and a solid copper conductor.

In the second trial the RF resistance each of the set of coils used in section 3.2.3 was measured when fitted around a NiFe conductor and the results compared to the same measurement taken with solid copper, SRA831 and SRA830 reed switches.

3.2.4.1 RF Losses with NiFe, Copper Plated NiFe and Solid Copper Conductors

The RF heating of a coil when mounted around conductors of different materials was measured. These materials were:

Bare NiFe wire (1.3mm diameter)

1.3mm NiFe wire with 10μm copper plating

1.3mm NiFe wire with 20μm copper plating

1.3mm NiFe wire with 40μm copper plating

Solid copper wire (2.3mm diameter)

Coil heating was measured as a function of RF current for each of the above conductors. The coil used for the experiment was C1 as described in section 3.1. The frequency of the current passed through the conductor was 30MHz.

Results

The results for RF coil heating against current for each of the conductors are shown below

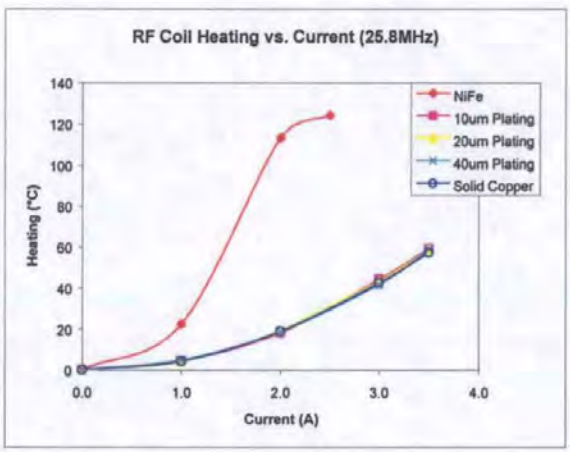

Figure 3.16 – RF Coil Heating with NiFe, Copper Plated NiFe & Copper Conductors

Discussion of Results

The results show that the heating of the coil recorded in the coil with a NiFe conductor passing through it is several times greater than that with a copper conductor. Also, the heating characteristic with the NiFe conductor does not follow a rough proportionality with the square of the current as that with the copper conductor does. Instead a characteristic similar to saturation is observed. A likely explanation for this is that, because the resistive losses in the NiFe conductor are very much greater than in copper, substantial heating of the NiFe was occurring and this was absorbed by the surrounding coil. The resistive losses in NiFe are much greater than those in copper at high frequencies as it has a lower conductivity and the skin depth, which is dependent upon magnetic permeability (see equation 3.7), is much smaller. The permeability of NiFe drops with increasing temperature and so as the

current in the NiFe conductor is increased, and its temperature rises accordingly, its permeability drops and the skin depth starts to increase. This would lead to a reduction in the resistance of the conductor and the levelling of coil heating against current characteristic seen with the NiFe conductor.

The results for the three copper plated conductors are all virtually identical to that of the solid copper conductor. This is surprising as the skin depth at 30MHz is 12μm - thicker than the plating thickness on one of the conductors. Also, as the skin depth is the depth above which ~2/3 of the current is flowing, and not the depth in which all the current is flowing, it might be expected that a small but significant proportion of the current would flow within the NiFe rather than the copper plate. However, the results suggest otherwise. It is possible that, as the NiFe is considerably more resistive than the copper plating, current flows almost entirely in the copper plating regardless of the skin depth expected. This being the case the cross sectional area of copper over the NiFe would become the significant factor. It should be noted that the cross sectional area of copper on the 10μm plated conductor (at 1.3mm diameter) is substantially more than that on an SRA831 reed blade (0.56mm diameter).

3.2.4.2 RF Resistance of Coils with a Solid NiFe Conductor

The second trial entailed measuring the RF heating of each of a set of coils, as those used in 3.2.3, when fitted around a 1.3mm NiFe wire, an SRA830 type reed switch and an SRA831 switch.

The significance of including the two switch types is that they are identical except for the copper plating on their blades. The SRA831 switch has nominally 3μm of rhodium sputtered on top of 3μm of copper on each contact. The rhodium is present only on the contact face and, to a lesser extent, the sides of the reed blade but the copper plating is present on all sides

of the reed blade. The SRA830 switch has only 3μm rhodium on the contact face and no copper. Both switch types have the same quantity (12μm) of copper plating on the reed blades away from the contact area. The difference stems from the application of the two switch types - the SRA830 has a minimal thickness of material on the contact in order to maximise the contact gap, and therefore breakdown voltage (for high voltage applications), and increase differential (for latching relay applications) whereas the SRA831 has additional copper plating to enhance current carrying performance (the SRA831 is rated at 3A carry at 30MHz whereas the SRA830 is rated at only 1.5A). The difference in differential and voltage breakdown characteristics can be seen by referring back to section 2.6.3 where test results, and accompanying explanation, are given for both switch types.

The coils, as already described in section 3.2.3, all had the same dimensions (inside diameter 4.8mm, outside diameter 8.0mm, length 8.4mm) but were wound with wire varying from 0.032 to 0.16mm diameter.

A current of 1A was passed through the NiFe wire (to avoid saturation – as suggested by the results in figure 3.16), and maximum rated currents of 1.5A and 3.0A through the SRA830 and SRA831 respectively. In all cases the frequency of the current was 30MHz and the RF resistance was determined using the "high power" technique described in section 3.1.

Results

The results for the RF resistance of the coils when fitted around the NiFe wire, SRA830 and SRA831 are shown below compared to those when fitted around a copper wire.

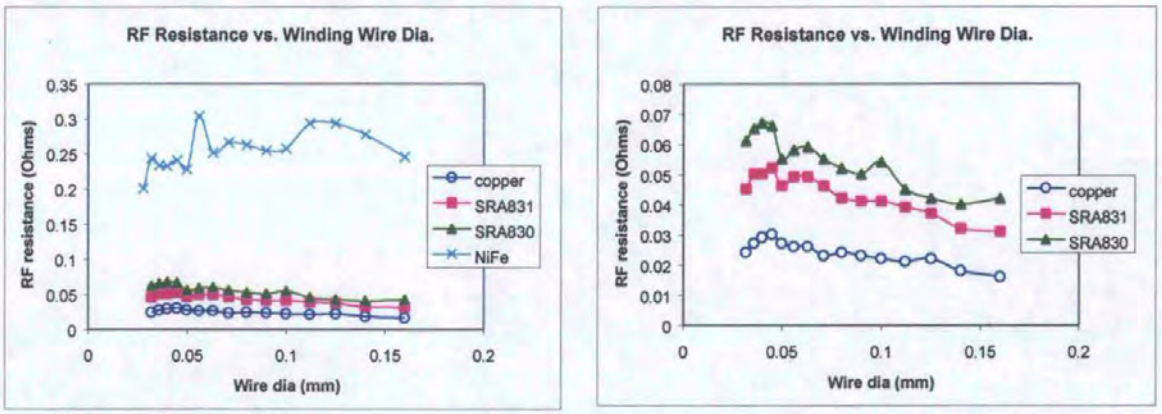

Figure 3.17 – RF Resistance vs. Winding Wire Dia for Copper, SRA831, SRA830 & NiFe

When expressed as a "loss factor" where:

$$F_{loss} = \frac{loss_{conductor}}{loss_{copper}} \qquad (3.15)$$

the results are as below

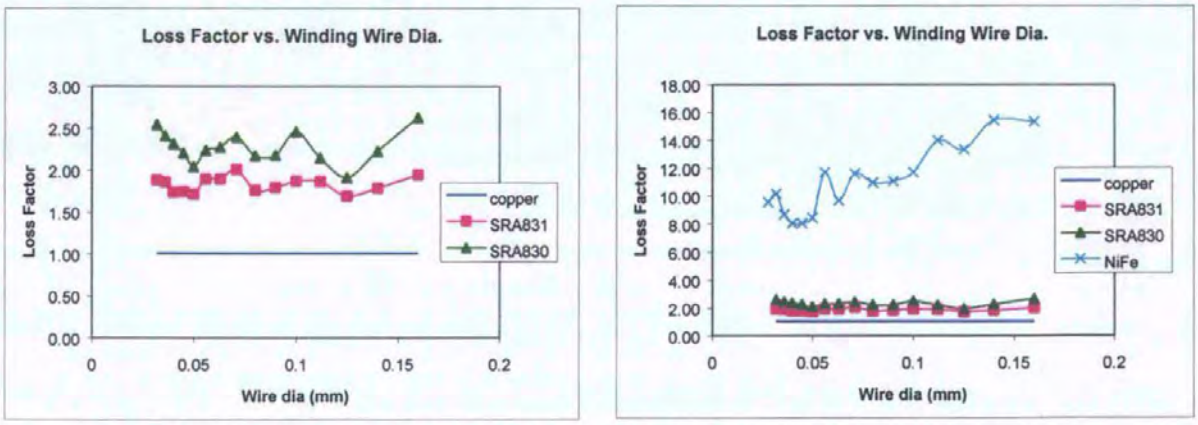

Figure 3.18 – Loss Factor vs. Winding Wire Dia for Copper, SRA831, SRA830 & NiFe

Discussion of Results

The above shows, again, that the presence of a ferromagnetic conductor passing through a coil will dramatically increase the RF power dissipated in it. The RF losses of the coils with a

NiFe conductor varies between 8 and 16 times that with a copper conductor. Again it is probable that losses within the conductor itself (due to the skin effect as already discussed in section 3.2.4.1) result in heating which is absorbed by the surrounding coil.

The losses measured with the two reed switch types are also significantly greater than that measured with a copper conductor. The "loss factor" is seen to be largely constant across the range of coils tested for each of the switch types at ~1.8 and ~2.3 for the SRA830 and SRA831 respectively. The "loss factor" for the SRA830 is greater than that for the SRA831 and this can be attributed to the lack of copper plating in the vicinity of the contacts on the SRA830. It is not clear whether the increased loss induced by the reed switches (when compared to a copper conductor) is due entirely to the reduced, or absent, copper plating in the contact area or whether some current flows in the NiFe core of the reed blades throughout their length (note that the copper plating is thinner in the contact area than over the rest of the blades). However, it is clear that RF coil heating is influenced by the ferromagnetic properties of the reed blade material and that both SRA830 and SRA831 switches would benefit considerably from more copper plating on the reed blades in order to reduce RF coil heating. Also, as the permeability of ferromagnetic materials generally decrease with frequency, another possible means of reducing RF coil losses might be to manufacture reed blades from a material whose permeability dropped to unity over the frequency range of interest (in this case 1-30MHz). It is likely that heating of the reed blades when carrying a high frequency current is transferred to the surrounding coil as with the NiFe conductor. A possible mechanism of this heat transfer (radiation) is investigated in 3.2.5.

The "loss factor" with the NiFe conductor varies across the range of coils tested. A possible explanation for this is that, if the heat transferred from the NiFe conductor to each coil was constant for any given current (as would be expected) this would have a proportionally larger influence on coils which would normally display a relatively low loss (heating). This theory

is in agreement with the results which show the "loss factor" to be at a maximum with coils with the greatest winding wire diameters tested.

The above highlights several areas for further work with a view to reducing the RF heating induced by reed switches and deriving a means by which "loss factor" can be determined by calculation. However, for the purposes of the present work, a "loss factor" determined by experiment is used in calculations for the RF resistance of a reed relay coil.

3.2.5 Effect of Radiated Heat from Reed Switch Contacts on RF Coil Heating

Introduction

A mechanism by which the RF coil heating measured with reed switches might be greater than that with a copper conductor was that of heat radiated from the reed switch contacts. The aim of the following experiment was to determine whether this mechanism had a significant effect.

Method

The RF heating of a coil mounted around a switch was measured with and without the presence of a reflective shield placed between the switch and coil. The shield was simply a wrap of aluminium foil. The current applied to the switch (SRA831) was 3A at 30MHz.

Results and Discussion

Tests on a number of different coil assemblies showed no difference in RF heating with or without the presence of the shield. It could only be concluded that radiated heat from the switch contacts was not the cause of the increased RF heating seen compared to a solid copper conductor. Furthermore, it was later discovered, after discussion with staff at Crydom, that the grade of glass used for the reed switch envelopes was specially chosen for its ability to absorb radiated heat from the seal making elements during manufacture. It was therefore unlikely that a significant quantity of radiated energy could be transmitted through the glass to the coil.

3.2.6 A Model for the Losses Occurring in the Coil of an RF Reed Relay

From the analysis and findings of the preceding sections the following is the relationship for the RF power dissipated in a coil of a reed relay

$$W_{RF} = \frac{I_{RF}^{\ 2}}{R_{RF}} \qquad (3.16)$$

where

$$R_{RF} = \frac{\rho}{2 \cdot \delta} \cdot dia_{wire} \cdot N \cdot \overline{\left(\frac{1}{r}\right)} \cdot F_{wire} \cdot F_{loss} \qquad (3.17)$$

and

$$\overline{\left(\frac{1}{r}\right)} = \frac{1}{r_2 - r_1} \cdot \ln\left(\frac{r_2}{r_1}\right) \qquad (3.11)$$

$$F_{wire} = \left[k \cdot \left(\frac{-2}{k} \cdot e^{-k \cdot r} + \frac{1 + e^{-2k \cdot r}}{k} \right) \right]^2 \quad (3.14) \quad ; \qquad k = \sqrt{\pi \cdot f \cdot \mu \cdot \sigma}$$

F_{loss} =1.8 for SRA831 and 2.3 for SRA830 switches (determined by experiment)

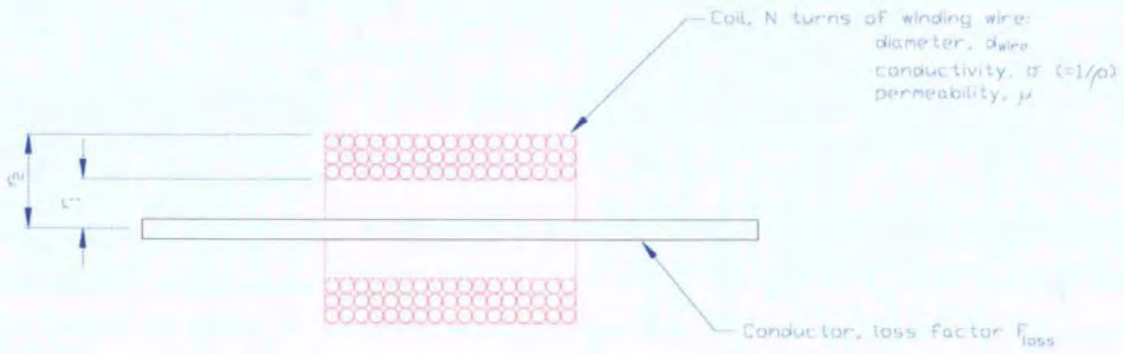

Figure 3.19 – RF Losses in a Reed Relay Coil

The above provides a means of obtaining a good estimate of RF losses in a reed relay coil from its geometry and winding, etc. In particular the link between coil geometry and RF loss is established. This is a key aim of the present research and opens up the possibility of using the above relationship in a design tool to optimise relay geometry for minimum losses.

4. ELECTROMAGNETIC FIELD MODEL FOR THE DESIGN OF RF REED RELAYS

The work from the preceding sections, covering the electromechanical model of a reed relay and the RF losses associated with a relay coil, was combined to form a computer program to be used as a tool for the design reed relays for RF applications. In this coil operating voltages, voltage isolation across the contacts, contact resistance and RF loss characteristics are predicted from reed switch and coil dimensions. This meets the original aim of linking relay dimensions to relay performance and essentially embodies a 3D electromagnetic field model of a reed relay.

The program is described and example results provided. In addition a case study of the application of the program to the development of a new product at Crydom Magnetics is detailed. Finally the commercial implications of the work are discussed.

4.1 RF Reed Relay Design Program

Introduction

The aim of the reed relay design program was to combine the work from the preceding sections to form a design tool for RF reed relays. Typically the principle design parameters of an RF reed relay are:

Size limitations

Nominal coil voltage

Max isolation voltage across contacts

Max RF carry current and frequency

Max operating temperature (ambient plus self heating)

From the above parameters RF and DC power dissipation in the coil were calculated. In doing so it was possible to assess the effect of altering reed and coil dimensions in order to minimise the power dissipated in the coil.

Structure

The reed switch design program, as described in section 2.6 was used as a base for the reed relay design program. In the reed switch design program the breakdown voltage for a given operate amp turn switch was calculated from reed and coil dimensions. For the present purpose this was reformed to provide the amp turns required to operate a switch with a given breakdown voltage. From the required amp turns the DC power dissipated in the coil can be calculated from:

$$W_{DC} = \frac{mmf^2 \cdot \rho \cdot MTL}{F_{pack} \cdot F_{cu} \cdot A_{coil}} \qquad (4.1)$$

where

mmf =magnetomotive force (AT)

ρ =resistivity (of copper)

MTL =mean turn length=$2*\pi*(r_2+r_1)/2$

A_{coil} =cross sectional area of the coil winding

F_{pack} =packing factor for a round wire occupying a square space=0.785

F_{cu} =proportion of winding wire cross sectional area which is copper. For the winding wire sizes used in reed relays (0.04-0.16mm) this is typically 0.65.

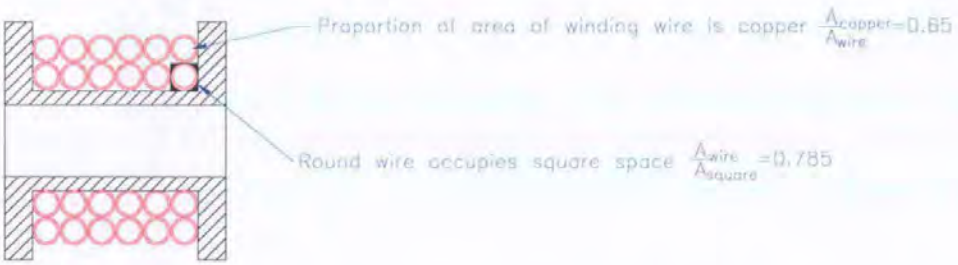

Figure 4.1 – Cross Section Through a Coil to show Winding Packing Factor

This relationship, the derivation of which is given in appendix 10, gives the power required to operate the switch at room temperature. To be of practical use the coil must be capable of operating the switch over the required temperature range. The resistance of the coil will increase with temperature and, as it is powered from a voltage source, the amp turns it produces will drop as temperature rises. The relationship for the change in resistance of a copper winding with temperature, as introduced in section 3.1, is given by:

$$R_2 = R_1 \cdot \frac{T_2 + 234.5}{T_1 + 234.5} \qquad (3.4)$$

In order for the coil to be capable of closing the switch at the nominal operating voltage and maximum temperature specified the amp turns delivered at room temperature will therefore be:

$$mmf = OAT \cdot \frac{T_2 + 234.5}{T_1 + 234.5} \qquad (4.2)$$

From the DC power corresponding to this and the nominal coil voltage the coil resistance can be determined from:

$$R = \frac{V^2}{W_{DC}} \qquad (4.3)$$

As the coil dimensions are known the diameter of the winding wire required to give this resistance is:

$$dia_{wire} = \left[\frac{16 \cdot \rho \cdot MTL \cdot A_{coil} \cdot F_{pack} \cdot F_{cu}}{\pi^2 \cdot R} \right]^{\frac{1}{4}} \qquad (4.4)$$

The derivation of equation 4.4 is given in appendix 10. The above gives all the details of the coil winding. From this the RF resistance and power dissipation can be calculated at the specified maximum frequency and magnitude of the RF current carried in the switch as described in section 3.2.

The summation of DC and RF power gives the total dissipated in the coil winding.

Example Results

As an illustrative example the results below are for a 12V (nominal) relay based around an SRA831 type reed switch of 25mm length. The effect of three different coil geometries are shown with a maximum RF current in the switch of 3A @ 30MHz. The maximum operating temperature of the coils was 180°C. The three coils were:

Coil#1 : 8mm OD, 4mm ID, 20mm length

Coil#2 : 8mm OD, 4mm ID, 10mm length

Coil#3 : 12mm OD, 8mm ID, 10mm length

The results for DC power, RF power and total power dissipated in each of the coils as a function of the maximum isolation voltage of the switch are shown overleaf. Note that, to relate back to the results from the reed switch design program, a higher maximum isolation voltage (i.e. breakdown voltage) implies a higher operate amp turn switch. The DC power requirement is therefore correspondingly greater. Once the winding details associated with this have been established, the RF power dissipated can be calculated from these and the RF current in the switch.

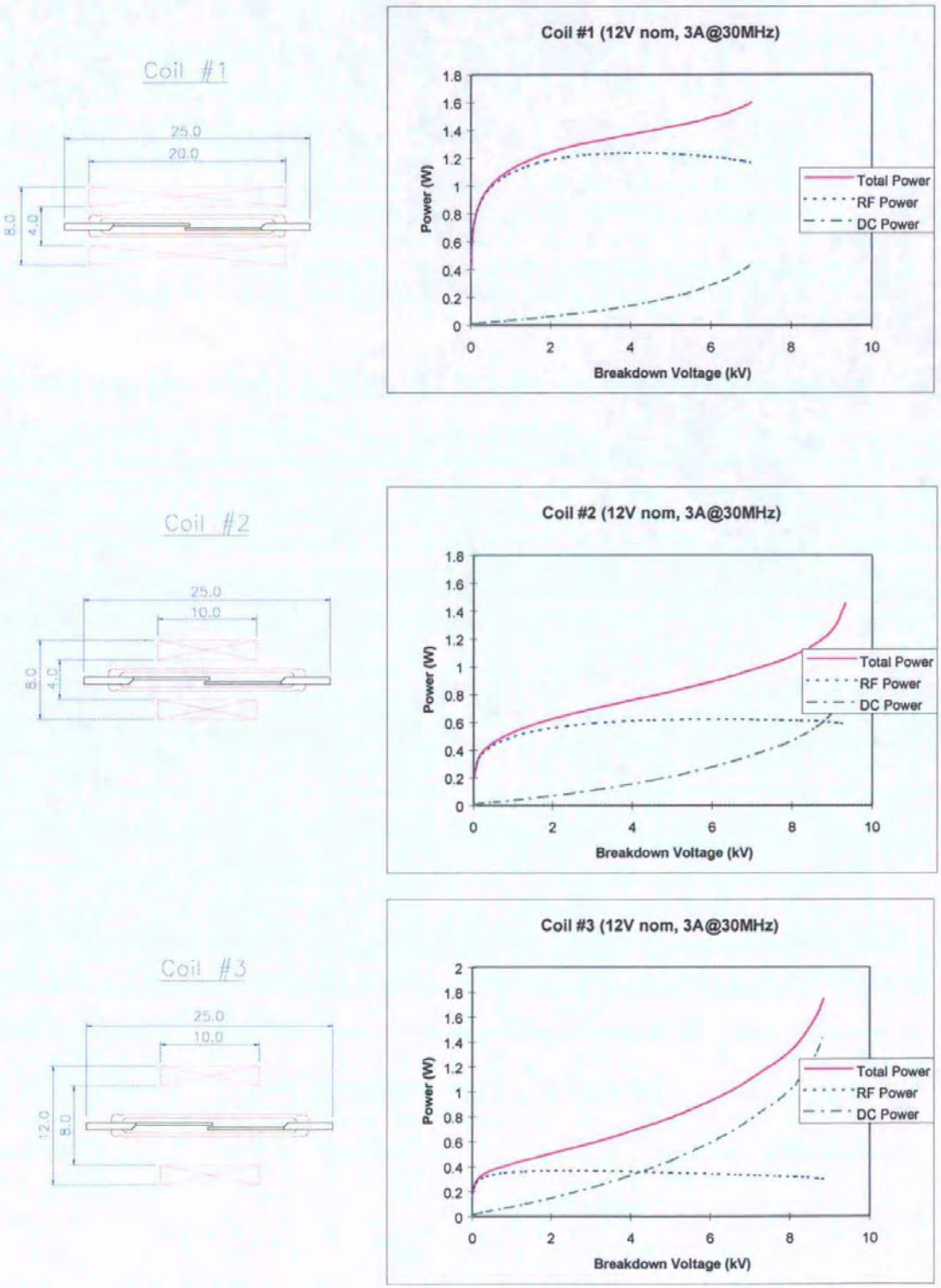

Figure 4.2 – RF, DC & Total Power Dissipated in Relay Coils #1-#3

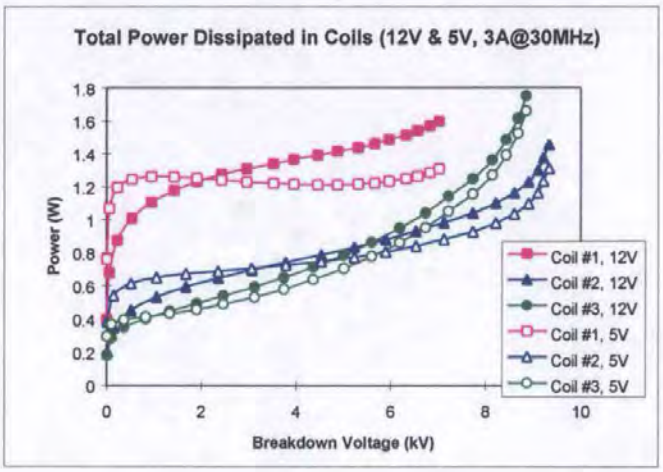

Figure 4.3 – Total Power Dissipated in Relay Coils #1-#3, 5V & 12V Nominal

Discussion of Results

The results show a substantial variation in the RF and DC power dissipated in the coil for a given switch isolation as geometry is varied.

With Coil#1 the DC power dissipated is low due to the large cross sectional area of the coil and its relatively small diameter. However, it can be seen that this arrangement leads to high RF power dissipation (more than four times greater than the DC power) and so would be unsuitable for an RF reed relay. Both these trends can be seen by referring to equations 4.1 and 3.17 for DC power dissipation and RF resistance respectively.

The results for Coil#2 show that, despite there being half the cross sectional area of Coil#1, the DC power dissipated for a given isolation voltage is similar. This is because the magnetic efficiency with the shorter coil is improved. The reduced cross sectional area of the coil results in a corresponding reduction in the RF losses in the coil - the RF power dissipated is roughly half that of Coil#1.

Coil#3 has the same cross sectional area as Coil#2 but larger inside and outside diameters. This has the effect of increasing the mean turn length of the winding and so reducing the DC efficiency of the coil. The magnetic efficiency will also reduce slightly and so the DC power dissipated in the coil is greater (by ~66%) than that for Coil#2 for a given switch isolation voltage. However, the increased diameter of the coil also results in much reduced RF losses (~60% of those in Coil#2). The net result is that the total power dissipated in Coil#3 is very similar to that in Coil#2 although the proportion of RF:DC losses is different. This would suggest that the coil winding diameter for minimum power dissipation for a 10mm long coil (and the other constraints detailed) lies somewhere between those of Coil#2 and Coil#3.

It should be noted that, in the above results, power dissipated, but not coil heating, is calculated. The power against temperature characteristic will vary with coil geometry and so a coil which provides minimum power dissipation may not provide minimum heating.

A further point is that the requirements on coil geometry for minimum DC power dissipation generally contradict those of minimum RF power dissipation. The optimal coil dimensions for a reed relay will therefore depend greatly upon the balance between the RF carry current and breakdown voltage requirements. A requirement for a high breakdown voltage but either small or low frequency carry current would yield a coil of large cross sectional area with the minimum possible inside diameter. Conversely a requirement for a high RF carry current at high frequency but only a low breakdown voltage requirement would result in a coil of minimal cross sectional area and relatively large inside diameter.

The effect of altering the nominal operating voltage is seen in figure 4.3. RF losses are dependent upon winding wire diameter and so are affected by changing the nominal operating voltage of the coil (as this entails changing winding wire diameter). There is no change to the DC power requirement. RF losses are at a maximum for wire sizes in the range

0.04mm to 0.63mm (this can be seen in the test results throughout section 3.2) which is unfortunate as most small 12V and 24V relays based around "SRA" type switches require this size of wire. Reducing the nominal operating voltage from 12V to 5V in the above example results in the size of winding wire required increasing above that at which maximum losses occur for most drive requirements. This gives the useful reduction in the total power dissipated in the coil shown. The significance of coil operating voltage upon RF losses occurring in it has not previously been noted.

A listing of the reed relay design program is included in appendix 8.

Conclusions

The discussion in section 4.1 demonstrates how the reed switch design program can be used to show the effect of relay dimensions on electrical performance. This was the aim of the present work. From this lies the possibility of using the program to optimise relay dimensions to fulfil a given electrical specification.

In practise, although relay requirements may be superficially similar, the exact set of constraints for each application are almost invariably different. For example, a requirement for a high voltage isolation between switch and coil could limit coil length, a weight limit could limit the mass of the coil winding or a spatial limitation coil restrict coil outside diameter. This makes it difficult to create a program to cater for all cases. As a result an attempt has not been made to develop a general piece of software which would return the optimal dimensions from any set of constraints. It is felt that this is outside the scope of the present work and, if undertaken, would constitute a research project in its own right.

4.2 Case Study - Crydom FRS42500 Series RF Reed Relay

Introduction

The development of the FRS42500 series reed relay is presented as an example of a practical application of the present research. In this instance the requirement was to produce an equivalent to an existing relay but at roughly half the manufactured cost. The only concession made was that the operating temperature range of the new product was to be restricted to -40°C to +65°C rather than -40°C to +85°C.

In order to reduce cost the number of component parts in the relay had to be reduced. The existing product featured electrostatic screening to reduce RF losses (and therefore heating). An aim of the new development was therefore to try and optimise coil geometry so that RF losses were reduced and the requirement for electrostatic screening eliminated.

Optimisation

In order to find the optimal coil geometry for the constraints given a program, similar to the reed relay design program, was written with the constraints as follows:

Coil

Nominal Coil Voltage	21V
Max OD	8mm
Max Length	10mm

Switch

Contact Isolation	800V
Max Carry Current	3.2A @ 30MHz
Max Length	25.4mm

Note that, despite the low isolation voltage specification, the use of a, cheaper, pressurised (rather than evacuated) switch was planned and so the amp turns required of the coil were not as low as would otherwise be expected. As a result the switches used were rated at 25-40AT (tested uncropped in an RSC09 test coil). The same switch, if evacuated, would have a breakdown voltage of roughly 2.5-4.0kV.

The parameters varied in the program were coil length and coil inside diameter. Coil outside diameter was fixed at its maximum value of 8mm as this was considered at or smaller than its optimal value.

DC power was calculated so that the coil would give performance equivalent to 40AT in an RSC09 test coil. Note that switch length was restricted to 25.4mm. A maximum coil temperature of 180°C was assumed.

In order to calculate RF losses the winding wire diameter to give the required drive at the nominal voltage was determined. This, the number of turns, the coil dimensions and the switch type then allowed the RF losses to be calculated.

Results

The results for the total power dissipated in 4, 6, 8 & 10mm long coils as coil inside diameter was varied are shown below:

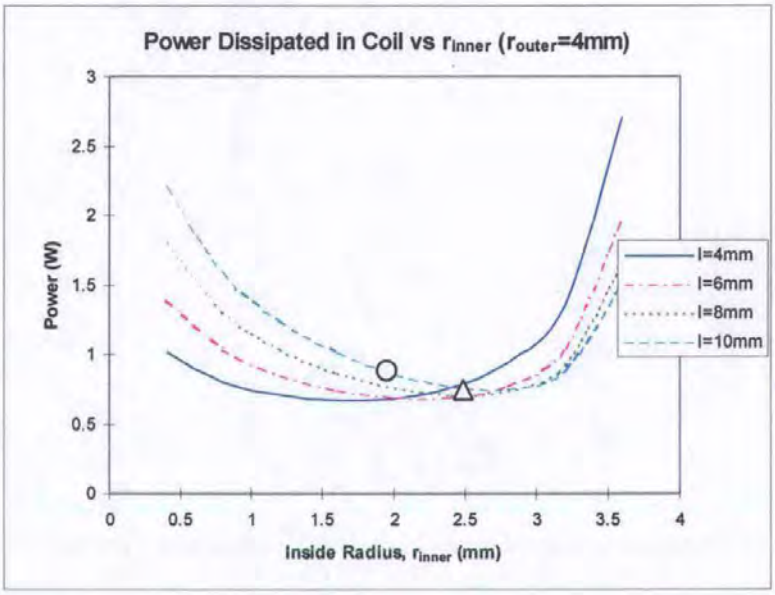

Figure 4.4 – Power Dissipated in Coil vs. r_{inner} (r_{outer}=4mm) for l=4,6,8&10mm

Discussion

The results show clearly an optimal inside diameter of the coil for each of the coil lengths considered. With a small inside diameter the cross sectional area of the coil is greater and so the DC power dissipated is small. However, in this case the RF power loss is very large. At the other end of the scale, with the inside diameter enlarged so that it is very close to the outside diameter, the cross sectional area of the coil is small and the DC power correspondingly large. Conversely, the RF losses diminish as inside diameter increases. The inside diameter for minimum total power dissipation obviously lies between these extremes.

Note that, although the minimum power dissipated for the shortest coils is lowest, as their surface area (and therefore ability to dissipate heat) will also be much lower they are likely to

run hotter. As a result a coil length close to the maximum 10mm is likely to give the lowest heating.

The round marker on the figure indicates the coil length/inside diameter combination for the existing product and the triangular one that of the FRS42500. A clear reduction in total power dissipated in the relay coil is shown.

Comparison Between FRS42500 and Existing Relays

On the basis of the above work and various packaging constraints the coil chosen for the new product were as shown below. Also shown are the dimensions of the existing relay coil and the total power dissipated in each for comparison.

	Existing	FRS42500	
Coil OD	7.0mm	8.0mm	
Coil ID	3.6mm	4.8mm	
Coil length	10mm	8.4mm	
DC Power*	0.29W	0.29W	(*calculated; 21V, 1500 Ohms)
RF Power*[2]	0.61W	0.39W	(*[2]calculated; 3.2A @ 30MHz)
Coil Heating*[3]	115°C	95°C	(*[3]measured with 21V to coil, 3.2A @30MHz through switch)

Note that the above figures for the existing coil are without electrostatic screening fitted for the purposes of comparison.

From the above results it can be seen that there is a 24% reduction in the power dissipated in the new coil. This allowed the new relay to be produced without electrostatic screening and still meet the RF carry current requirements. As a result of this and a design for manufacture

exercise to reduce the component count in the relay a considerable saving in manufactured cost was made.

The FRS42500 series relay has since entered into production and been used to address low cost markets which would previously have proved uneconomic.

4.3 Application of Reed Relay Design Program

The reed relay design program can be used to facilitate cost reduction and/or performance enhancement of RF reed relays. In the example already described cost reduction was achieved by tuning coil dimensions so that electrostatic screen components could be removed whilst still allowing performance criteria to be met. An alternative approach using the same technique might be to enhance performance by tuning coil dimensions and retaining the screen components.

The balance between relay cost and performance is determined by customer preferences. In general customers building equipment for civilian applications will err on the side of low cost whereas those catering for military applications will be more inclined to push the limits of relay performance. The reed relay design program offers potential improvements in both these areas and is therefore applicable to all of the RF reed relays manufactured by Crydom Magnetics Ltd.

In the example described new business worth ~£80k pa was realised. This is significant for small firm of approximately 70 employees turning over around £4M pa. At the time of writing RF reed relays are the largest single product group and account for ~£1.5M pa. It is difficult to make an accurate assessment of the full extent of the financial implications of the present research in terms of giving access to new or maintaining existing business. However, the work forms an important part in improving the competitiveness of Crydom's RF reed relays in the market place. It is not advisable for any business to stand still and this is especially true of manufacturing concerns. Crydom Magnetics Ltd is no exception to this and, viewed in this light, the work is therefore of significant value.

5. CONCLUSIONS

The original work contained in the present research is:

- Verification of Roters' technique for the calculation of permeance through capacitance measurements (section 2.1).

- Finite element analysis of a simplified, 2D axisymmetric, model of a reed switch and coil (section 2.2).

- Incorporation of the works of Cullen and Takamisawa to form a procedure for calculating the breakdown voltage of an evacuated reed switch (section 2.5).

- Development of the reed switch design program including elements from all of the above to link the electromechanical aspects of reed relay performance to reed and coil dimensions (section 2.6).

- Experimental measurement of RF losses occurring in reed relay coils (section 3.1).

- Development of a relationship to calculate the RF loss in a reed relay coil from the dimensions of the coil (section 3.2).

- Development of the reed relay design program incorporating all of the above for use as a design tool for RF reed relays (section 4.1).

The key result (and original aim) of the present research is the establishment of the link between relay dimensions and relay performance. This is true of both electromechanical characteristics (i.e. DC coil power, contact gap, breakdown voltage, etc) and RF loss characteristics (i.e. RF power dissipated in the relay coil). It is shown that the ideal proportions for DC and RF efficiency are, to some extent, in conflict. The reed relay design program can therefore be used to find optimal dimensions for given required performance characteristics.

The work has implications for both cost reduction and performance enhancement, as demonstrated in the case study provided, and is relevant to all reed relays manufactured by Crydom Magnetics Ltd.

6. SCOPE FOR FURTHER WORK

6.1 Electromechanical Model

The electromechanical model of the reed relay presented in section 2.6 is considered to be as detailed as is possible without resorting to a full 3D finite element model. However, this still leaves parts of the model, in particular in the vicinity of the contact gap, where the actual form of the field cannot be analysed. To further the understanding of the electromechanical aspects of a reed relay the next logical step would be to "bite the bullet" and create a full 3D finite element model of the reed switch and coil. This would not, however, be a straightforward exercise.

A 3D model, because of the reed switch's overlapped contacts, would not be able to take advantage of symmetry and so all of the coil, reed blades and surrounding volume of air would have to be modelled. Also, a complex mesh would be required as a fine mesh in the contact gap, which will have a minimum value of only 6um for an SRA830 model, will mean using elements with an edge length of the order of 1um. As the total length of the model for the same switch will be approximately 70mm it can be seen that the model size, in computational terms, will become very large indeed. Also, representing the motion of the reed blades could mean re-meshing the model for every gap size analysed.

These issues will inevitably ease as computing power and software continue to improve. A possible alternative is the use of the boundary element modelling technique which does not involve the creation of a mesh as in finite element modelling. Software packages of this type are available for magnetic field analysis although the author has no experience of them or any limitations they may have.

A further possibility with increasingly sophisticated software is that of combined field analysis. This could be used to model both the magnetic and mechanical aspects of the reed relay using the finite (or boundary) element technique. It may also be possible to include electrostatic force calculation with this in order to improve the accuracy of breakdown voltage calculations.

6.2 Coil Heating

One obvious shortcoming of the electromagnetic model presented in the current work is that a means of calculating coil temperature rise from the power dissipated in it and it dimensions is not included. Some initial research on the subject (Backe (30), Giese (31) & Rice (32)) yielded the fundamental relationships for each of the three forms of heat transfer. These are:

Conduction $$Q = \frac{A}{L} \cdot K \cdot \Delta T \qquad (6.1)$$

Radiation $$Q = A \cdot e \cdot \sigma \cdot T_{abs}^{\ 4} \qquad (6.2)$$

Convection (natural) $$Q = A \cdot K_2 \cdot \Delta T^{1.25} \qquad (6.3)$$

Convection (gaseous) $$Q = \frac{2 \cdot \pi \cdot r \cdot L \cdot K_3 \cdot \Delta T}{r \cdot \ln(r/R)} \qquad (6.4)$$

where

Q	=heat flow (W)
A	=area (CSA for conduction, surface for convection, radiation)
K	=thermal conductivity
ΔT	=difference between body temp and ambient
T_{abs}	=absolute temperature
E	=surface emissivity
σ	=Stephan Boltzman constant
K_2	=convection constant

K_3 =gaseous thermal conductivity over range ΔT

r,L =radius and length of heated cylinder at body temp

R =radius of surrounding cylinder at ambient temp

Experiments by the author involving the measurement of the power vs. heating characteristic for coils or different proportions in air failed to identify coefficients for the relevant heat transfer mechanisms (convection and radiation - conduction was disregarded in this case). However, a more thorough investigation might well achieve more success.

Alternatively, this topic would make another ideal candidate for finite element analysis as packages created specially to model the heating of electronic components are becoming increasingly prevalent. It may also be possible to include this characteristic in a combined field model.

A complication arising from the construction of reed relays is that some coils are surrounded largely by air and some are encapsulated using an epoxy or silicone compound. This will clearly influence heat transfer characteristics of the coil and the finite element technique may be better suited to accommodate this.

6.3 Optimisation

The electromagnetic model presented in the current work describes the relationship between coil and reed switch dimensions and their electromechanical and RF loss characteristics. It does not, however, incorporate a general means by which optimal relay dimensions can be calculated from any given set of performance criteria. If such a means could be developed it would exploit the maximum potential from the present work and would form an interesting topic for further work.. Optimisation algorithms of this type are a part of some finite element analysis packages and analysis in this field is becoming increasingly popular. Ideally, this

would be included with the combined field analysis outlined above. However, the complexity of a 3D model incorporating magnetic, mechanical, electrostatic and thermal analysis would be considerable.

6.4 Effect of Ferromagnetic Materials on RF Coil Losses

The effect of the ferromagnetic nature of reed blade material on RF losses in the coil has been identified in the present work but not fully explored. In particular, the exact mechanisms determining "loss factor" have not been identified. A mathematical model of the effect of a copper plated reed blade to allow "loss factor" to be calculated from plating thickness and material properties would form a useful addition to the present work.

To improve RF reed relay performance in the short term it has been shown that simply increasing the thickness of copper plating on the reed blades until "loss factor" is reduced to unity would be one approach. However, should this prove impractical from a manufacturing perspective, further research may yield a more convenient means of achieving the same end.

Also, as there is a conflict between additional copper plating at the contacts and switch breakdown voltage, this is another feature which would, ideally, be included in a combined field model for an optimum, or best compromise, solution to be found.

7. REFERENCES

1. R.L.Peek, "Magnetisation of Pull Characteristics of Mating Magnetic Reeds", Bell Systems Technical Journal, March 1968

2. K.Kato, "Analysis on Magnetisation Characteristics of Reed Switches", Proceedings 19th Annual Relay Conference, 1971

3. G.W.Cullen, "A Practical Theory for Reed Switches", Proceedings 19th Annual Relay Conference, 1971

4. T.Handa , T.Hamahata , S.Iida, "Development of a Dry-Reed Sealer Transfer Contact", Proceedings 19th Annual Relay Conference, 1971

5. H.Rensch ,"Characteristics and Applications of Reed Contacts", Electrical Communication, Vol. 40, No.3, 1965

6. B.C.Stickley, "Magnetic Characteristics of Miniature Reed Relays", Proceedings 14th Annual Relay Conference, 1966

7. H.C.Roters, "Magnetic Devices", Wiley, 1948

8. T.Sekiya, T.Umemoto, T.Takeuchi, "Performance-Up for reed switch contacts by means of Ruthenium Plating", Proceedings 3rd International Relay Conference, 1974

9. G.W.Cullen, "Periodic Table of the Elements as it Pertains to Electrical Contacts", Internal Report, 1973

10. J.A.Augis, L.L.Hines, "Sputtered Ruthenium as a Contact Material for Sealed Reeds", Proceedings 23rd Holm Conference, 1977

11. Y.Hayashi, H.Tanaka, T.Hara, "Contact Resistance Characteristics of Rhodium Plated Contacts in Dry Reed Switch", Proceedings 19th Holm Seminar, 1973

12. T.Dabrowska , W.Francyk ,"Influence of contact material and Direction of Current Flow on Durability , Reliability and Contact Resistance of Reed Relay Contacts", Proceedings 24th Holm Conference, 1978

13. K.Izumi, N.Oode, K.Sato, H.Nakatani, "Ionplating Technique for Reed Switch Contacts", Proceedings 25th Holm Seminar, 1979

14. H.Matsueda, K .Nakamura, T.Kobayashi, T.Miyata, "A Study of Contact Surface Phenomena After the Surface Deactivation Treatment", Proceedings 41st Annual Relay Conference, 1993

15. T.Yokogawa, C.Kawagita , "High Reliability Reed Switches with Rhodium Plated Contacts", 21st Annual National Relay Conference, 1973

16. T.Yokokawa, T.Yano, C.Kawakita, K.Hinohara, A.Nagai, T.Kobayashi, "A Study of the Thickness of Rhodium Oxide Film Produced by the Surface Deactivation Treatment of Rhodium Plated Contact Reed Switches", Proceedings 31st Holm Conference, 1985

17. S.Orgen ,"Formation of a Highly Resistive Deposit in the Reed Contact Unit", Proceedings 25th Holm Conference, 1979

18. G.D.Theophilus, R.G. Van Heeswijk, K.D.Srivastava, "Differences Between 60Hz A.C.Breakdown and D.C. Breakdown of Vacuum Gaps", Proceedings 5th International Symposium on Discharges and Electrical Insulation in Vacuum, 1972

19. K.Takamisawa, "The Mechanism of the Electrical Breakdown in Vacuum", Proceedings 5th International Symposium on Discharges and Electrical Insulation in Vacuum, 1972

20. G.W.Cullen, "Prediction of Electrostatic Attraction in Reed Switch ", Internal Report, 1975

21. T.Hara, H.Tanaka, F.Kume, "Strange Behaviours in High Current Dry Reed Switch", Proceedings 20th Holm Seminar, 1974

22. J.Kaczmerek and H.J.Wierzba, "Phenomena Occurring in Dry Reed at High Current Loads", Proceedings 22nd Holm Seminar, 1976

23. H.Kulikjan, "A Method of Sample Measurements of Reed Relays Resistance in High Frequency Applications", Proceedings 30th Holm Seminar, 1984

24. J.N.Mason, "A Method of Measuring RF Loss Resistance in Reed Relays", Internal Report, 1995

25. J.Zawislanski, J.Stasiuk, M.Burzynski, B.Miedzinski, "Performance of HF Reed Relay Under Radio Frequency Conditions", Proceedings 41st Annual Relay Conference, 1993

26. J.Fullem, J.Bateman, "Reed Relays Designed to Handle Fast Pulses and RF Applications", Proceedings 37th Annual Relay Conference, 1989

27. ANSYS FEA Manuals, Vols. 1 and 2 , Swanson Analysis Systems Inc. , 1994

28. D.G.Watterson, M.Bradford, "Finite Element Modelling of Magnetic Devices", ERA Report 93-0978R

29. J.F.van Oss, "Magnetic Analysis of Solenoids", Moog Inc., Proceedings ANSYS 5th International Conference and Exhibition, 1991

30. "Temperature Rise of a Winding", BS EN 60950:1992, Annexe E

31. R.J.Backe, "Relay Coil Temperature Rise at Simulated Outer Space Pressure Levels", Proceedings 17th Annual National Relay Conference, 1969

32. B. Giese, "Approximate Power - Temperature Relationships for Copper Wire Coils", Proceedings 11th Annual National Relay Conference, 1963

33. L.A. Rice, "The Application of Basic Heat Transfer Principals in Optimising Relay Design", Proceedings 10th Annual National Relay Conference, 1962

Appendix 1 – Example ANSYS Input Data File

Below is an example of an ANSYS input data file which contains the information required to construct the 2D axisymmetric finite element model of a reed switch and coil. Included are material properties, dimensions of the model, meshing criteria, boundary conditions, loading, force calculations and solution procedure. It should be noted that commands generated during normal use of the software relating to display functions (e.g. zoom, numbering options, etc) have been removed from the listing for clarity.

```
/BATCH
/COM,ANSYS REVISION 5.0        A     08:22:19   03/25/1996
/input,start   ,ans    ,C:\ANSYS50A\DOCU\              ,,,,,,,,,,,,,,,,,1

/PREP7                    !enter preprocesor
ET,1,53,0,,1              !specify element type
TB,BH,1,,16               !enter BH characteristic for material 1(NiFe)
TBLE
STAT,TABLE
TBPT,,  4.19000000   , 5.000000000E-02
TBPT,,  12.6000000   , 0.150000000
TBPT,,  20.9000000   , 0.250000000
TBPT,,  29.3000000   , 0.350000000
TBPT,,  37.7000000   , 0.450000000
TBPT,,  46.1000000   , 0.550000000
TBPT,,  54.4000000   , 0.650000000
TBPT,,  62.8000000   , 0.750000000
TBPT,,  71.2000000   , 0.850000000
TBPT,,  79.6000000   , 0.950000000
TBPT,,  95.0000000   ,  1.05000000
TBPT,,  151.200000   ,  1.15000000
TBPT,,  246.000000   ,  1.25000000
TBPT,,  397.000000   ,  1.35000000
TBPT,,  637.000000   ,  1.45000000
TBPT,,  1161.00000   ,  1.55000000
TBPLOT,BH,1
MP,murx,2,1               !relative permeability of material 2 (air)
MP,murx,3,1               !relative permeability of material 3 (coil)
MPLIST

gap=0.2e-3                !dimensions of model
reed_l=27.2e-3
reed_r=0.279e-3
coil_l=15e-3
coil_id=4e-3
coil_od=16e-3
blockx=25e-3
blocky=30e-3

K,1,0,blocky              !define keypoints
```

```
K,2,reed_r,blocky
K,3,coil_id/4,blocky
K,4, blockx,9e-3
K,5,0,reed_l+gap/2
K,6,reed_r,reed_l+gap/2
K,7,coil_id/4,reed_l+gap/2
K,8,coil_id/2,coil_l/2
K,9,coil_od/2,coil_l/2
K,10,0,gap/2
K,11,reed_r,gap/2
K,12,coil_id/4,gap/2
K,13,0,0
K,14,reed_r,0
K,15,coil_id/4,0
K,16,coil_id/2,0
K,17,coil_od/2,0
K,18,blockx,0
K,19,19e-3,25e-3
K,20, 8e-3,blocky

A,1,2,6,5              !define areas
A,2,3,7,6
A,5,6,11,10
A,6,7,12,11
A,10,11,14,13
A,11,12,15,14
A,8,9,17,16
A,3,20,19,4,18,17,9,8,16,15,12,7

AGLUE,ALL

LESIZE,2,0.45e-3       !define element size along line
LESIZE, 4,0.45e-3
LESIZE,1,,,5
LESIZE, 3,,,5
ESHAPE,2               !set element shape to quadrilateral
MAT,2                  !set element material to 2 (air)
AMESH,1                !mesh area 1

LESIZE, 6,0.45e-3
KESIZE,3,0.5e-3        !define element size at keypoint
KESIZE,7,0.5e-3
ESHAPE,2
MAT,2
AMESH,2                !mesh area 2

LESIZE,8,,,62
LESIZE, 10,,,62
LESIZE, 9,,,5
ESHAPE,2
MAT,1                  !set element material to 1 (NiFe)
AMESH,3                !mesh area 3

LESIZE,11,,,62
KESIZE,12,0.5e-3
ESHAPE,2
MAT,2
AMESH,4                !mesh area 4
```

```
LESIZE, 14,,,5
LESIZE, 13,,,10
LESIZE, 15,,,10
ESHAPE,2
MAT,2
AMESH,5              !mesh area 5

ESHAPE,0             !set element shape to quad/tri mix
MAT,2
AMESH,6              !mesh area 6

LESIZE, 20,,,12
LESIZE, 22,,,12
LESIZE, 23,,,10
LESIZE, 25,,,10
ESHAPE,2
MAT,3                !set element material to 3 (coil)
AMESH,7              !mesh area 7

MAT,2
ESHAPE,0
AMESH,8              !mesh area 8

FINISH               !leave preprocessor

/SOLU                !enter solver

!note that boundary conditions default to those required - flux parallel on y (axisymmetric) axis and flux
perpendicular elsewhere

ESEL,MAT,3           !apply current density to coil
BFE,ALL,JS,1,,,2.0833e4
ESEL,ALL

ESEL,S,MAT,,1        !set up calculation of force on reed by virtual displacement method
NSLE,S
BF,ALL,MVDI,1
NSEL,INVE
BF,ALL,MVDI,0
ALLSEL

!apply the two step method to compute a converged solution

!first load step
NSUBST,5             !no. of substeps is 5
NEQIT,1              !no. of equilibrium iterations is 1
KBC,0                !ramp the current load
SOLVE                !solve first load step

!second load step
NSUBST,1             !no. of substeps is 5
NEQIT,20             !no. of equilibrium iterations is 20
CNVTOL,CSG,,1E-5     !convergence criteria is the out of balance load vector with a tolerance of 1e-
5
OUTRES,,LAST         !store data from last substep only
SOLVE                !solve second load step

FINISH               !leave solver
```

```
/POST1                  !enter post processor
PLF2D,27                !display flux lines using plf2d macro
ETABLE,FVX,NMISC,3      !Fx by virtual work
ETABLE,FVY,NMISC,4      !Fy by virtual work
ESEL,S,MAT,,2           !select the air elements around the armature
SSUM                    !sum up the forces

FINISH                  !leave post processor
```

Appendix 2 – Return Path Reluctance Calculated from FEA Model

Selected results for return path reluctance calculated from the 2D axisymmetric finite element model are presented and discussed in section 2.2.3. It was not appropriate to include all the data obtained at this point. The full set of results collected from the model are shown overleaf.

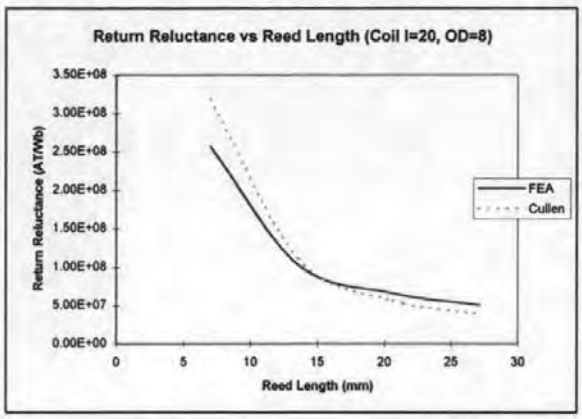
Return Reluctance vs Reed Length (Coil l=20, OD=8)
Return Reluctance (AT/Wb)
3.50E+08
3.00E+08
2.50E+08
2.00E+08
1.50E+08
1.00E+08
5.00E+07
0.00E+00
0
5
10
15
20
25
30
Reed Length (mm)
FEA
Cullen

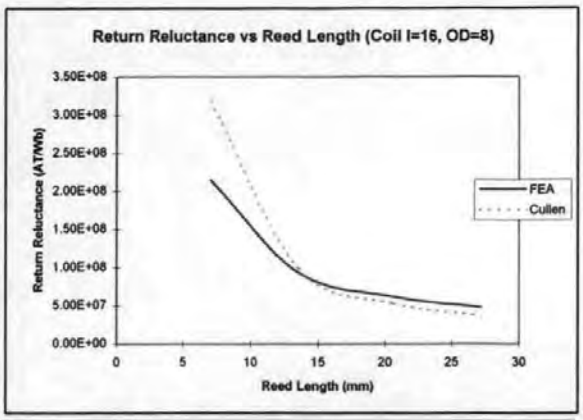
Return Reluctance vs Reed Length (Coil l=16, OD=8)
Return Reluctance (AT/Wb)
3.50E+08
3.00E+08
2.50E+08
2.00E+08
1.50E+08
1.00E+08
5.00E+07
0.00E+00
0
5
10
15
20
25
30
Reed Length (mm)
FEA
Cullen

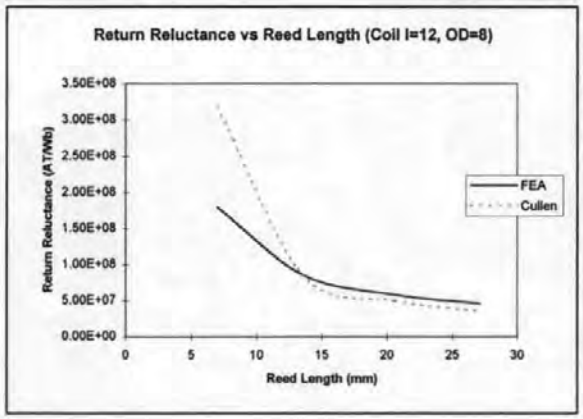
Return Reluctance vs Reed Length (Coil l=12, OD=8)
Return Reluctance (AT/Wb)
3.50E+08
3.00E+08
2.50E+08
2.00E+08
1.50E+08
1.00E+08
5.00E+07
0.00E+00
0
5
10
15
20
25
30
Reed Length (mm)
FEA
Cullen

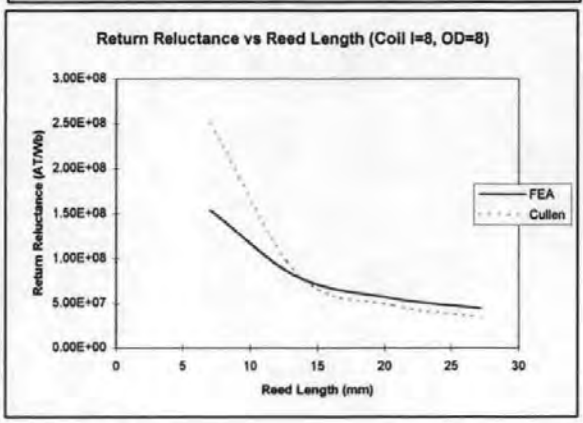
Return Reluctance vs Reed Length (Coil l=8, OD=8)
Return Reluctance (AT/Wb)
3.00E+08
2.50E+08
2.00E+08
1.50E+08
1.00E+08
5.00E+07
0.00E+00
0
5
10
15
20
25
30
Reed Length (mm)
FEA
Cullen

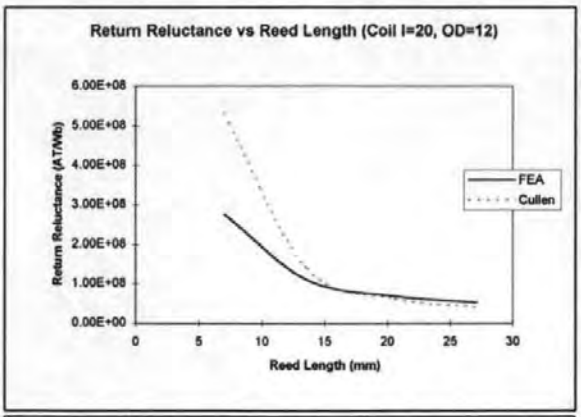
Return Reluctance vs Reed Length (Coil l=20, OD=12)
Return Reluctance (AT/Wb)
6.00E+08
5.00E+08
4.00E+08
3.00E+08
2.00E+08
1.00E+08
0.00E+00
0
5
10
15
20
25
30
Reed Length (mm)
FEA
Cullen

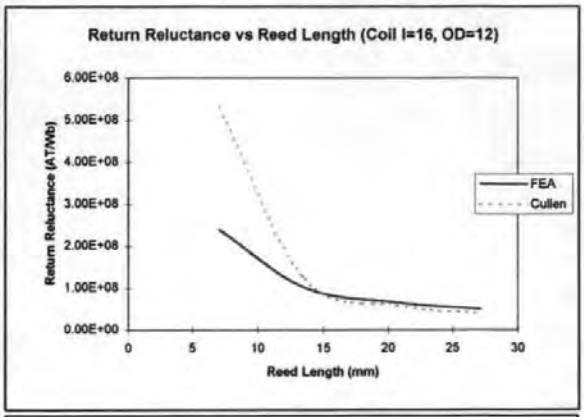
Return Reluctance vs Reed Length (Coil l=16, OD=12)
Return Reluctance (AT/Wb)
6.00E+08
5.00E+08
4.00E+08
3.00E+08
2.00E+08
1.00E+08
0.00E+00
0
5
10
15
20
25
30
Reed Length (mm)
FEA
Cullen

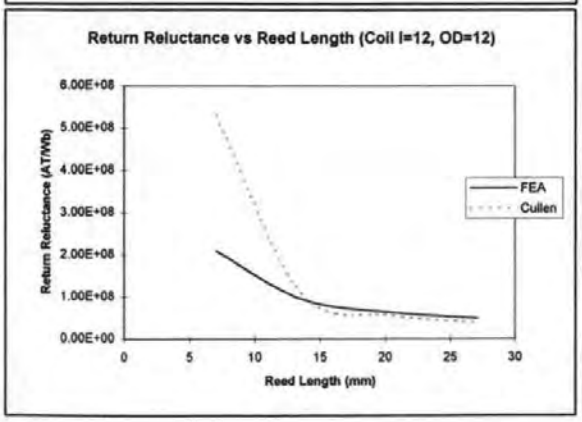
Return Reluctance vs Reed Length (Coil l=12, OD=12)
Return Reluctance (AT/Wb)
6.00E+08
5.00E+08
4.00E+08
3.00E+08
2.00E+08
1.00E+08
0.00E+00
0
5
10
15
20
25
30
Reed Length (mm)
FEA
Cullen

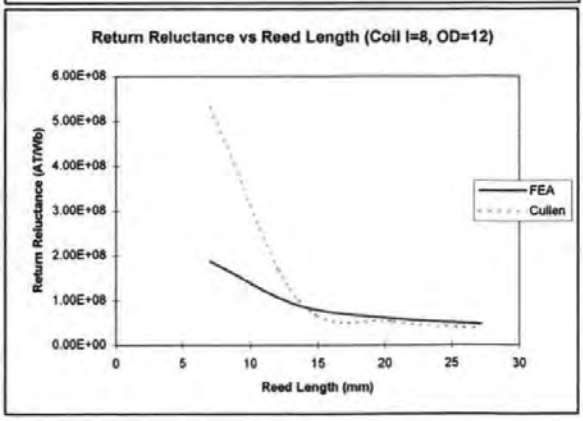
Return Reluctance vs Reed Length (Coil l=8, OD=12)
Return Reluctance (AT/Wb)
6.00E+08
5.00E+08
4.00E+08
3.00E+08
2.00E+08
1.00E+08
0.00E+00
0
5
10
15
20
25
30
Reed Length (mm)
FEA
Cullen

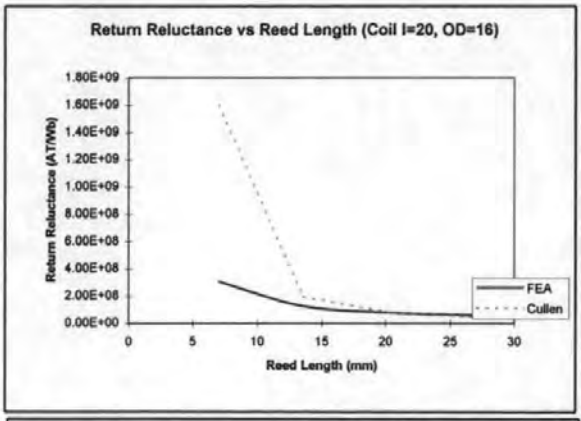
Return Reluctance vs Reed Length (Coil l=20, OD=16)
Return Reluctance (AT/Wb)
1.80E+09
1.60E+09
1.40E+09
1.20E+09
1.00E+09
8.00E+08
6.00E+08
4.00E+08
2.00E+08
0.00E+00
0
5
10
15
20
25
30
Reed Length (mm)
FEA
Cullen

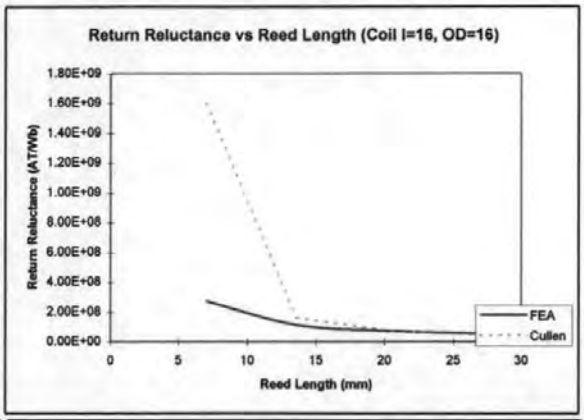
Return Reluctance vs Reed Length (Coil l=16, OD=16)
Return Reluctance (AT/Wb)
1.80E+09
1.60E+09
1.40E+09
1.20E+09
1.00E+09
8.00E+08
6.00E+08
4.00E+08
2.00E+08
0.00E+00
0
5
10
15
20
25
30
Reed Length (mm)
FEA
Cullen

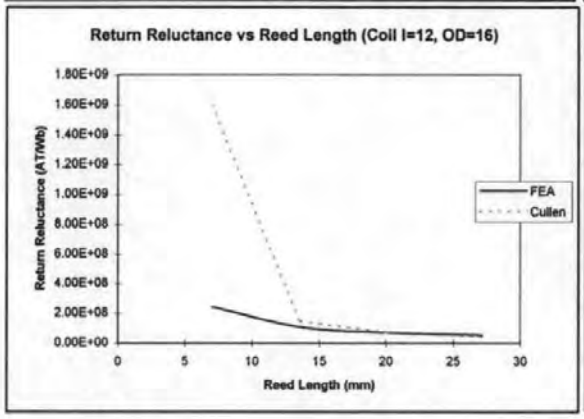
Return Reluctance vs Reed Length (Coil l=12, OD=16)
Return Reluctance (AT/Wb)
1.80E+09
1.60E+09
1.40E+09
1.20E+09
1.00E+09
8.00E+08
6.00E+08
4.00E+08
2.00E+08
0.00E+00
0
5
10
15
20
25
30
Reed Length (mm)
FEA
Cullen

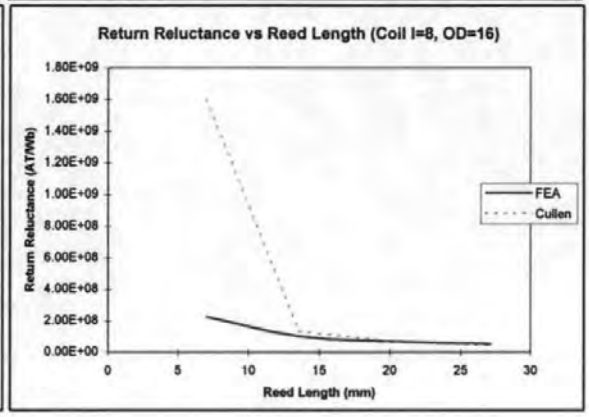
Return Reluctance vs Reed Length (Coil l=8, OD=16)
Return Reluctance (AT/Wb)
1.80E+09
1.60E+09
1.40E+09
1.20E+09
1.00E+09
8.00E+08
6.00E+08
4.00E+08
2.00E+08
0.00E+00
0
5
10
15
20
25
30
Reed Length (mm)
FEA
Cullen

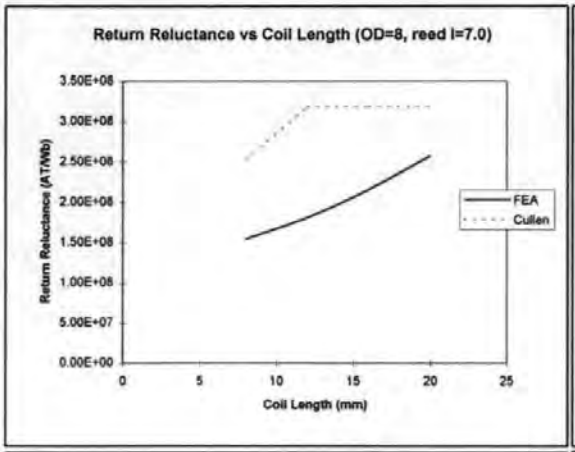
Return Reluctance vs Coil Length (OD=8, reed l=7.0)
Return Reluctance (AT/Wb)
3.50E+08
3.00E+08
2.50E+08
2.00E+08
1.50E+08
1.00E+08
5.00E+07
0.00E+00
0
5
10
15
20
25
Coil Length (mm)
FEA
Cullen

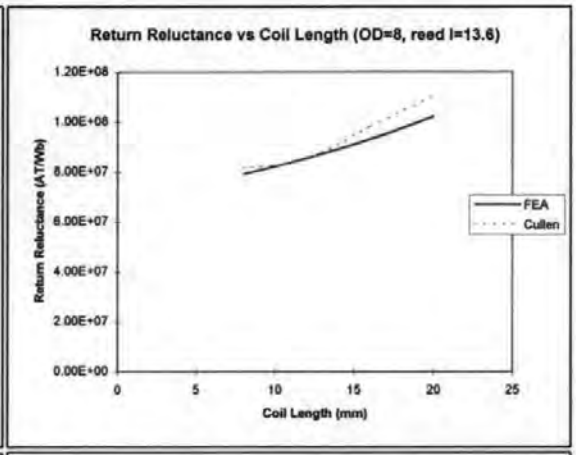
Return Reluctance vs Coil Length (OD=8, reed l=13.6)
Return Reluctance (AT/Wb)
1.20E+08
1.00E+08
8.00E+07
6.00E+07
4.00E+07
2.00E+07
0.00E+00
0
5
10
15
20
25
Coil Length (mm)
FEA
Cullen

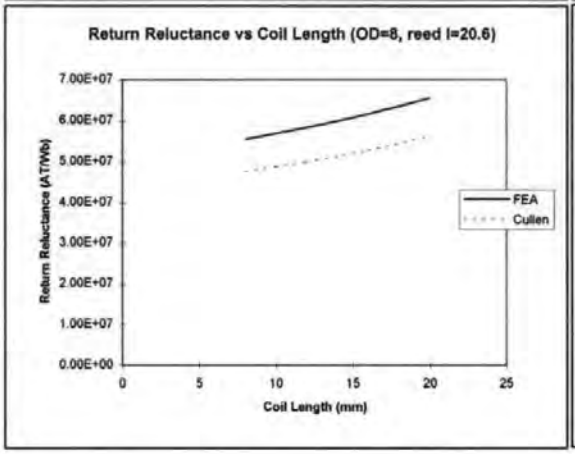
Return Reluctance vs Coil Length (OD=8, reed l=20.6)
Return Reluctance (AT/Wb)
7.00E+07
6.00E+07
5.00E+07
4.00E+07
3.00E+07
2.00E+07
1.00E+07
0.00E+00
0
5
10
15
20
25
Coil Length (mm)
FEA
Cullen

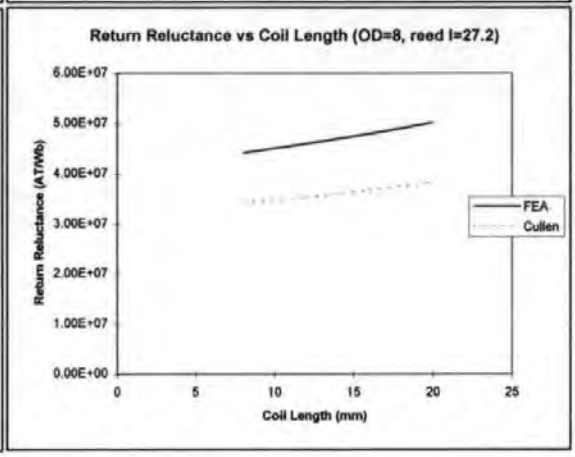
Return Reluctance vs Coil Length (OD=8, reed l=27.2)
Return Reluctance (AT/Wb)
6.00E+07
5.00E+07
4.00E+07
3.00E+07
2.00E+07
1.00E+07
0.00E+00
0
5
10
15
20
25
Coil Length (mm)
FEA
Cullen

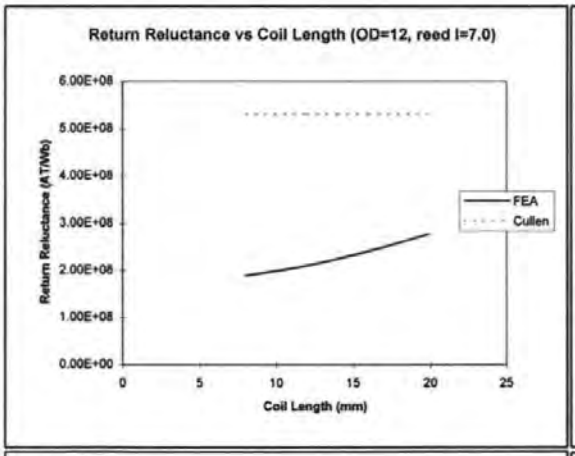
Return Reluctance vs Coil Length (OD=12, reed l=7.0)
Return Reluctance (AT/Wb)
6.00E+08
5.00E+08
4.00E+08
3.00E+08
2.00E+08
1.00E+08
0.00E+00
0
5
10
15
20
25
Coil Length (mm)
FEA
Cullen

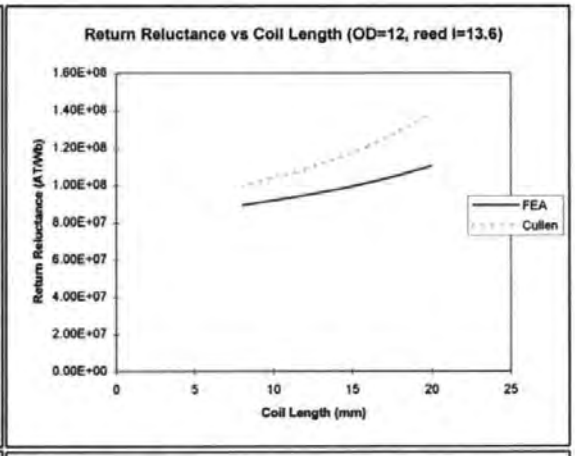
Return Reluctance vs Coil Length (OD=12, reed l=13.6)
Return Reluctance (AT/Wb)
1.60E+08
1.40E+08
1.20E+08
1.00E+08
8.00E+07
6.00E+07
4.00E+07
2.00E+07
0.00E+00
0
5
10
15
20
25
Coil Length (mm)
FEA
Cullen

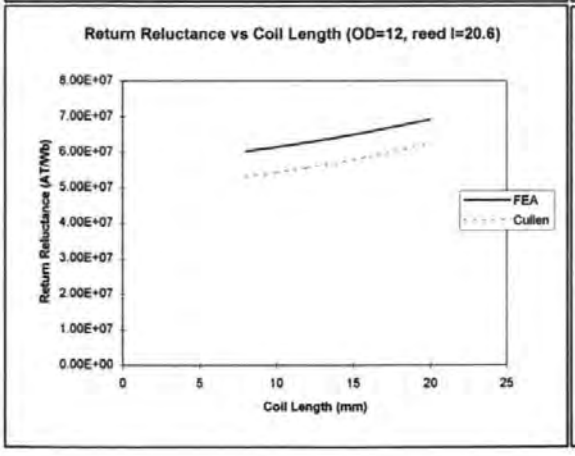
Return Reluctance vs Coil Length (OD=12, reed l=20.6)
Return Reluctance (AT/Wb)
8.00E+07
7.00E+07
6.00E+07
5.00E+07
4.00E+07
3.00E+07
2.00E+07
1.00E+07
0.00E+00
0
5
10
15
20
25
Coil Length (mm)
FEA
Cullen

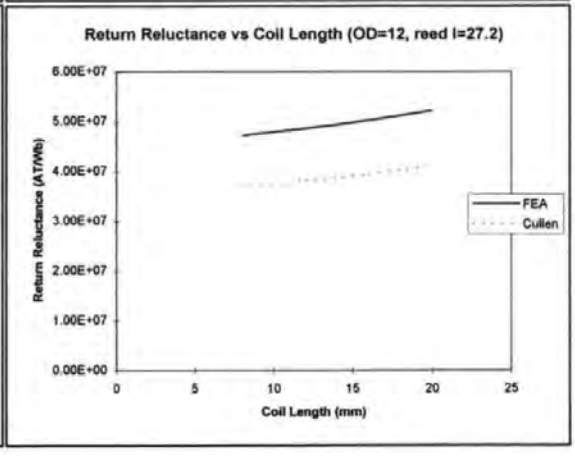
Return Reluctance vs Coil Length (OD=12, reed l=27.2)
Return Reluctance (AT/Wb)
6.00E+07
5.00E+07
4.00E+07
3.00E+07
2.00E+07
1.00E+07
0.00E+00
0
5
10
15
20
25
Coil Length (mm)
FEA
Cullen

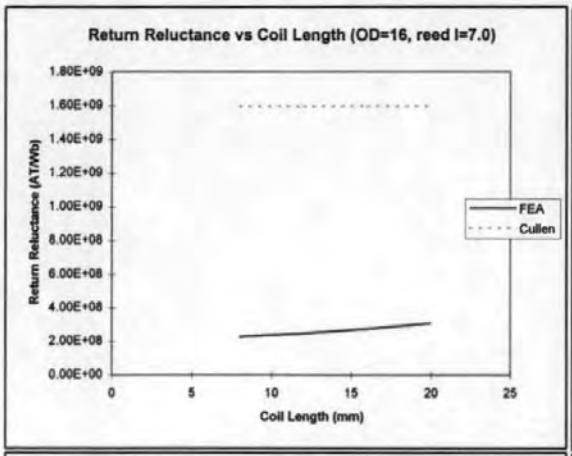
Return Reluctance vs Coil Length (OD=16, reed l=7.0)
Return Reluctance (AT/Wb)
1.80E+09
1.60E+09
1.40E+09
1.20E+09
1.00E+09
8.00E+08
6.00E+08
4.00E+08
2.00E+08
0.00E+00
0
5
10
15
20
25
Coil Length (mm)
FEA
Cullen

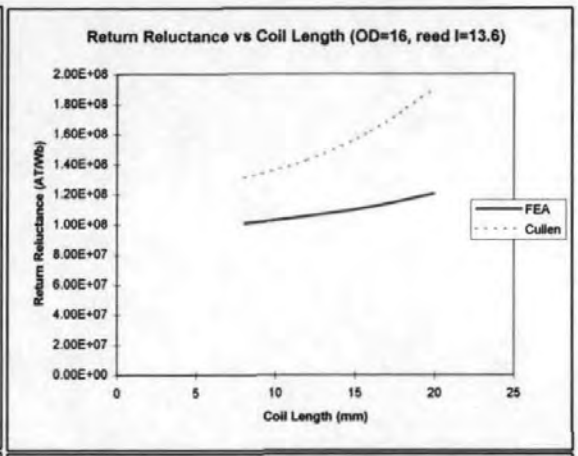
Return Reluctance vs Coil Length (OD=16, reed l=13.6)
Return Reluctance (AT/Wb)
2.00E+08
1.80E+08
1.60E+08
1.40E+08
1.20E+08
1.00E+08
8.00E+07
6.00E+07
4.00E+07
2.00E+07
0.00E+00
0
5
10
15
20
25
Coil Length (mm)
FEA
Cullen

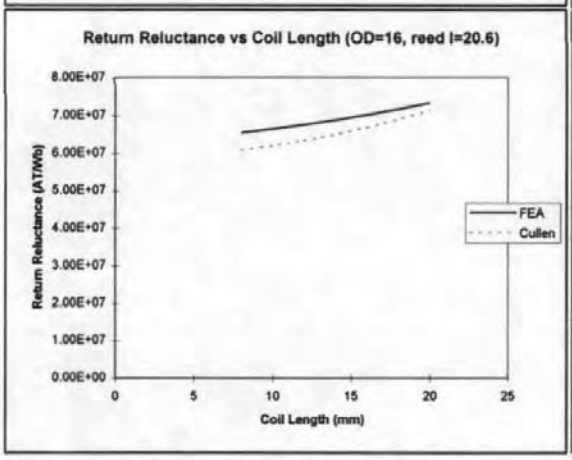
Return Reluctance vs Coil Length (OD=16, reed l=20.6)
Return Reluctance (AT/Wb)
8.00E+07
7.00E+07
6.00E+07
5.00E+07
4.00E+07
3.00E+07
2.00E+07
1.00E+07
0.00E+00
0
5
10
15
20
25
Coil Length (mm)
FEA
Cullen

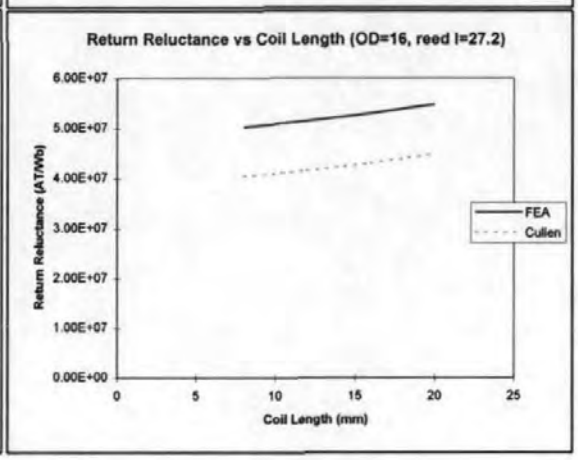
Return Reluctance vs Coil Length (OD=16, reed l=27.2)
Return Reluctance (AT/Wb)
6.00E+07
5.00E+07
4.00E+07
3.00E+07
2.00E+07
1.00E+07
0.00E+00
0
5
10
15
20
25
Coil Length (mm)
FEA
Cullen

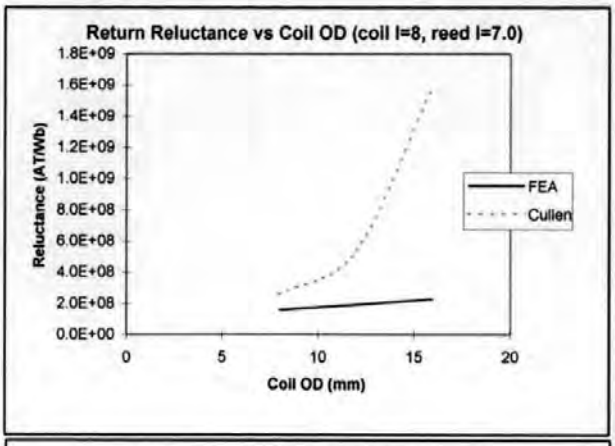
Return Reluctance vs Coil OD (coil l=8, reed l=7.0)
Reluctance (AT/Wb)
1.8E+09
1.6E+09
1.4E+09
1.2E+09
1.0E+09
8.0E+08
6.0E+08
4.0E+08
2.0E+08
0.0E+00
0
5
10
15
20
Coil OD (mm)
FEA
Cullen

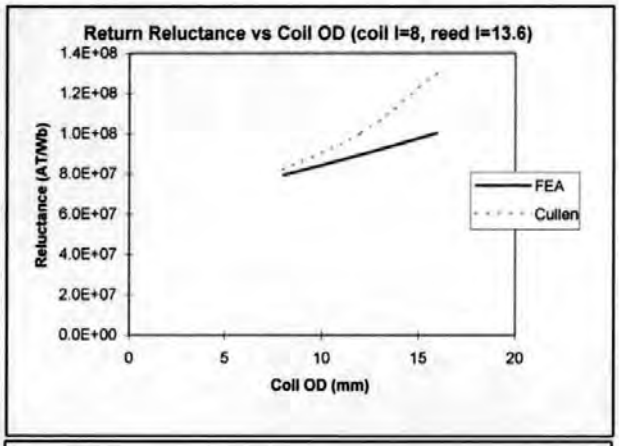
Return Reluctance vs Coil OD (coil l=8, reed l=13.6)
Reluctance (AT/Wb)
1.4E+08
1.2E+08
1.0E+08
8.0E+07
6.0E+07
4.0E+07
2.0E+07
0.0E+00
0
5
10
15
20
Coil OD (mm)
FEA
Cullen

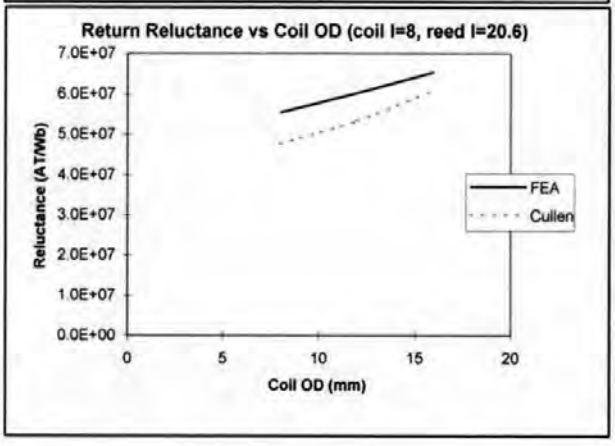
Return Reluctance vs Coil OD (coil l=8, reed l=20.6)
Reluctance (AT/Wb)
7.0E+07
6.0E+07
5.0E+07
4.0E+07
3.0E+07
2.0E+07
1.0E+07
0.0E+00
0
5
10
15
20
Coil OD (mm)
FEA
Cullen

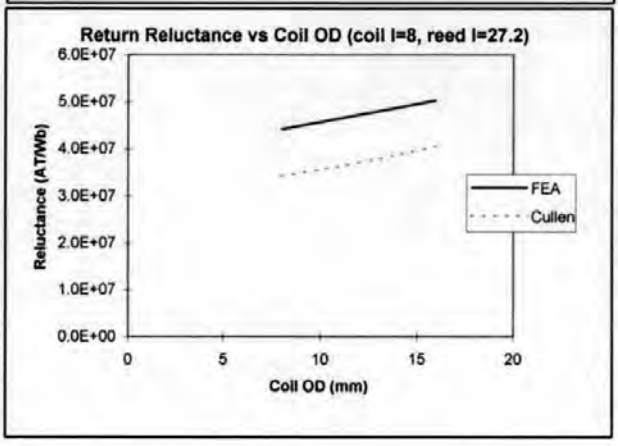
Return Reluctance vs Coil OD (coil l=8, reed l=27.2)
Reluctance (AT/Wb)
6.0E+07
5.0E+07
4.0E+07
3.0E+07
2.0E+07
1.0E+07
0.0E+00
0
5
10
15
20
Coil OD (mm)
FEA
Cullen

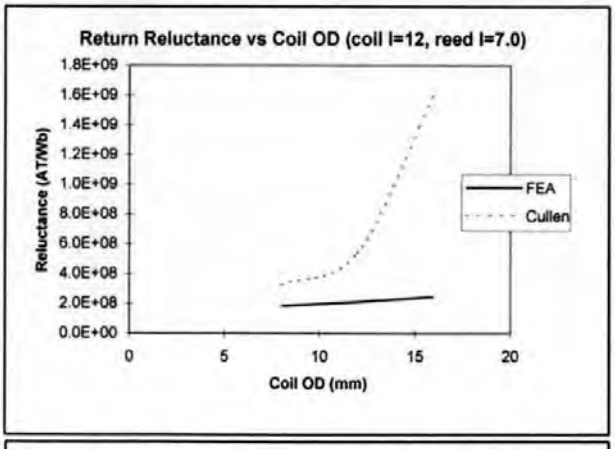
Return Reluctance vs Coil OD (coil l=12, reed l=7.0)
Reluctance (AT/Wb)
1.8E+09
1.6E+09
1.4E+09
1.2E+09
1.0E+09
8.0E+08
6.0E+08
4.0E+08
2.0E+08
0.0E+00
0
5
10
15
20
Coil OD (mm)
FEA
Cullen

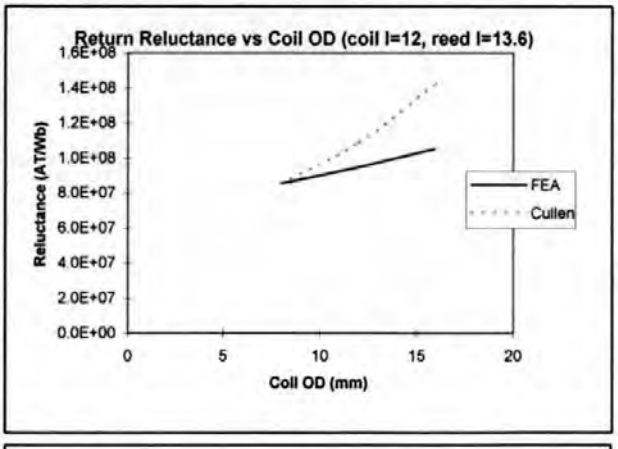
Return Reluctance vs Coil OD (coil l=12, reed l=13.6)
Reluctance (AT/Wb)
1.6E+08
1.4E+08
1.2E+08
1.0E+08
8.0E+07
6.0E+07
4.0E+07
2.0E+07
0.0E+00
0
5
10
15
20
Coil OD (mm)
FEA
Cullen

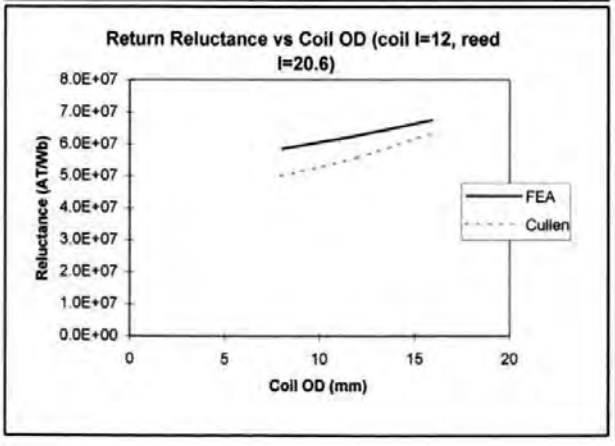
Return Reluctance vs Coil OD (coil l=12, reed l=20.6)
Reluctance (AT/Wb)
8.0E+07
7.0E+07
6.0E+07
5.0E+07
4.0E+07
3.0E+07
2.0E+07
1.0E+07
0.0E+00
0
5
10
15
20
Coil OD (mm)
FEA
Cullen

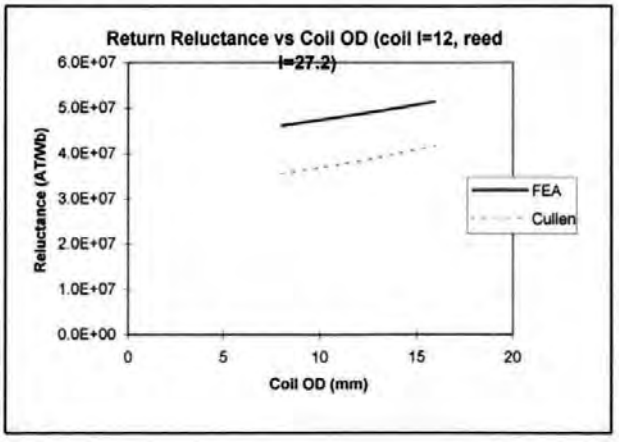
Return Reluctance vs Coil OD (coil l=12, reed l=27.2)
Reluctance (AT/Wb)
6.0E+07
5.0E+07
4.0E+07
3.0E+07
2.0E+07
1.0E+07
0.0E+00
0
5
10
15
20
Coil OD (mm)
FEA
Cullen

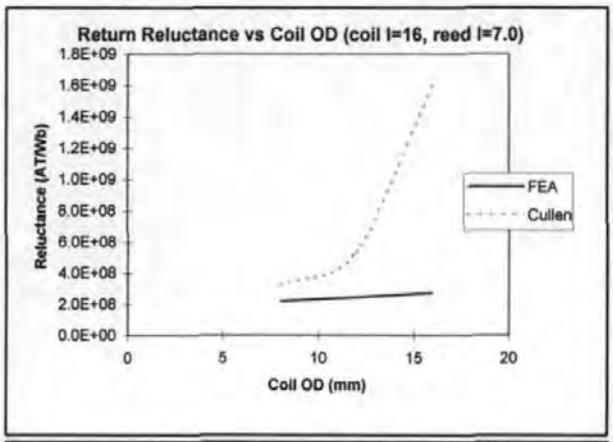
Return Reluctance vs Coil OD (coil l=16, reed l=7.0)
Reluctance (AT/Wb)
1.8E+09
1.6E+09
1.4E+09
1.2E+09
1.0E+09
8.0E+08
6.0E+08
4.0E+08
2.0E+08
0.0E+00
0
5
10
15
20
Coil OD (mm)
FEA
Cullen

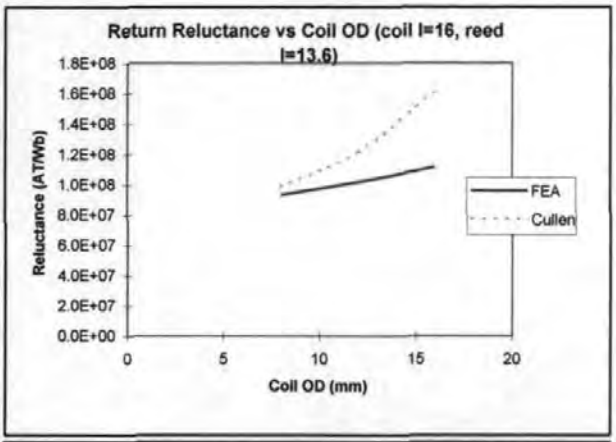
Return Reluctance vs Coil OD (coil l=16, reed l=13.6)
Reluctance (AT/Wb)
1.8E+08
1.6E+08
1.4E+08
1.2E+08
1.0E+08
8.0E+07
6.0E+07
4.0E+07
2.0E+07
0.0E+00
0
5
10
15
20
Coil OD (mm)
FEA
Cullen

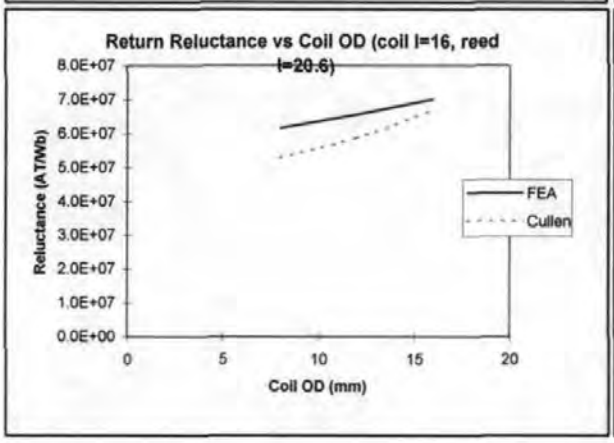
Return Reluctance vs Coil OD (coil l=16, reed l=20.6)
Reluctance (AT/Wb)
8.0E+07
7.0E+07
6.0E+07
5.0E+07
4.0E+07
3.0E+07
2.0E+07
1.0E+07
0.0E+00
0
5
10
15
20
Coil OD (mm)
FEA
Cullen

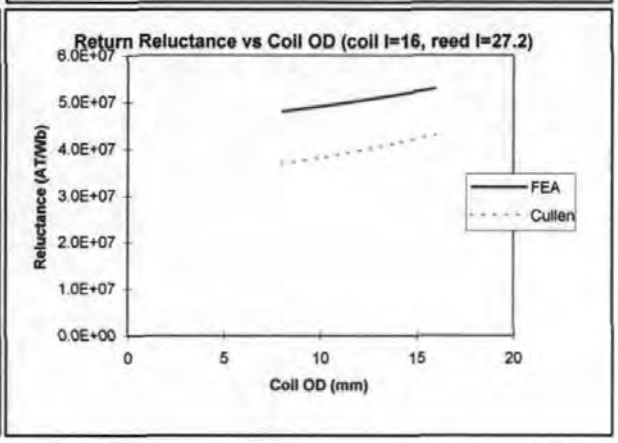
Return Reluctance vs Coil OD (coil l=16, reed l=27.2)
Reluctance (AT/Wb)
6.0E+07
5.0E+07
4.0E+07
3.0E+07
2.0E+07
1.0E+07
0.0E+00
0
5
10
15
20
Coil OD (mm)
FEA
Cullen

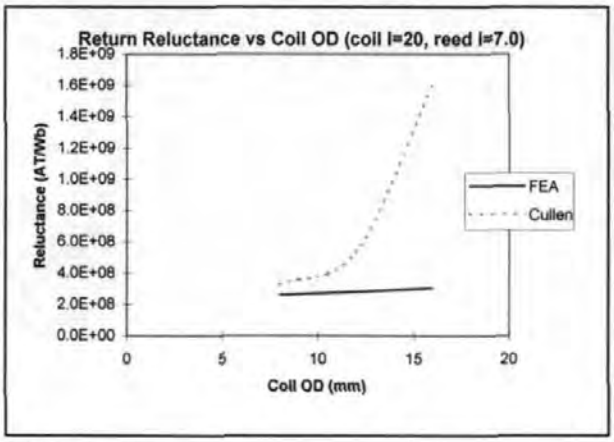
Return Reluctance vs Coil OD (coil l=20, reed l=7.0)
Reluctance (AT/Wb)
1.8E+09
1.6E+09
1.4E+09
1.2E+09
1.0E+09
8.0E+08
6.0E+08
4.0E+08
2.0E+08
0.0E+00
0
5
10
15
20
Coil OD (mm)
FEA
Cullen

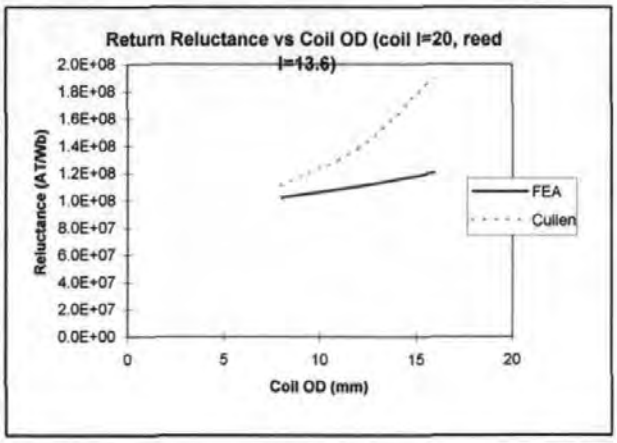
Return Reluctance vs Coil OD (coil l=20, reed l=13.6)
Reluctance (AT/Wb)
2.0E+08
1.8E+08
1.6E+08
1.4E+08
1.2E+08
1.0E+08
8.0E+07
6.0E+07
4.0E+07
2.0E+07
0.0E+00
0
5
10
15
20
Coil OD (mm)
FEA
Cullen

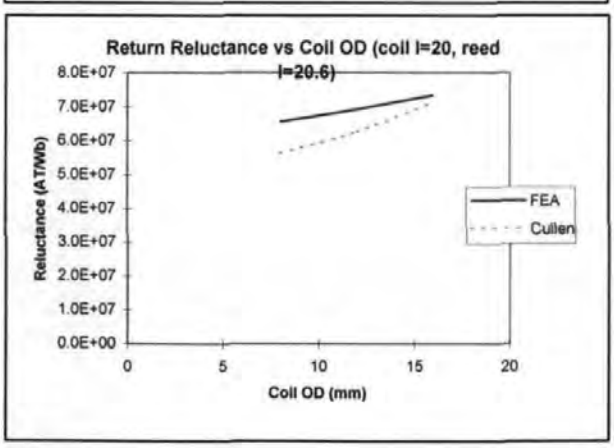
Return Reluctance vs Coil OD (coil l=20, reed l=20.6)
Reluctance (AT/Wb)
8.0E+07
7.0E+07
6.0E+07
5.0E+07
4.0E+07
3.0E+07
2.0E+07
1.0E+07
0.0E+00
0
5
10
15
20
Coil OD (mm)
FEA
Cullen

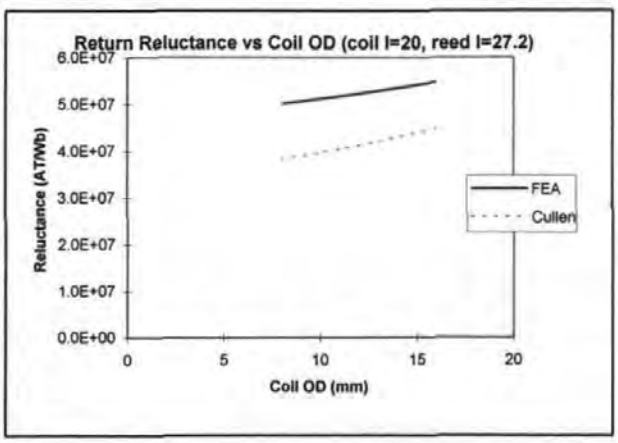
Return Reluctance vs Coil OD (coil l=20, reed l=27.2)
Reluctance (AT/Wb)
6.0E+07
5.0E+07
4.0E+07
3.0E+07
2.0E+07
1.0E+07
0.0E+00
0
5
10
15
20
Coil OD (mm)
FEA
Cullen

Appendix 3 – Fringing Reluctance vs. Coil and Reed Dimensions (FEA Results)

Selected results for fringing reluctance calculated from the 2D axisymmetric finite element model are presented and discussed in section 2.2.5. It was not appropriate to include all the data obtained at this point. The full set of results collected from the model are shown below and overleaf. In all cases the contact gap was fixed at 0.04mm (S_g=1.3*10^8).

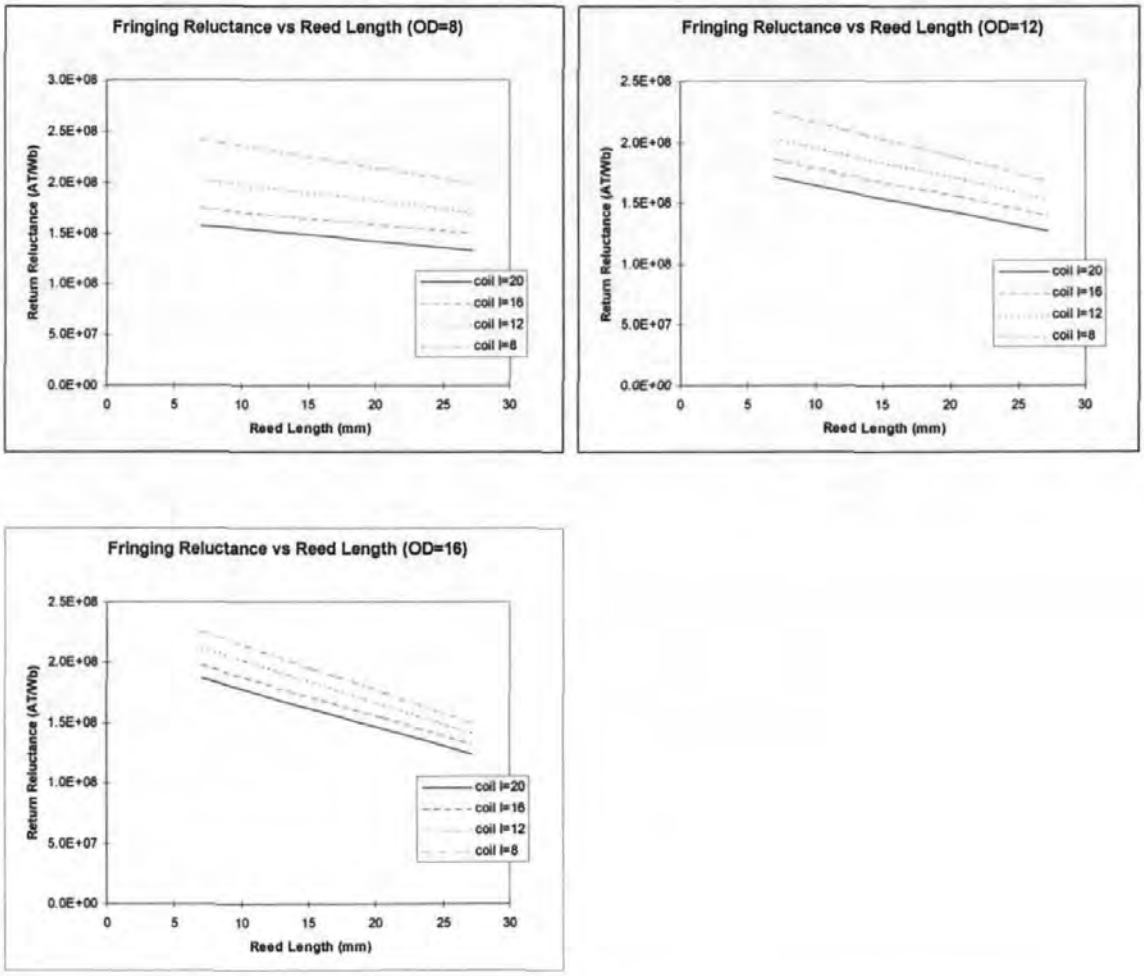

Figure A3.1 – Variation of Fringing Reluctance with Reed Length

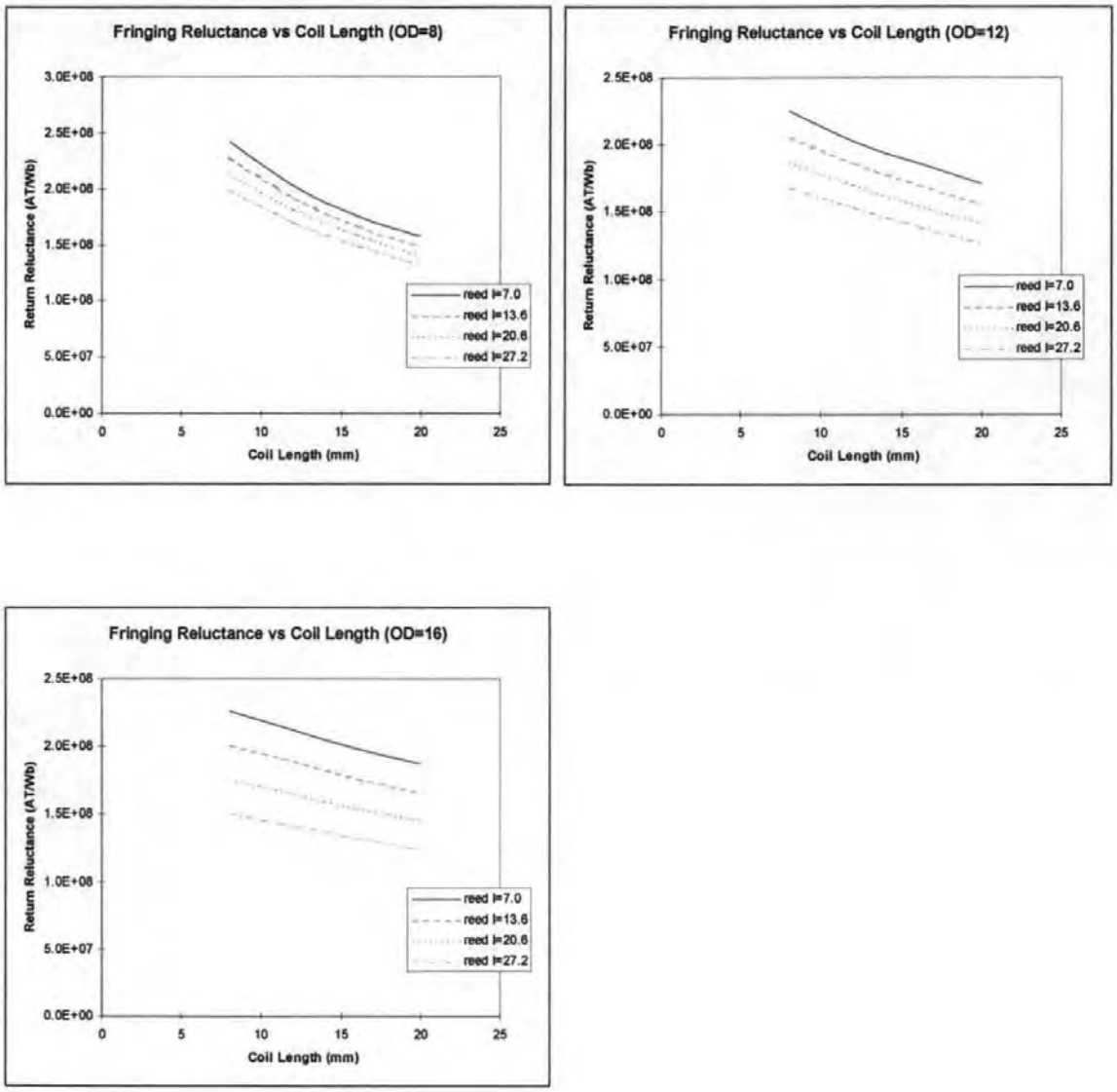

Figure A3.2 – Variation in Fringing Reluctance with Coil Length

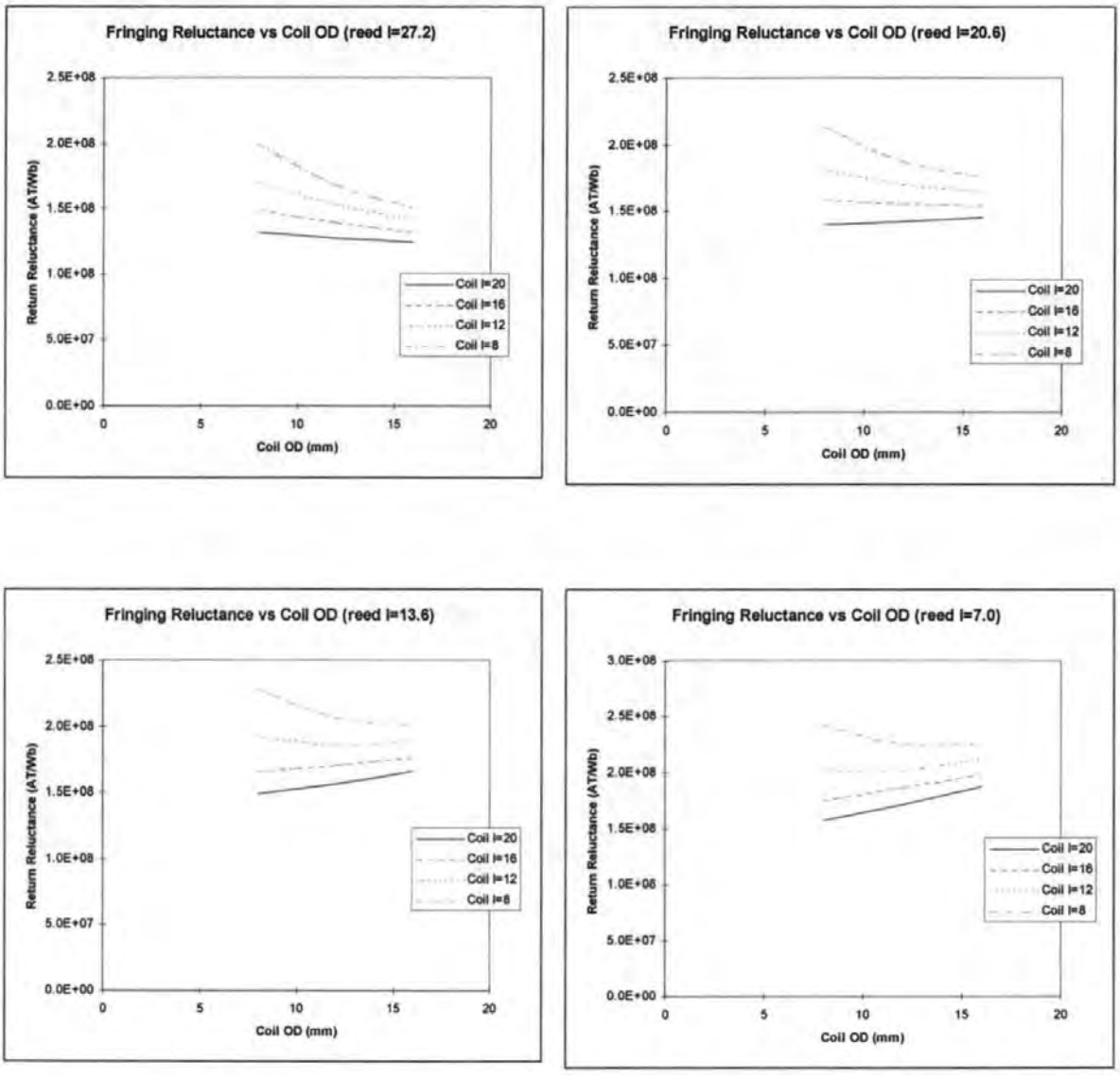

Figure A3.3 – Variation in Fringing Reluctance with Coil Outside Diameter

Appendix 4 – Fringing Reluctance vs. Contact Gap Reluctance (FEA Results)

Selected results for the variation in fringing reluctance with contact gap reluctance calculated from the 2D axisymmetric finite element model are presented and discussed in section 2.2.5. It was not appropriate to include all the data obtained at this point. Further results are shown below.

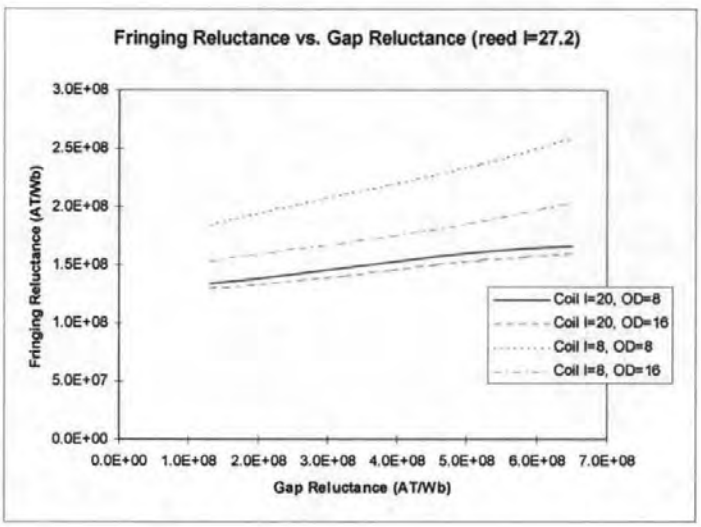

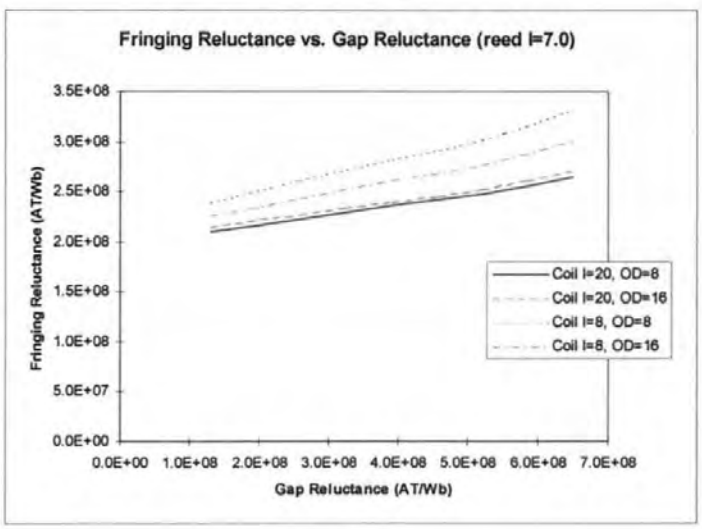

Figure A4.1 – Fringing Reluctance vs. Gap Reluctance

Appendix 5 – Reed Switch Design Program Listing

An annotated listing of the Reed Switch Design Program, as described in section 2.6 and written using Mathcad software, is provided overleaf.

Calculation of "SRA 83X" Blade Performance

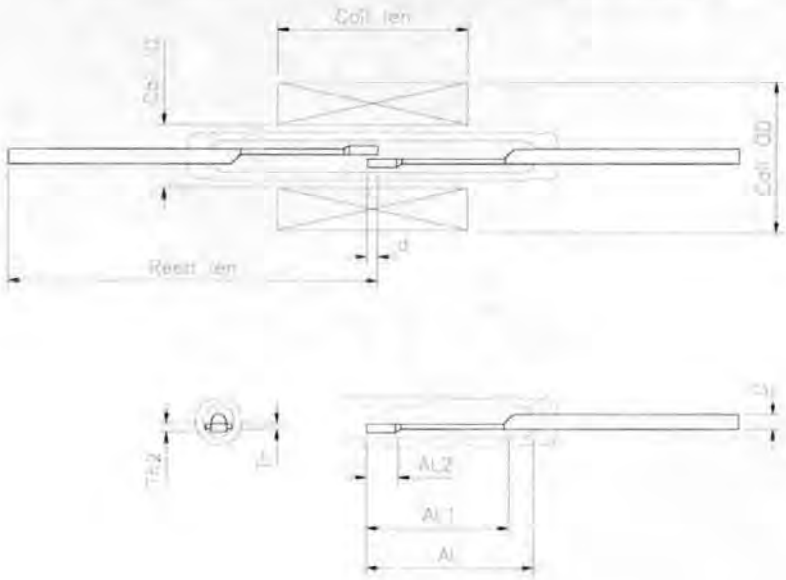

USER DEFINED VARIABLES

$Th_0 := 0.010 \cdot 25.4 \cdot 10^{-3}$ **Thickness of middle flat section(m) - First Blade**

$Th_1 := 0.010 \cdot 25.4 \cdot 10^{-3}$ **Thickness of middle flat section(m) - Second Blade**

$Th = \begin{matrix} 0.00025 \\ 0.00025 \end{matrix}$

$Th2_0 := 0.010 \cdot 25.4 \cdot 10^{-3}$ **Thickness of end flat section(m) - First Blade**

$Th2_1 := 0.010 \cdot 25.4 \cdot 10^{-3}$ **Thickness of end flat section(m) - Second Blade**

$Th2 = \begin{matrix} 0.00025 \\ 0.00025 \end{matrix}$

$AL_0 := 8.5 \cdot 10^{-3}$ **Reed length inside the glass(m) - First Blade**

$AL_1 := 8.0 \cdot 10^{-3}$ **Reed length inside the glass(m) - Second Blade**

$AL = \begin{matrix} 0.0085 \\ 0.008 \end{matrix}$

$AL1_0 := \left(6.6 + \frac{0.3}{2}\right) \cdot 10^{-3}$ **Reed middle flat section length (m) - First Blade**

$AL1_1 := 6.0 \cdot 10^{-3}$ **Reed middle flat section length (m) - Second Blade**

$AL1 = \begin{matrix} 0.00675 \\ 0.006 \end{matrix}$

$AL2_0 := \left(2.795 - \frac{0.2}{2}\right) \cdot 10^{-3}$ **Reed end flat section length (m) - First Blade**

$AL2_1 := \left(2.795 - \frac{0.2}{2}\right) \cdot 10^{-3}$ **Reed end flat section length (m) - Second Blade**

$AL2 = \begin{matrix} 0.0027 \\ 0.0027 \end{matrix}$

$D := 0.022 \cdot 25.4 \cdot 10^{-3}$ **Reed diameter (m) - First blade** $D = 0.00056$

$Di := 0.015 \cdot 25.4 \cdot 10^{-3}$ **Tube inner diameter (m) - Second blade** $Di = 0.00038$

$Do := 0.030 \cdot 25.4 \cdot 10^{-3}$ **Tube outer diameter (m) - Second blade** $Do = 0.00076$

$d := 0.28 \cdot 10^{-3}$ **Depth of overlap (m)** $d = 0.00028$

$b := 0.85 \cdot 10^{-3}$ **Width of blade tip at overlap point** $b = 0.00085$

$NMG := 0.006 \cdot 10^{-3}$ **Plating thickness (m) - SRA830**

$reedlen := 27.2 \cdot 10^{-3}$ **Length of a single reed (m).**

$coillen := 19.0 \cdot 10^{-3}$ **Length of the coil (m)**

$coilOD := 7.6 \cdot 10^{-3}$ **Coil winding outside diameter (m)**

CONSTANTS

$\mu := 1.256637 \cdot 10^{-6}$ **Permeability of free space (Wb/AT.m)**

$\varepsilon := 8.854188 \cdot 10^{-12}$ **Permitivity of free space**

$E := 15.47 \cdot 10^{10}$ **N/m2**

COUNTER VARIABLES

$bl := 0, 1 .. 1$ **Blade identification ; 0 or 1 (for asymmetric blades)**

$cg := 0, 1 .. 49$ **Gap counter**

$g_{cg} := (0.00022 \cdot (cg + 1))^2$ **Main gap, excluding plating thickness (m)** $g_0 \cdot 1000 = 0.00005$ $g_{49} \cdot 1000 = 0.121$

$cn := 0, 1 .. 19$ **amp-turn counter**

$at_{cn} := (cn \cdot 5) + 5$ **Range of amp-turns to be used in calculations** $at_0 = 5$
Note that altering this range will affect CR calcs. $at_{19} = 100$

Initial Calculations

$a := \pi \cdot \frac{D^2}{4}$ **Reed cross-sectional area (mm2)** $a = 2.45246 \cdot 10^{-7}$

$l := coillen \cdot \frac{4}{3}$ **Assumed reed length (mm)** $l = 0.02533$

$t := \frac{Th2_0 + Th2_1}{2}$ **Average thickness of blades at tip(mm)** $t = 0.00025$

$L3 := AL - \frac{d}{2}$ **Distance from the seal to the middle of the overlap** $L3 = \begin{matrix} 0.00836 \\ 0.00786 \end{matrix}$

$L2 := AL - AL2$ **Distance from the seal to the end of middle section** $L2 = \begin{matrix} 0.00581 \\ 0.00531 \end{matrix}$

$L1 := AL - AL1$ **Distance from the seal to the end of the first section** $L1 = \begin{matrix} 0.00175 \\ 0.002 \end{matrix}$

Blade Stiffness Calculations

Calculate blade widths B and B2

$B_{bl} := \frac{\frac{\pi \cdot D^2}{4}}{Th_{bl}}$ $B = \begin{matrix} 0.00097 \\ 0.00097 \end{matrix}$ $B2_{bl} := \frac{\frac{\pi \cdot D^2}{4}}{Th2_{bl}}$ $B2 = \begin{matrix} 0.00097 \\ 0.00097 \end{matrix}$

Calculate I for the round section

$I1_0 := \frac{\pi \cdot D^4}{64}$ $I1 = 4.78625 \cdot 10^{-15}$ $I1_1 := \frac{\pi \cdot Do^4 - Di^4}{64}$ $I1_1 = 1.55153 \cdot 10^{-14}$

Calculate I for flat sections

$I2_{bl} := \frac{B_{bl} \cdot Th_{bl}^3}{12}$ $I2 = \begin{matrix} 1.31853 \cdot 10^{-15} \\ 1.31853 \cdot 10^{-15} \end{matrix}$

$I3_{bl} := \frac{B2_{bl} \cdot \left[Th2_{(bl)}\right]^3}{12}$ $I3 = \begin{matrix} 1.31853 \cdot 10^{-15} \\ 1.31853 \cdot 10^{-15} \end{matrix}$

$F := 1$ **N**

$$yl_{bl} := \frac{F}{6 \cdot E \cdot Il_{bl}} \cdot \left[3 \cdot L3_{bl} \cdot Ll_{bl}^{2} - Ll_{bl}^{3} \right]$$

$$y2_{bl} := \frac{F}{6 \cdot E \cdot I2_{bl}} \cdot \left[3 \cdot L3_{bl} \cdot L2_{bl}^{2} - L2_{bl}^{3} - 3 \cdot L3_{bl} \cdot Ll_{bl}^{2} + Ll_{bl}^{3} \right]$$

$$y3_{bl} := \frac{F}{6 \cdot E \cdot I3_{bl}} \cdot \left[2 \cdot L3_{bl}^{3} - 3 \cdot L3_{bl} \cdot L2_{bl}^{2} + L2_{bl}^{3} \right]$$

$$y_{bl} := yl_{bl} + y2_{bl} + y3_{bl} \qquad y = \begin{matrix} 0.00091 \\ 0.00073 \end{matrix}$$

$$st_{bl} := \frac{F}{y_{bl}} \qquad st = \begin{matrix} 1095.87099 \\ 1371.74253 \end{matrix} \quad \textbf{N/m}$$

$$stif := \frac{1}{\frac{1}{st_0} + \frac{1}{st_1}}$$ **(effect of two blade spring rates added in series)** $stif = 609.19298$ **N/m**

$stif \cdot \frac{1}{9.81} = 62.09918$ **g/mm**

Generation of Pull Curves

Range of Flux assummed - generated on basis of standard flux density values to link with BH data

$Q := 0, 1 .. 33$

$FL_Q := Q \cdot 5 \cdot 10^{-2} \cdot a$ **(Wb)**

Permeance for each sector of the contact gap field (c.f. "A Practical Theory for Reed Switches")

$$Pg_{cg} := \frac{\mu \cdot b \cdot d}{g_{cg}}$$

$$Pl_{cg} := \frac{\mu \cdot 4 \cdot b}{\pi} \cdot \ln\left(1 + \frac{t}{g_{cg}}\right)$$

$$P2_{cg} := \frac{\mu \cdot 2 \cdot d}{\pi} \cdot \ln\left(1 + \frac{2 \cdot t}{g_{cg}}\right)$$

$P3_{cg} := \mu \cdot 1.04 \cdot b$

$P4 := \mu \cdot 0.52 \cdot d$

$P5_{cg} := \mu \cdot 0.308 \cdot g_{cg}$

$P6 := \mu \cdot t$

The following section derives air return path reluctance from FEA results

Counter variables and coil length, od and reed length data which FEA results correspond to

$cl := 0, 1 .. 3$ $\quad rl := 0, 1 .. 3$ $\quad cd := 0, 1 .. 2$

$$coil\_l := \begin{bmatrix} 8 \\ 12 \\ 16 \\ 20 \end{bmatrix} \quad reed\_l := \begin{bmatrix} 7 \\ 13.6 \\ 20.6 \\ 27.2 \end{bmatrix} \quad coil\_od := \begin{matrix} 8 \\ 12 \\ 16 \end{matrix}$$

Return path reluctance for 8mm OD coils (no gap):

$$Rr8 := \begin{bmatrix} 1.54\cdot10^{8} & 1.80\cdot10^{8} & 2.15\cdot10^{8} & 2.57\cdot10^{8} \\ 7.90\cdot10^{7} & 8.52\cdot10^{7} & 9.28\cdot10^{7} & 1.02\cdot10^{8} \\ 5.53\cdot10^{7} & 5.82\cdot10^{7} & 6.15\cdot10^{7} & 6.54\cdot10^{7} \\ 4.41\cdot10^{7} & 4.59\cdot10^{7} & 4.79\cdot10^{7} & 5.01\cdot10^{7} \end{bmatrix}$$

Return path reluctance for 12mm OD coils (no gap):

$$Rr12 := \begin{bmatrix} 1.86\cdot10^{8} & 2.09\cdot10^{8} & 2.40\cdot10^{8} & 2.77\cdot10^{8} \\ 8.90\cdot10^{7} & 9.44\cdot10^{7} & 1.01\cdot10^{8} & 1.10\cdot10^{8} \\ 6.01\cdot10^{7} & 6.25\cdot10^{7} & 6.55\cdot10^{7} & 6.90\cdot10^{7} \\ 4.71\cdot10^{7} & 4.85\cdot10^{7} & 5.07\cdot10^{7} & 5.22\cdot10^{7} \end{bmatrix}$$

Return path reluctance for 16mm OD coils (no gap):

$$Rr16 := \begin{bmatrix} 2.23\cdot10^{8} & 2.43\cdot10^{8} & 2.70\cdot10^{8} & 3.03\cdot10^{8} \\ 1.00\cdot10^{8} & 1.05\cdot10^{8} & 1.11\cdot10^{8} & 1.20\cdot10^{8} \\ 6.53\cdot10^{7} & 6.74\cdot10^{7} & 7.00\cdot10^{7} & 7.32\cdot10^{7} \\ 5.02\cdot10^{7} & 5.14\cdot10^{7} & 5.29\cdot10^{7} & 5.47\cdot10^{7} \end{bmatrix}$$

Reed and coil dimensions used in interpolation

$reed := reedlen\cdot10^{3}$ **Reed length in mm** reed = 27.2

$coil := coillen\cdot10^{3}$ **Coil length in mm** coil = 19

$od := coilOD\cdot10^{3}$ **Coil OD in mm** od = 7.6

Interpolation for 8mm OD coil

"reed" and 8mm coil

$R_{rl} := Rr8_{rl,0}$ $vs := pspline(reed\_l, R)$ $R0 := interp(vs, reed\_l, R, reed)$

"reed" and 12mm coil

$R_{rl} := Rr8_{rl,1}$ $vs := pspline(reed\_l, R)$ $R1 := interp(vs, reed\_l, R, reed)$

"reed" and 16mm coil

$R_{rl} := Rr8_{rl,2}$ $vs := pspline(reed\_l, R)$ $R2 := interp(vs, reed\_l, R, reed)$

"reed" and 20mm coil

$R_{rl} := Rr8_{rl,3}$ $vs := pspline(reed\_l, R)$ $R3 := interp(vs, reed\_l, R, reed)$

$$Rr\_8 := \begin{bmatrix} R0 \\ R1 \\ R2 \\ R3 \end{bmatrix}$$

"reed" and "coil"

$vs := lspline(coil\_l, Rr\_8)$ $R8 := interp(vs, coil\_l, Rr\_8, coil)$

Return Path Reluctance (no gap) for 8mm coil OD

$R8 = 4.95406 \cdot 10^{7}$

Interpolation for 12mm OD coil

"reed" and 8mm coil

$R_{rl} := Rr12_{rl,0}$ vs := pspline(reed_l,R) R0 := interp(vs,reed_l,R,reed)

"reed" and 12mm coil

$R_{rl} := Rr12_{rl,1}$ vs := pspline(reed_l,R) R1 := interp(vs,reed_l,R,reed)

"reed" and 16mm coil

$R_{rl} := Rr12_{rl,2}$ vs := pspline(reed_l,R) R2 := interp(vs,reed_l,R,reed)

"reed" and 20mm coil

$R_{rl} := Rr12_{rl,3}$ vs := pspline(reed_l,R) R3 := interp(vs,reed_l,R,reed)

$$Rr\_12 := \begin{bmatrix} R0 \\ R1 \\ R2 \\ R3 \end{bmatrix}$$

"reed" and "coil"

vs := lspline(coil_l,Rr_12) R12 := interp(vs,coil_l,Rr_12,coil)

Return Path Reluctance (no gap) for 12mm coil OD

$R12 = 5.18813 \cdot 10^{7}$

Interpolation for 16mm OD coil

"reed" and 8mm coil

$R_{rl} := Rr16_{rl,0}$ vs := pspline(reed_l,R) R0 := interp(vs,reed_l,R,reed)

"reed" and 12mm coil

$R_{rl} := Rr16_{rl,1}$ vs := pspline(reed_l,R) R1 := interp(vs,reed_l,R,reed)

"reed" and 16mm coil

$R_{rl} := Rr16_{rl,2}$ vs := pspline(reed_l,R) R2 := interp(vs,reed_l,R,reed)

"reed" and 20mm coil

$R_{rl} := Rr16_{rl,3}$ vs := pspline(reed_l,R) R3 := interp(vs,reed_l,R,reed)

$$Rr\_16 := \begin{bmatrix} R0 \\ R1 \\ R2 \\ R3 \end{bmatrix}$$

"reed" and "coil"

vs := lspline(coil_l,Rr_16) R16 := interp(vs,coil_l,Rr_16,coil)

Return Path Reluctance (no gap) for 16mm coil OD

$R16 = 5.42359 \cdot 10^{7}$

Interpolate between results for 8,12 and 16mm od coils to find return path reluctance (no gap)

$$Rret := \begin{matrix} R8 \\ R12 \\ R16 \end{matrix} \qquad Rret = \begin{matrix} 4.95406 \cdot 10^7 \\ 5.18813 \cdot 10^7 \\ 5.42359 \cdot 10^7 \end{matrix}$$

$vs := lspline(coil\_od, Rret)$ $\quad Rreturn := interp(vs, coil\_od, Rret, od)$ $\quad Rreturn = 4.93069 \cdot 10^7$

Function to model change in return path reluctance with working gap reluctance, Rg

$o := -4.5 \cdot 10^{-18}$

$p := \frac{1}{(reed + 13.2)} \cdot (0.275 \cdot od + 2.6) \cdot 10^{-8}$ $\quad p = 1.16089 \cdot 10^{-9}$

$q := 1$

$fn_{cg} := o \cdot \left(\frac{1}{Pg_{cg}}\right)^2 + p \cdot \frac{1}{Pg_{cg}} + q$

$R\_return_{cg} := Rreturn \cdot fn_{cg}$

The following section derives fringing (leakage) reluctance from FEA results

Fringing reluctance for 8mm OD coils (R gap=1.3e8):

$$Rfr8 := \begin{bmatrix} 2.42 \cdot 10^8 & 2.02 \cdot 10^8 & 1.75 \cdot 10^8 & 1.57 \cdot 10^8 \\ 2.28 \cdot 10^8 & 1.92 \cdot 10^8 & 1.66 \cdot 10^8 & 1.49 \cdot 10^8 \\ 2.13 \cdot 10^8 & 1.81 \cdot 10^8 & 1.58 \cdot 10^8 & 1.40 \cdot 10^8 \\ 1.99 \cdot 10^8 & 1.70 \cdot 10^8 & 1.49 \cdot 10^8 & 1.32 \cdot 10^8 \end{bmatrix}$$

Fringing reluctance for 12mm OD coils (R gap=1.3e8):

$$Rfr12 := \begin{bmatrix} 2.25 \cdot 10^8 & 2.02 \cdot 10^8 & 1.86 \cdot 10^8 & 1.71 \cdot 10^8 \\ 2.06 \cdot 10^8 & 1.86 \cdot 10^8 & 1.70 \cdot 10^8 & 1.56 \cdot 10^8 \\ 1.87 \cdot 10^8 & 1.70 \cdot 10^8 & 1.55 \cdot 10^8 & 1.42 \cdot 10^8 \\ 1.68 \cdot 10^8 & 1.53 \cdot 10^8 & 1.39 \cdot 10^8 & 1.27 \cdot 10^8 \end{bmatrix}$$

Fringing reluctance for 16mm OD coils (R gap=1.3e8):

$$Rfr16 := \begin{bmatrix} 2.26 \cdot 10^8 & 2.12 \cdot 10^8 & 1.98 \cdot 10^8 & 1.87 \cdot 10^8 \\ 2.01 \cdot 10^8 & 1.89 \cdot 10^8 & 1.76 \cdot 10^8 & 1.66 \cdot 10^8 \\ 1.75 \cdot 10^8 & 1.65 \cdot 10^8 & 1.54 \cdot 10^8 & 1.45 \cdot 10^8 \\ 1.50 \cdot 10^8 & 1.41 \cdot 10^8 & 1.32 \cdot 10^8 & 1.24 \cdot 10^8 \end{bmatrix}$$

Interpolation for 8mm OD coil

"reed" and 8mm coil

$R_{rl} := Rfr8_{rl,0}$ vs := pspline(reed_l, R) R0 := interp(vs, reed_l, R, reed)

"reed" and 12mm coil

$R_{rl} := Rfr8_{rl,1}$ vs := pspline(reed_l, R) R1 := interp(vs, reed_l, R, reed)

"reed" and 16mm coil

$R_{rl} := Rfr8_{rl,2}$ vs := pspline(reed_l, R) R2 := interp(vs, reed_l, R, reed)

"reed" and 20mm coil

$R_{rl} := Rfr8_{rl,3}$ vs := pspline(reed_l, R) R3 := interp(vs, reed_l, R, reed)

$$Rfr\_8 := \begin{bmatrix} R0 \\ R1 \\ R2 \\ R3 \end{bmatrix}$$

"reed" and "coil"

vs := lspline(coil_l, Rfr_8) Rfr8 := interp(vs, coil_l, Rfr_8, coil)

Interpolation for 12mm OD coil

"reed" and 8mm coil

$R_{rl} := Rfr12_{rl,0}$ vs := pspline(reed_l, R) R0 := interp(vs, reed_l, R, reed)

"reed" and 12mm coil

$R_{rl} := Rfr12_{rl,1}$ vs := pspline(reed_l, R) R1 := interp(vs, reed_l, R, reed)

"reed" and 16mm coil

$R_{rl} := Rfr12_{rl,2}$ vs := pspline(reed_l, R) R2 := interp(vs, reed_l, R, reed)

"reed" and 20mm coil

$R_{rl} := Rfr12_{rl,3}$ vs := pspline(reed_l, R) R3 := interp(vs, reed_l, R, reed)

$$Rfr\_12 := \begin{bmatrix} R0 \\ R1 \\ R2 \\ R3 \end{bmatrix}$$

"reed" and "coil"

vs := lspline(coil_l, Rfr_12) Rfr12 := interp(vs, coil_l, Rfr_12, coil)

Fringing reluctance for 12mm coil od(R gap=1.3e8)

$Rfr12 = 1.29891 \cdot 10^{8}$

Interpolation for 16mm OD coil

"reed" and 8mm coil

$R_{rl} := Rfr16_{rl,0}$ vs := pspline(reed_l, R) R0 := interp(vs, reed_l, R, reed)

"reed" and 12mm coil

$R_{rl} := Rfr16_{rl,1}$ vs := pspline(reed_l, R) R1 := interp(vs, reed_l, R, reed)

"reed" and 16mm coil

$R_{rl} := Rfr16_{rl,2}$ vs := pspline(reed_l, R) R2 := interp(vs, reed_l, R, reed)

"reed" and 20mm coil

$R_{rl} := Rfr16_{rl,3}$ vs := pspline(reed_l, R) R3 := interp(vs, reed_l, R, reed)

$$Rfr\_16 := \begin{bmatrix} R0 \\ R1 \\ R2 \\ R3 \end{bmatrix}$$

"reed" and "coil"

vs := lspline(coil_l, Rfr_16) Rfr16 := interp(vs, coil_l, Rfr_16, coil)

Fringing reluctance for 16mm coil od(R gap=1.3e8)

$Rfr16 = 1.25938 \cdot 10^8$

Interpolate between results for 8,12 and 16mm od coils to find the fringing reluctance (R gap=1.3e8)

$$Rfringe := \begin{matrix} Rfr8 \\ Rfr12 \\ Rfr16 \end{matrix} \qquad Rfringe = \begin{matrix} 1.36125 \cdot 10^8 \\ 1.29891 \cdot 10^8 \\ 1.25938 \cdot 10^8 \end{matrix}$$

vs := lspline(coil_od, Rfringe) Rfr := interp(vs, coil_od, Rfringe, od) $Rfr = 1.36805 \cdot 10^8$

Pfr is the permeance of the fringing path around the gap which does not create any force between the blades

u := 0.9

$$m := \frac{(1-u)\cdot Rfr}{1.30\cdot 10^8} \qquad m = 0.10523$$

$c := u \cdot Rfr$ $c = 1.23124 \cdot 10^8$

$$Rfr_{cg} := m \cdot \frac{1}{Pg_{cg}} + c$$

$$Pfr_{cg} := \frac{1}{Rfr_{cg}}$$

Total gap permeance and reluctance

$$P\_cull_{cg} := Pg_{cg} + P1_{cg} + P2_{cg} + P3_{cg} + P4 + P5_{cg} + P6 + Pfr_{cg}$$

$$R\_gap_{cg} := \frac{1}{P\_cull_{cg}}$$

dP/dg for all non-zero components of gap permeance

$$dPg_{cg} := \frac{\mu \cdot b \cdot d}{g_{cg}^2}$$

$$dP1_{cg} := \frac{\mu \cdot 4 \cdot b}{\pi} \cdot \frac{g_{cg}}{t + g_{cg}}$$

$$dP2_{cg} := \frac{\mu \cdot 2 \cdot d}{\pi} \cdot \frac{g_{cg}}{g_{cg} + 2 \cdot t}$$

$$dP5 := 0.308 \cdot \mu$$

$$dP\_cull_{cg} := dPg_{cg} + dP1_{cg} + dP2_{cg} + dP5$$

Nickel Iron Permeability or B-H Curve

$cpc := 0, 1 .. 19$

$N_{cpc} := cpc \cdot 4.1883 \cdot 10^{-3}$

$N_{20} := 0.0875$ $N_{21} := 0.0955$ $N_{22} := 0.1273$

$N_{23} := 0.1512$ $N_{24} := 0.1910$ $N_{25} := 0.2467$ $N_{26} := 0.3024$ $N_{27} := 0.3979$ $N_{28} := 0.5013$ $N_{29} := 0.6366$

$N_{30} := 0.8157$ $N_{31} := 1.1618$ $N_{32} := 2.1088$ $N_{33} := 10^6$

Flux Density, B (Wb/mm2)

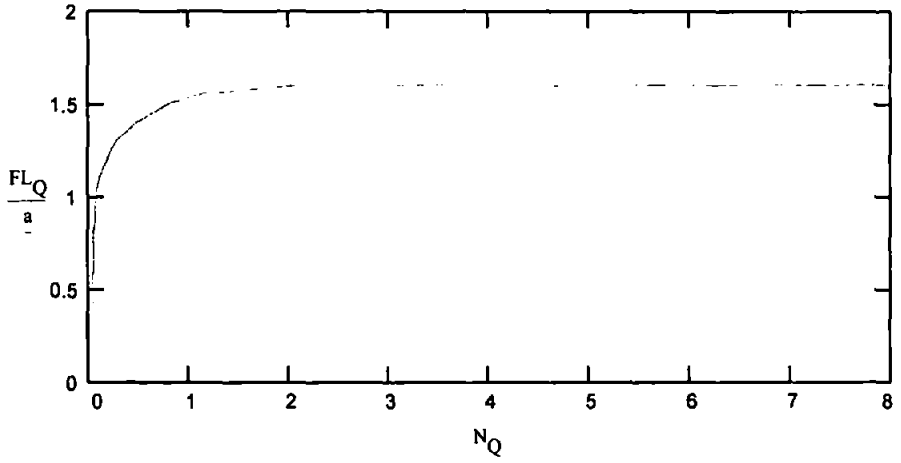

Field Strength, H (AT/mm)

Reluctance of NiFe blades

$$R\_blades_Q := \frac{N_Q \cdot l \cdot 10^3}{FL_Q}$$

mmf across return path, reeds and contact gap

$mmf_{cg,Q} := FL_Q \cdot (R\_return_{cg} + R\_blades_Q + R\_gap_{cg})$

$p := 0, 1 .. 32$

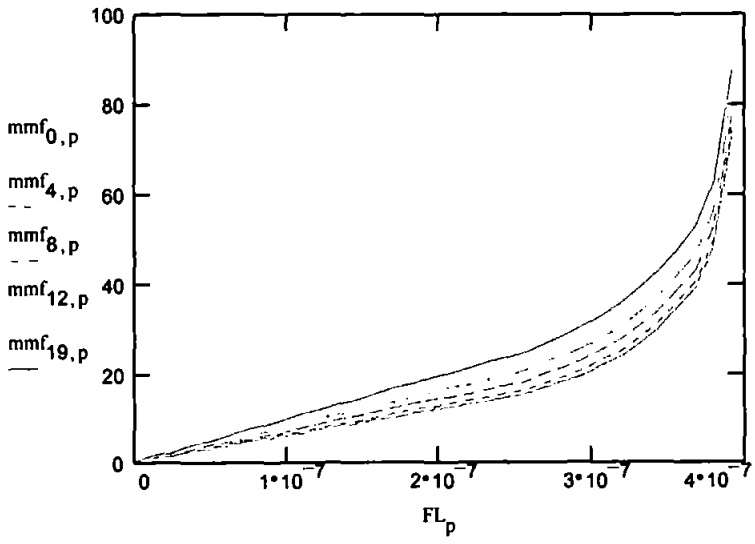

Interpolation to find the flux across the contact gap corresponding to various AT applied to the whole circuit

$v_Q := mmf_{0,Q}$ $vs := pspline(v, FL)$ $Y_{cn,0} := interp\ vs, v, FL, at_{cn}$

$v_Q := mmf_{1,Q}$ $vs := pspline(v, FL)$ $Y_{cn,1} := interp\ vs, v, FL, at_{cn}$

$v_Q := mmf_{2,Q}$ $vs := pspline(v, FL)$ $Y_{cn,2} := interp\ vs, v, FL, at_{cn}$

$v_Q := mmf_{3,Q}$ $vs := pspline(v, FL)$ $Y_{cn,3} := interp\ vs, v, FL, at_{cn}$

$v_Q := mmf_{4,Q}$ $vs := pspline(v, FL)$ $Y_{cn,4} := interp\ vs, v, FL, at_{cn}$

$v_Q := mmf_{5,Q}$ $vs := pspline(v, FL)$ $Y_{cn,5} := interp\ vs, v, FL, at_{cn}$

$v_Q := mmf_{6,Q}$ $vs := pspline(v, FL)$ $Y_{cn,6} := interp\ vs, v, FL, at_{cn}$

$v_Q := mmf_{7,Q}$ $vs := pspline(v, FL)$ $Y_{cn,7} := interp\ vs, v, FL, at_{cn}$

$v_Q := mmf_{8,Q}$ $vs := pspline(v, FL)$ $Y_{cn,8} := interp\ vs, v, FL, at_{cn}$

$v_Q := mmf_{9,Q}$ $vs := pspline(v, FL)$ $Y_{cn,9} := interp\ vs, v, FL, at_{cn}$

$v_Q := mmf_{10,Q}$ $vs := pspline(v, FL)$ $Y_{cn,10} := interp\ vs, v, FL, at_{cn}$

$v_Q := mmf_{11,Q}$ $vs := pspline(v, FL)$ $Y_{cn,11} := interp\ vs, v, FL, at_{cn}$

$v_Q := mmf_{12,Q}$ $vs := pspline(v, FL)$ $Y_{cn,12} := interp\ vs, v, FL, at_{cn}$

$v_Q := mmf_{13,Q}$ $vs := pspline(v, FL)$ $Y_{cn,13} := interp\ vs, v, FL, at_{cn}$

$v_Q := mmf_{14,Q}$ $vs := pspline(v, FL)$ $Y_{cn,14} := interp\ vs, v, FL, at_{cn}$

$v_Q := mmf_{15,Q}$ $vs := pspline(v, FL)$ $Y_{cn,15} := interp\ vs, v, FL, at_{cn}$

$v_Q := mmf_{16,Q}$ $vs := pspline(v, FL)$ $Y_{cn,16} := interp\ vs, v, FL, at_{cn}$

$v_Q := mmf_{17,Q}$ $vs := pspline(v, FL)$ $Y_{cn,17} := interp\ vs, v, FL, at_{cn}$

$v_Q := mmf_{18,Q}$ $vs := pspline(v, FL)$ $Y_{cn,18} := interp\ vs, v, FL, at_{cn}$

$v_Q := mmf_{19,Q}$ $vs := pspline(v, FL)$ $Y_{cn,19} := interp\ vs, v, FL, at_{cn}$

$v_Q := mmf_{20,Q}$ $vs := pspline(v, FL)$ $Y_{cn,20} := interp\ vs, v, FL, at_{cn}$

$v_Q := mmf_{21,Q}$ $vs := pspline(v, FL)$ $Y_{cn,21} := interp\ vs, v, FL, at_{cn}$

$v_Q := mmf_{22,Q}$ $vs := pspline(v, FL)$ $Y_{cn,22} := interp\ vs, v, FL, at_{cn}$

$v_Q := mmf_{23,Q}$ $vs := pspline(v, FL)$ $Y_{cn,23} := interp\ vs, v, FL, at_{cn}$

$v_Q := mmf_{24,Q}$ $vs := pspline(v, FL)$ $Y_{cn,24} := interp\ vs, v, FL, at_{cn}$

$v_Q := mmf_{25,Q}$ $vs := pspline(v, FL)$ $Y_{cn,25} := interp\ vs, v, FL, at_{cn}$

$v_Q := mmf_{26,Q}$ $vs := pspline(v, FL)$ $Y_{cn,26} := interp\ vs, v, FL, at_{cn}$

$v_Q := mmf_{27,Q}$ $vs := pspline(v, FL)$ $Y_{cn,27} := interp\ vs, v, FL, at_{cn}$

$v_Q := mmf_{28,Q}$ $vs := pspline(v, FL)$ $Y_{cn,28} := interp\ vs, v, FL, at_{cn}$

$v_Q := mmf_{29,Q}$ $vs := pspline(v, FL)$ $Y_{cn,29} := interp\ vs, v, FL, at_{cn}$

$v_Q := mmf_{30,Q}$ $vs := pspline(v, FL)$ $Y_{cn,30} := interp\ vs, v, FL, at_{cn}$

$v_Q := mmf_{31,Q}$ $vs := pspline(v, FL)$ $Y_{cn,31} := interp\ vs, v, FL, at_{cn}$

$v_Q := mmf_{32,Q}$ $vs := pspline(v, FL)$ $Y_{cn,32} := interp\ vs, v, FL, at_{cn}$

$v_Q := mmf_{33,Q}$ $vs := pspline(v, FL)$ $Y_{cn,33} := interp\ vs, v, FL, at_{cn}$

$v_Q := mmf_{34,Q}$ $vs := pspline(v, FL)$ $Y_{cn,34} := interp\ vs, v, FL, at_{cn}$

$v_Q := mmf_{35,Q}$ $vs := pspline(v, FL)$ $Y_{cn,35} := interp\ vs, v, FL, at_{cn}$

$v_Q := mmf_{36,Q}$ $vs := pspline(v, FL)$ $Y_{cn,36} := interp\ vs, v, FL, at_{cn}$

$v_Q := mmf_{37,Q}$ $vs := pspline(v, FL)$ $Y_{cn,37} := interp\ vs, v, FL, at_{cn}$

$v_Q := mmf_{38,Q}$ $vs := pspline(v, FL)$ $Y_{cn,38} := interp\ vs, v, FL, at_{cn}$

$v_Q := mmf_{39,Q}$ $vs := pspline(v, FL)$ $Y_{cn,39} := interp\ vs, v, FL, at_{cn}$

$v_Q := mmf_{40,Q}$ $vs := pspline(v, FL)$ $Y_{cn,40} := interp\ vs, v, FL, at_{cn}$

$v_Q := mmf_{41,Q}$ $vs := pspline(v, FL)$ $Y_{cn,41} := interp\ vs, v, FL, at_{cn}$

$v_Q := mmf_{42,Q}$ $vs := pspline(v, FL)$ $Y_{cn,42} := interp\ vs, v, FL, at_{cn}$

$v_Q := mmf_{43,Q}$ $vs := pspline(v, FL)$ $Y_{cn,43} := interp\ vs, v, FL, at_{cn}$

$v_Q := mmf_{44,Q}$ $vs := pspline(v, FL)$ $Y_{cn,44} := interp\ vs, v, FL, at_{cn}$

$v_Q := mmf_{45,Q}$ $vs := pspline(v, FL)$ $Y_{cn,45} := interp\ vs, v, FL, at_{cn}$

$v_Q := mmf_{46,Q}$ $vs := pspline(v, FL)$ $Y_{cn,46} := interp\ vs, v, FL, at_{cn}$

$v_Q := mmf_{47,Q}$ $vs := pspline(v, FL)$ $Y_{cn,47} := interp\ vs, v, FL, at_{cn}$

$v_Q := mmf_{48,Q}$ $vs := pspline(v, FL)$ $Y_{cn,48} := interp\ vs, v, FL, at_{cn}$

$v_Q := mmf_{49,Q}$ $vs := pspline(v, FL)$ $Y_{cn,49} := interp\ vs, v, FL, at_{cn}$

Graph of Flux against Gap for various Ampere-turns.

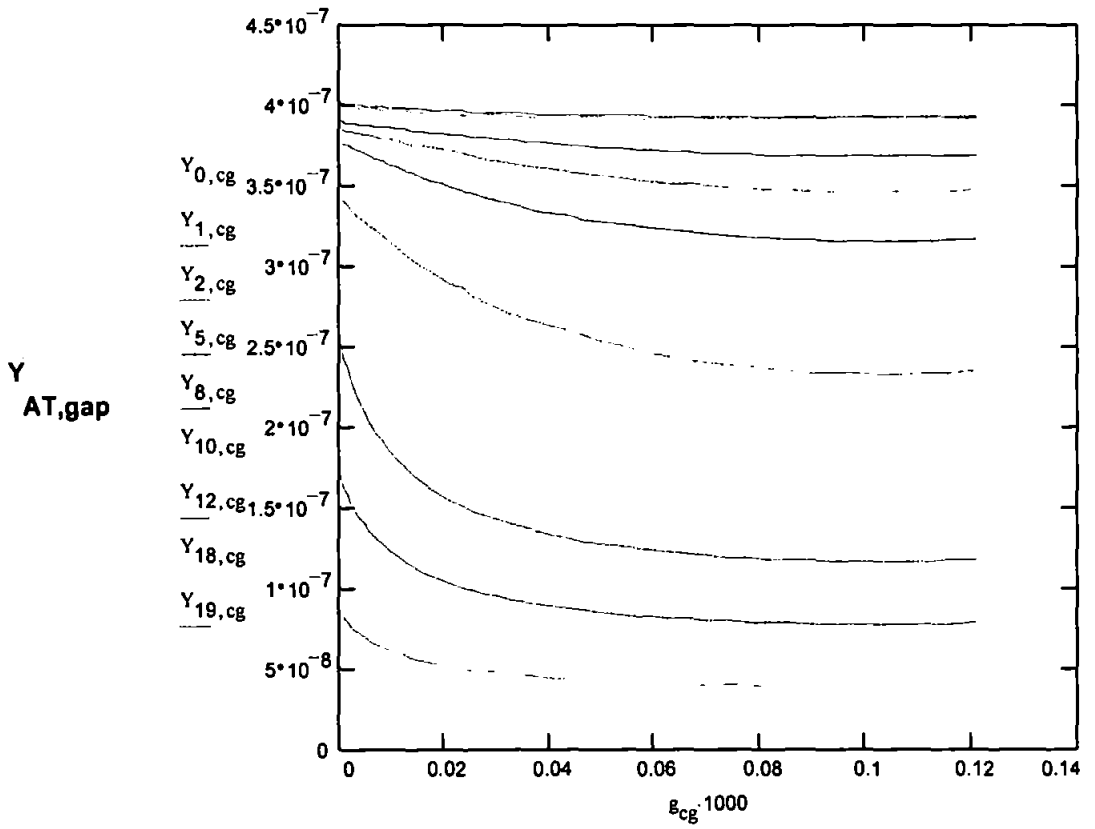

Total attractive force between reed blades

$$F\_cull_{cn,cg} := \frac{1}{2} \cdot \left(\frac{Y_{cn,cg}}{P\_cull_{cg}} \right)^2 \cdot dP\_cull_{cg}$$

Interpolate to find magnetic force at NMG

$w_{cg} := F\_cull_{0,cg}$ $ws := lspline(g, w)$ $FM_0 := interp(ws, g, w, NMG)$

$w_{cg} := F\_cull_{1,cg}$ $ws := lspline(g, w)$ $FM_1 := interp(ws, g, w, NMG)$

$w_{cg} := F\_cull_{2,cg}$ $ws := lspline(g, w)$ $FM_2 := interp(ws, g, w, NMG)$

$w_{cg} := F\_cull_{3,cg}$ $ws := lspline(g, w)$ $FM_3 := interp(ws, g, w, NMG)$

$w_{cg} := F\_cull_{4,cg}$ $ws := lspline(g, w)$ $FM_4 := interp(ws, g, w, NMG)$

$w_{cg} := F\_cull_{5,cg}$ $ws := lspline(g, w)$ $FM_5 := interp(ws, g, w, NMG)$

$w_{cg} := F\_cull_{6,cg}$ $ws := lspline(g, w)$ $FM_6 := interp(ws, g, w, NMG)$

$w_{cg} := F\_cull_{7,cg}$ $ws := lspline(g, w)$ $FM_7 := interp(ws, g, w, NMG)$

$w_{cg} := F\_cull_{8,cg}$ $ws := lspline(g, w)$ $FM_8 := interp(ws, g, w, NMG)$

$w_{cg} := F\_cull_{9,cg}$ $ws := lspline(g, w)$ $FM_9 := interp(ws, g, w, NMG)$

$w_{cg} := F\_cull_{10,cg}$ $ws := lspline(g, w)$ $FM_{10} := interp(ws, g, w, NMG)$

$w_{cg} := F\_cull_{11,cg}$ $ws := lspline(g, w)$ $FM_{11} := interp(ws, g, w, NMG)$

$w_{cg} := F\_cull_{12,cg}$ $ws := lspline(g, w)$ $FM_{12} := interp(ws, g, w, NMG)$

$w_{cg} := F\_cull_{13,cg}$ $ws := lspline(g, w)$ $FM_{13} := interp(ws, g, w, NMG)$

$w_{cg} := F\_cull_{14,cg}$ $ws := lspline(g, w)$ $FM_{14} := interp(ws, g, w, NMG)$

$w_{cg} := F\_cull_{15,cg}$ $ws := lspline(g, w)$ $FM_{15} := interp(ws, g, w, NMG)$

$w_{cg} := F\_cull_{16,cg}$ $ws := lspline(g, w)$ $FM_{16} := interp(ws, g, w, NMG)$

$w_{cg} := F\_cull_{17,cg}$ $ws := lspline(g, w)$ $FM_{17} := interp(ws, g, w, NMG)$

$w_{cg} := F\_cull_{18,cg}$ $ws := lspline(g, w)$ $FM_{18} := interp(ws, g, w, NMG)$

$w_{cg} := F\_cull_{19,cg}$ $ws := lspline(g, w)$ $FM_{19} := interp(ws, g, w, NMG)$

To find dF/dg:

$n := 0, 1 .. (last(g) - 1)$ $last(g) = 49$

$$m\_int_{cn,n} := \frac{F\_cull_{cn,n+1} - F\_cull_{cn,n}}{g_{n+1} - g_n}$$

Take average of gradients between data points to give gradients at data points

$nn := 1, 2 .. (last(g) - 1)$

$$m_{cn,nn} := \frac{1}{2} \cdot m\_int_{cn,nn} + m\_int_{cn,nn-1}$$

Approximate first data point - assume dF/dg is proportional to 1/gap^3 for very small gaps

$$m_{cn,0} := \left(\frac{g_1}{g_0}\right)^3 \cdot m_{cn,1}$$

Approximate last data point - assume constant rate of change of gradient over last points

$$m_{cn,last(g)} := m_{cn,last(g)-1} + 2 \cdot m\_int_{cn,last(g)-1} - m_{cn,last(g)-1}$$

$$dF\_cull_{cn,cg} := -m_{cn,cg}$$

Closure condition

$Closure_{cn,cg} := if\ dF\_cull_{cn,cg} > stif, 1, 0$

$$cl_{cn} := \sum_{cg} Closure_{cn,cg}$$

$stif = 609.19298$

Magnetic gap for given OAT

$$gap_{cn} := g_{cl_{cn}} + \frac{F\_cull_{cn,cl_{cn}}}{stif}$$

$$gap_{cn} := if\left[g_{cl_{cn}} > NMG, g_{cl_{cn}} + \frac{F\_cull_{cn,cl_{cn}}}{stif}, NMG + \frac{FM_{cn}}{stif}\right]$$

Stiffness line corresponding to operate condition

$STL_{cn,cg} := -stif \cdot g_{cg} + stif \cdot gap_{cn}$

$STL_{cn,cg} := \text{if } STL_{cn,cg} < 0, 0, STL_{cn,cg}$

$aa := 19 \qquad bb := 4,5..49$

$ba := 8$

$ca := 1$

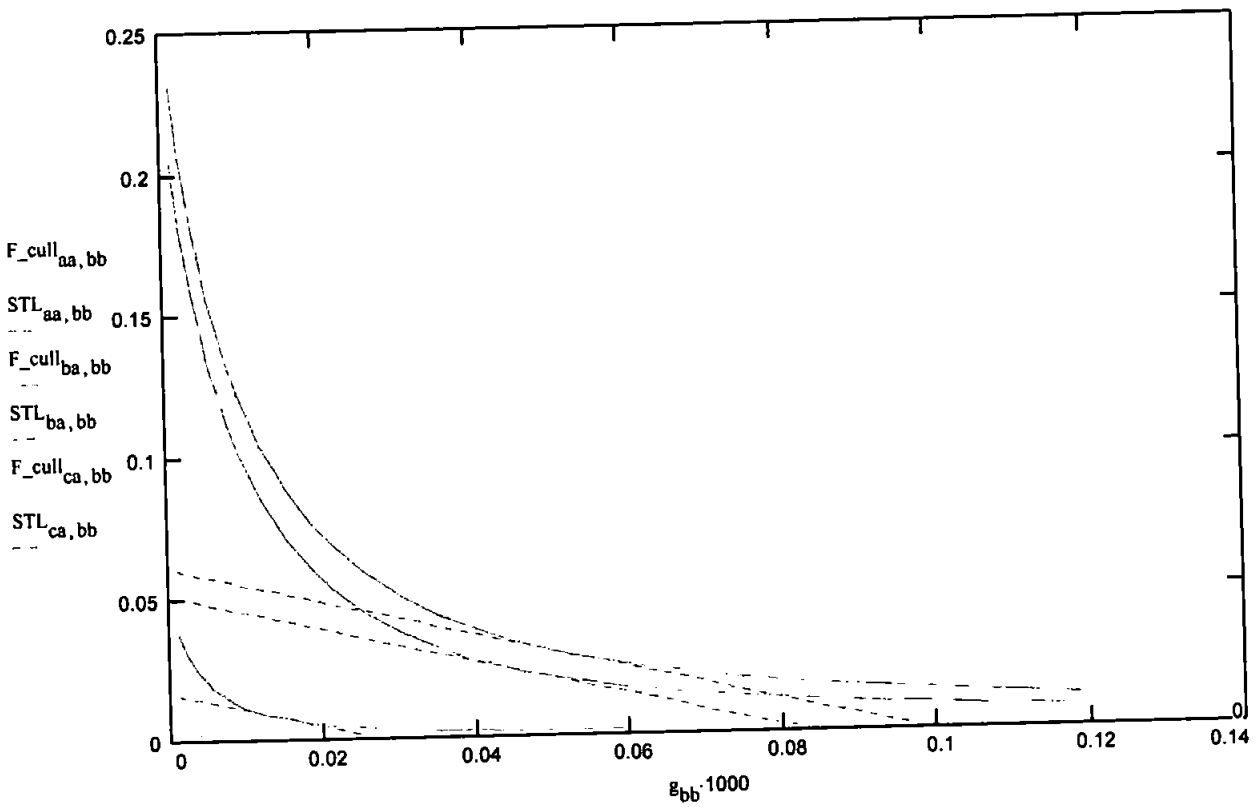

Contact gap for given OAT

$gap_{cn} := gap_{cn} - NMG$

$gap_{cn} := \text{if } gap_{cn} \le 0, 0, gap_{cn}$ **(prevents calculations with -ve gaps taking place)**

To calculate RAT:

$fm_{cn} := gap_{cn} \cdot stif$ **fm=magnetic force at point of release (=spring force at NMG)**

FM=magnetic force at operate condition

$spl := lspline(FM, at)$ **spline of magnetic force at operation against AT**

$RAT_{cn} := interp\ spl, FM, at, fm_{cn}$ **AT corresponding to fm**

$diff_{cn} := at_{cn} - RAT_{cn}$ **differential AT**

Contact force at OAT

$CF_{cn} := FM_{cn} - fm_{cn}$

Contact resistance data for Rhodium (figures in mOhms for 0.5g steps in CF) :

$cfc := 0,1..99$

$cfcr_{cfc} := 0.5 \cdot cfc \cdot \frac{9.81}{1000}$

$cr_0 := 300 \quad cr_1 := 119 \quad cr_2 := 53 \quad cr_3 := 38 \quad cr_4 := 31 \quad cr_5 := 26 \quad cr_6 := 22 \quad cr_7 := 20 \quad cr_8 := 17 \quad cr_9 := 16$

$cr_{10} := 15 \quad cr_{11} := 14 \quad cr_{12} := 13.5 \quad cr_{13} := 13.5 \quad cr_{14} := 13.5$

$cfd := 15..99$

$cr_{cfd} := 15$

$ss := 0,1..14$

Interpolate to find CR corresponding to CF for various OAT switches.

$spl := lspline(cfcr, cr) \qquad CR_{cn} := interp\ spl, cfcr, cr, CF_{cn}$

Calculate the variation in contact resistance for specific OAT switches with AT.

$CF1_{cn} := FM_{cn} - fm_5$

$CF1_{cn} := if\ CF1_{cn} > 0, CF1_{cn}, 0$

$c1 := 5..19 \qquad r1 := 0,1..5$

$CR1_{c1} := interp\ spl, cfcr, cr, CF1_{c1}$

$cr1_{r1} := interp\ spl, cfcr, cr, CF1_{r1}$

$CF2_{cn} := FM_{cn} - fm_7$

$CF2_{cn} := if\ CF2_{cn} > 0, CF2_{cn}, 0$

$c2 := 7..19 \qquad r2 := 3,4..7$

$CR2_{c2} := interp\ spl, cfcr, cr, CF2_{c2}$

$cr2_{r2} := interp\ spl, cfcr, cr, CF2_{r2}$

$CF3_{cn} := FM_{cn} - fm_9$

$CF3_{cn} := if\ CF3_{cn} > 0, CF3_{cn}, 0$

$c3 := 9..19 \qquad r3 := 3,4..9$

$CR3_{c3} := interp\ spl, cfcr, cr, CF3_{c3}$

$cr3_{r3} := interp\ spl, cfcr, cr, CF3_{r3}$

$CF4_{cn} := FM_{cn} - fm_{11}$

$CF4_{cn} := if\ CF4_{cn} > 0, CF4_{cn}, 0$

$c4 := 11..19 \qquad r4 := 3,4..11$

$CR4_{c4} := interp\ spl, cfcr, cr, CF4_{c4}$

$cr4_{r4} := interp\ spl, cfcr, cr, CF4_{r4}$

$CF5_{cn} := FM_{cn} - fm_{13}$

$CF5_{cn} := if\ CF5_{cn} > 0, CF5_{cn}, 0$

$c5 := 13..19 \qquad r5 := 3,4..13$

$CR5_{c5} := interp\ spl, cfcr, cr, CF5_{c5}$

$cr5_{r5} := interp\ spl, cfcr, cr, CF5_{r5}$

$CF6_{cn} := FM_{cn} - fm_{15}$

$CF6_{cn} := if\ CF6_{cn} > 0, CF6_{cn}, 0$

$c6 := 15..19 \qquad r6 := 3,4..15$

$CR6_{c6} := interp\ spl, cfcr, cr, CF6_{c6}$

$cr6_{r6} := interp\ spl, cfcr, cr, CF6_{r6}$

Calculate the contact resistance of various OAT switches when overdriven by 10 AT.

$cnn := 0,1..17$

$CFplus10_{cnn} := FM_{cnn+2} - fm_{cnn}$

$CRplus10_{cnn} := interp\ spl, cfcr, cr, CFplus10_{cnn}$

Graph of RAT against OAT

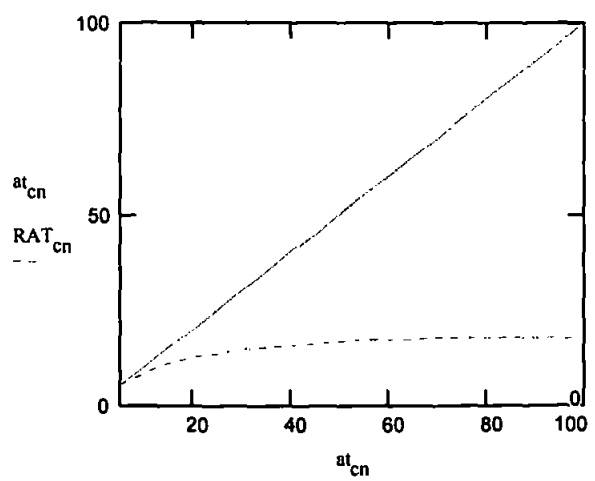

Graph of differential against OAT

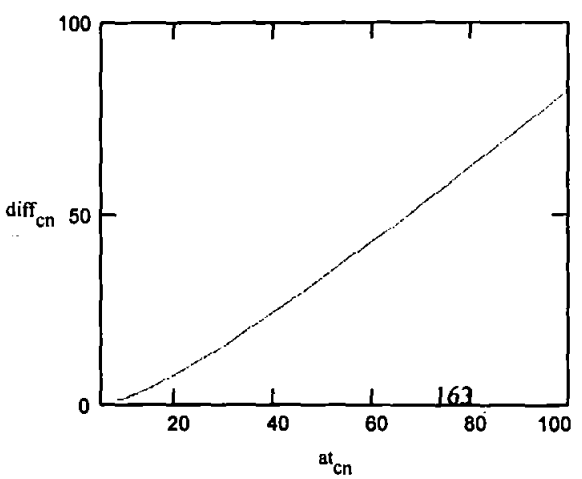

Voltage Breakdown Calculations

Intercontact capacitance (from Cullen's method of predicting permeance)

$$C\_cull_{cg} := \frac{\varepsilon}{\mu} \cdot P\_cull_{cg}$$

dC/dg

$$dC\_cull_{cg} := \frac{\varepsilon}{\mu} \cdot dP\_cull_{cg}$$

To find d2C/dg2:

$n := 0, 1 .. (last(g) - 1)$ $\quad last(g) = 49$

$$mc\_int_n := \frac{dC\_cull_{n+1} - dC\_cull_n}{g_{n+1} - g_n}$$

Take average of gradients between data points to give gradients at data points

$nn := 1, 2 .. (last(g) - 1)$

$$mc_{nn} := \frac{1}{2} \cdot \left(mc\_int_{nn} + mc\_int_{nn-1} \right)$$

Approximate first data point - assume dF/dg is proportional to 1/gap^3 for very small gaps

$$mc_0 := \left(\frac{g_1}{g_0} \right)^3 \cdot mc_1$$

Approximate last data point - assume constant rate of change of gradient over last points

$$mc_{last(g)} := mc_{last(g)-1} + 2 \cdot \left(mc\_int_{last(g)-1} - mc_{last(g)-1} \right)$$

$$d2C\_cull_{cg} := -mc_{cg}$$

$cg := 49, 48 .. 0$

$STL2_{cn,cg} := STL_{cn,cg} - stif \cdot NMG$ **convert to actual gap from magnetic gap**

$STL2_{cn,cg} := if\ STL2_{cn,cg} \le 0, 0, STL2_{cn,cg}$

Voltage breakdown criteria

$$V_{cn,cg} := \sqrt{2 \cdot STL2_{cn,cg} \cdot \frac{1}{dC\_cull_{cg}}}$$ **Voltage at which Fe=spring force for each gap considered**

$$V\_arc_{cg} := 13.4 \cdot 10^{-3} \cdot \frac{1}{\sqrt{C\_cull_{cg}}} \cdot g_{cg} \cdot 1000^{0.641}$$ **Voltage at which arcing occurs for each of the gaps considered .**

$$Fe_{cn,cg} := \frac{1}{2} \cdot V_{cn,cg}^2 \cdot dC\_cull_{cg}$$

$dFe_{cn,cg} := \frac{1}{2} \cdot V_{cn,cg}^{2} \cdot d2C\_cull_{cg}$ **dFe/dg for each of the gaps considered .**

$Closure_{cn,cg} := \text{if } dFe_{cn,cg} > stif, 1, 0$ **If dFe/dg > k then failure through closure - Closure:=1**

$Arc_{cn,cg} := \text{if } V_{cn,cg} > V\_arc_{cg}, 1, 0$ **If V > V_arc then failure through arcing - Arc:=1**

$closure_{cn} := \sum_{cg} Closure_{cn,cg}$ **The Closure flags are summed to give cg at failure (through closure)**

$arc_{cn} := \sum_{cg} Arc_{cn,cg}$ **The Arc flags are summed to give cg at failure (through arcing) condition**

$vb_{cn} := \text{if } arc_{cn} > closure_{cn}, arc_{cn}, closure_{cn}$ **vb is cg at the first failure condition to occur**

$Vat_{cn,1} := V_{cn,vb_{cn}} \cdot 10^{-3}$ $Vat_{cn,0} := at_{cn}$ **Places Vbd-AT results into a single array (in kV)**

Graph of Breakdown Voltage against OAT

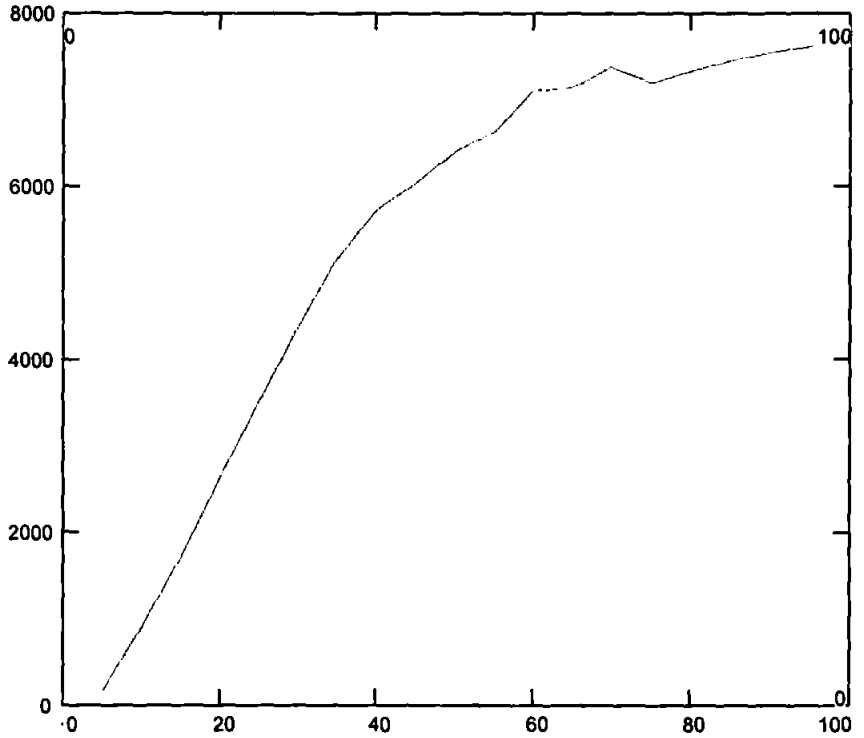

$$Vat = \begin{bmatrix} 5 & 0.16 \\ 10 & 0.88 \\ 15 & 1.69 \\ 20 & 2.59 \\ 25 & 3.51 \\ 30 & 4.4 \\ 35 & 5.17 \\ 40 & 5.72 \\ 45 & 6.02 \\ 50 & 6.4 \\ 55 & 6.64 \\ 60 & 7.08 \\ 65 & 7.15 \\ 70 & 7.38 \\ 75 & 7.18 \\ 80 & 7.33 \\ 85 & 7.45 \\ 90 & 7.54 \\ 95 & 7.61 \\ 100 & 7.69 \end{bmatrix}$$

Graph of Gap (mm) against OAT

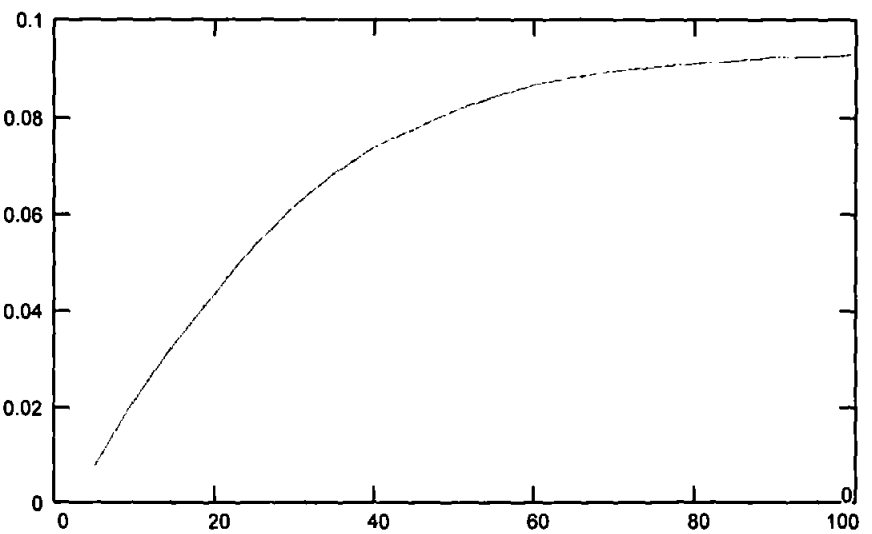

Graph of Contact Force (g) (at pull in) against OAT

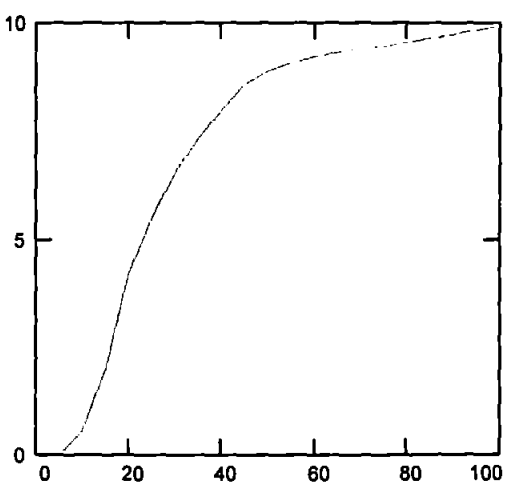

Graph of differential and RAT against OAT

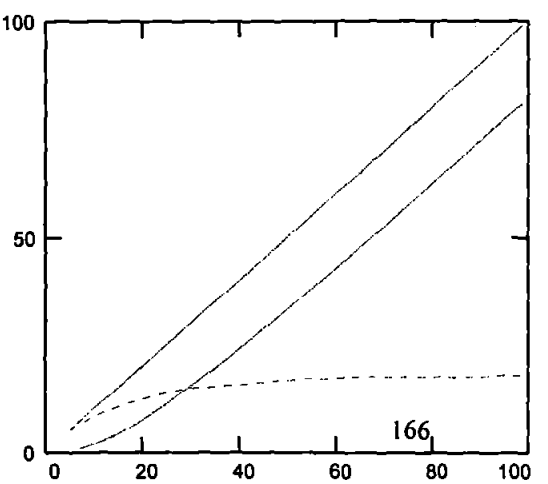

Graph of Voltage Breakdown against Gap (mm)

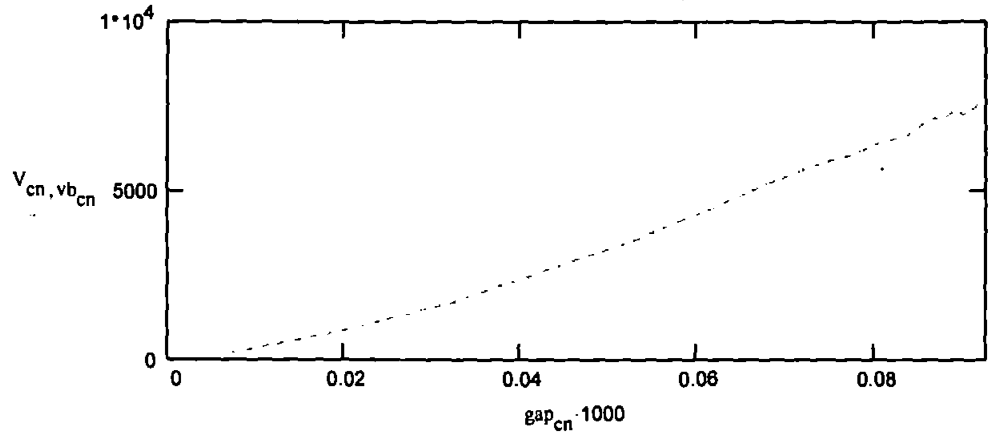

Graph of Contact Resistance (at OAT+10) against OAT

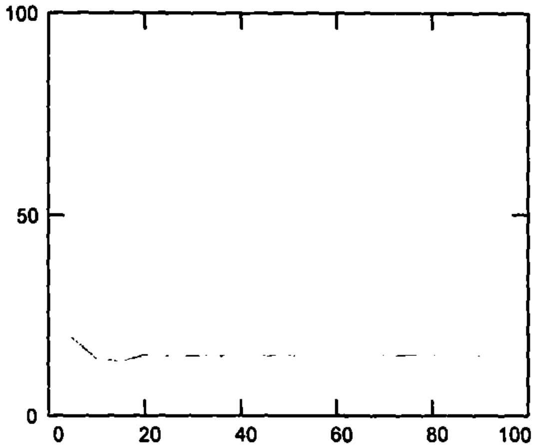

Graph of CR (mOhms) against CF (N) (for Rhodium)

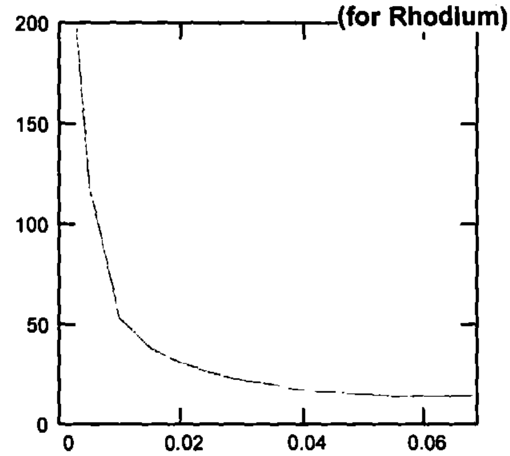

Graphs of contact resistance (mOhms) against drive (AT) for 30,40,50,60,70 & 80 OAT switches.

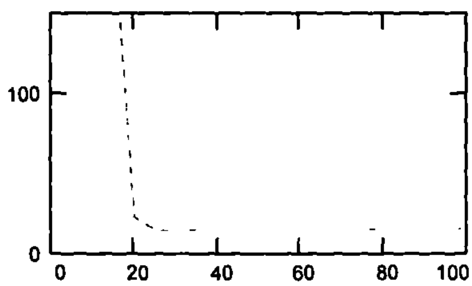

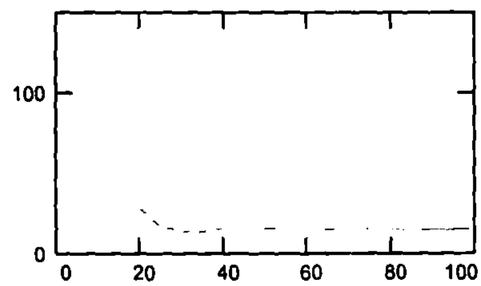

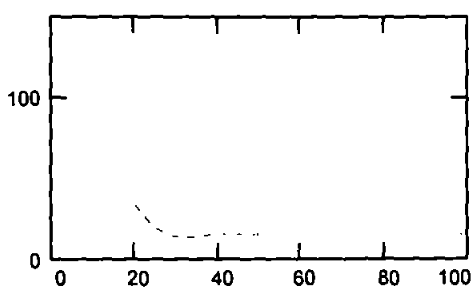

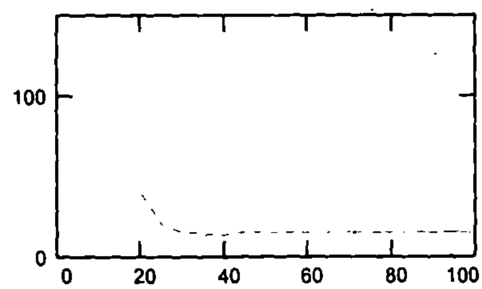

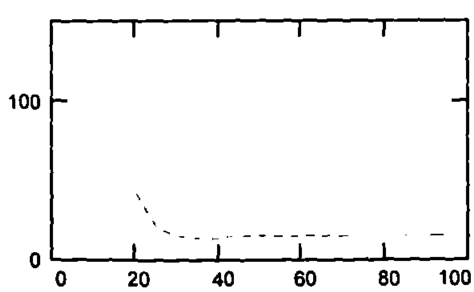

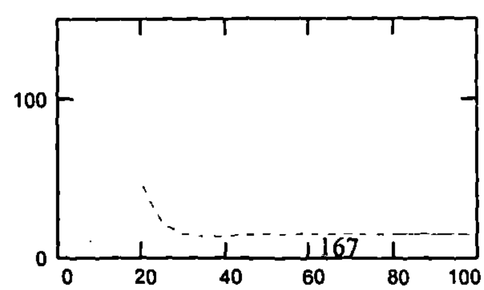

Appendix 6 - Calculated and Measured RF Resistance for Coil Sets 1-4

The relationship presented in section 3.2.2 was used to calculate the RF resistance presented by the coils used in the experiments in section 3.1 to a conductor passing through them. The results, compared to measurements taken in section 3.1 using "low power" and "high power" techniques are shown overleaf.

A good match between measured and calculated results over the range of coil geometries is shown.

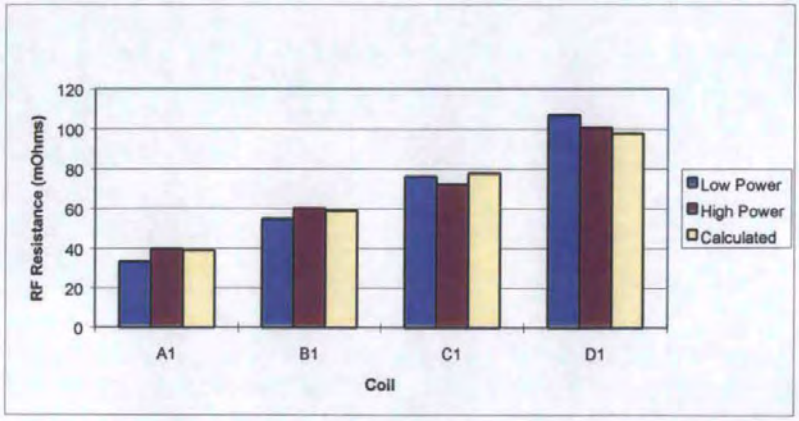

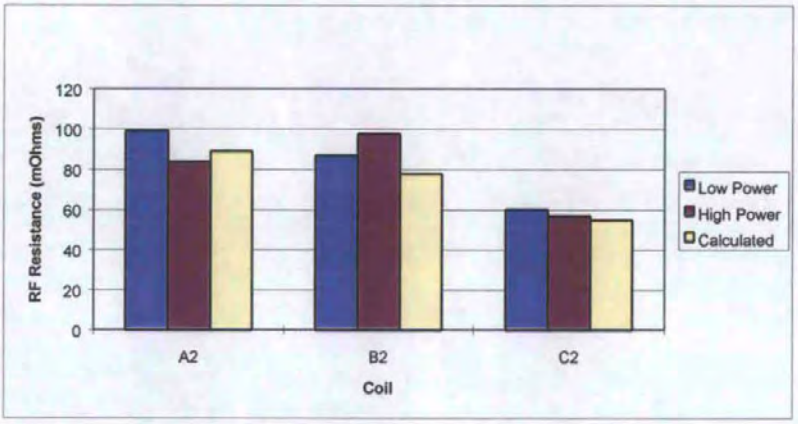

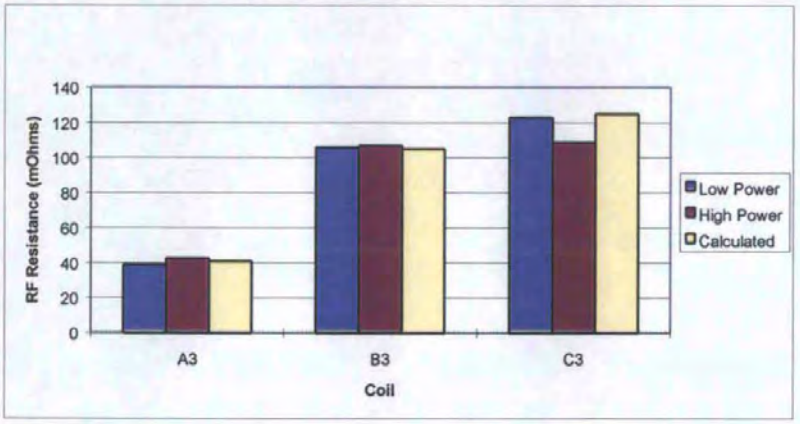

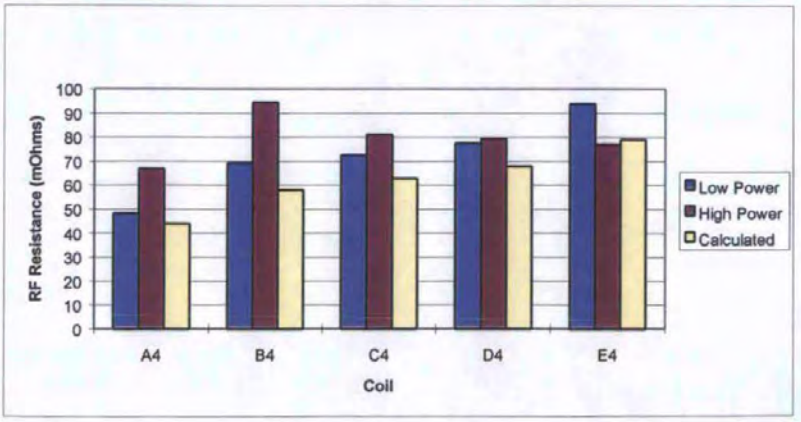

Figure A6.1 – Calculated and Measured (High and Low Power) for Coil Sets 1-4

Appendix 7 - Repeatability of RF Resistance Measurements using the "High Power" Technique

During the course of the investigations into the RF resistance presented by a coil on a reed switch passing through it the measurements presented in section 3.2.3 were repeated using a slightly different experimental technique. The results are included here as an illustration of the repeatability of measurements taken using the "high power" technique as described in section 3.1.

The measurements presented in section 3.2.3 were of the RF resistance presented by a series of coils mounted around an SRA831 reed switch all with the following overall dimensions but with different sizes of winding wire.

Inside diameter	4.8mm
Outside diameter	8.0mm
Length	8.4mm

Clearly the number of turns of each of the windings was different in order to achieve this. A full description of each of the coils is contained in section 3.2.2.

The "high power" technique used in section 3.2.3 involved measuring the change in resistance if the coil to determine heating (and therefore the effective resistance presented by the coil) whilst the reed switch was held closed with a magnet.

This measurement was also repeated with the coil itself, rather than a magnet, used to operate the reed switch. This involved measuring the current and voltage applied to the coil both with and without the RF current applied to the reed switch. The resistance of the coil was

determined directly from Ohms law in each case and this used to determine RF coil heating and the effective RF resistance of the coil as before.

The results of the two sets of measurements are shown overleaf and can be seen to concur. This demonstrates the degree of repeatability which can be expected when using the "high power" technique to measure the RF resistance of a coil.

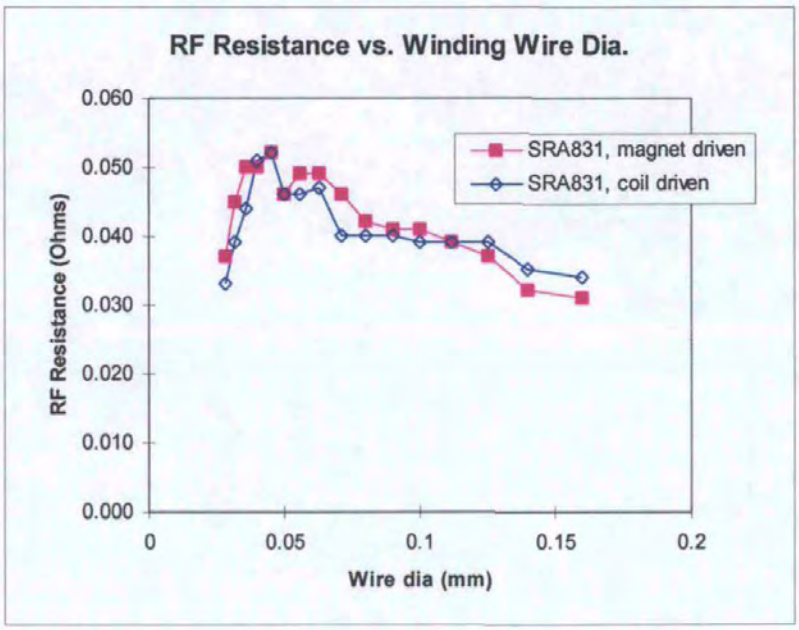

Figure A7.1 – RF Resistance vs. Winding Wire Diameter – Illustration of Repeatability

Appendix 8 – Reed Relay Design Program Listing

An annotated listing of the Reed Relay Design Program, as described in section 4.1 and written using Mathcad software, is provided overleaf.

Calculation of Reed Relay Performance

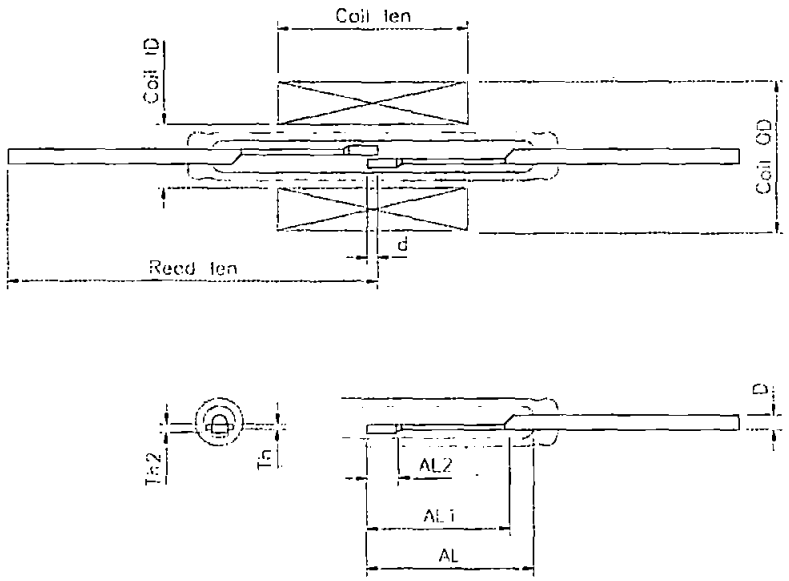

USER DEFINED VARIABLES

$Th_0 := 0.010 \cdot 25.4 \cdot 10^{-3}$ **Thickness of middle flat section(m) - First Blade**

$Th_1 := 0.010 \cdot 25.4 \cdot 10^{-3}$ **Thickness of middle flat section(m) - Second Blade**

$Th = \begin{matrix} 0.00025 \\ 0.00025 \end{matrix}$

$Th2_0 := 0.010 \cdot 25.4 \cdot 10^{-3}$ **Thickness of end flat section(m) - First Blade**

$Th2_1 := 0.010 \cdot 25.4 \cdot 10^{-3}$ **Thickness of end flat section(m) - Second Blade**

$Th2 = \begin{matrix} 0.00025 \\ 0.00025 \end{matrix}$

$AL_0 := 8.5 \cdot 10^{-3}$ **Reed length inside the glass(m) - First Blade**

$AL_1 := 8.0 \cdot 10^{-3}$ **Reed length inside the glass(m) - Second Blade**

$AL = \begin{matrix} 0.0085 \\ 0.008 \end{matrix}$

$AL1_0 := 6.6 + \frac{0.3}{2} \cdot 10^{-3}$ **Reed middle flat section length (m) - First Blade**

$AL1_1 := 6.0 \cdot 10^{-3}$ **Reed middle flat section length (m) - Second Blade**

$AL1 = \begin{matrix} 0.00675 \\ 0.006 \end{matrix}$

$AL2_0 := 2.795 - \frac{0.2}{2} \cdot 10^{-3}$ **Reed end flat section length (m) - First Blade**

$AL2_1 := 2.795 - \frac{0.2}{2} \cdot 10^{-3}$ **Reed end flat section length (m) - Second Blade**

$AL2 = \begin{matrix} 0.0027 \\ 0.0027 \end{matrix}$

$D := 0.022 \cdot 25.4 \cdot 10^{-3}$ **Reed diameter (m) - First blade** $D = 0.00056$

$Di := 0.015 \cdot 25.4 \cdot 10^{-3}$ **Tube inner diameter (m) - Second blade** $Di = 0.00038$

$Do := 0.030 \cdot 25.4 \cdot 10^{-3}$ **Tube outer diameter (m) - Second blade** $Do = 0.00076$

$d := 0.28 \cdot 10^{-3}$ **Depth of overlap (m)** $d = 0.00028$

$b := 0.85 \cdot 10^{-3}$ **Width of blade tip at overlap point** $b = 0.00085$

$NMG := 0.014 \cdot 10^{-3}$ **Plating thickness (m) - SRA831**

$reedlen := 12.5 \cdot 10^{-3}$ **Length of a single reed (m). Take an average for asymmetric blades .**

$coillen := 10.0 \cdot 10^{-3}$ **Length of the coil (m)**

$coilOD := 12.0 \cdot 10^{-3}$ **Coil winding outside diameter (m)**

$coilID := 8.0 \cdot 10^{-3}$ **Coil winding inside diameter (m)**

CONSTANTS

$\mu := 1.256637 \cdot 10^{-6}$ **Permeability of free space (Wb/AT.m)**

$\varepsilon := 8.854188 \cdot 10^{-12}$ **Permitivity of free space**

$E := 15.47 \cdot 10^{10}$ **N/m^2**

COUNTER VARIABLES

$bl := 0, 1 .. 1$ **Blade identification ; 0 or 1 (for asymmetric blades)**

$cg := 0, 1 .. 49$ **Gap counter**

$g_{cg} := (0.00022 \cdot (cg + 1))^2$ **Main gap, excluding plating thickness (m)** $g_0 \cdot 1000 = 0.00005$ $g_{49} \cdot 1000 = 0.121$

$cn := 0, 1 .. 19$ **amp-turn counter**

$at_{cn} := (cn \cdot 5) + 5$ **Range of amp-turns to be used in calculations. Note that altering this range will affect CR calcs.** $at_0 = 5$ $at_{19} = 100$

Initial Calculations

$a := \pi \cdot \frac{D^2}{4}$ **Reed cross-sectional area (mm2)** $a = 2.45246 \cdot 10^{-7}$

$l := coillen \cdot \frac{4}{3}$ **Assumed reed length (mm)** $l = 0.01333$

$t := \frac{Th2_0 + Th2_1}{2}$ **Average thickness of blades at tip(mm)** $t = 0.00025$

$L3 := AL - \frac{d}{2}$ **Distance from the seal to the middle of the overlap** $L3 = \begin{matrix} 0.00836 \\ 0.00786 \end{matrix}$

$L2 := AL - AL2$ **Distance from the seal to the end of middle section** $L2 = \begin{matrix} 0.00581 \\ 0.00531 \end{matrix}$

$L1 := AL - AL1$ **Distance from the seal to the end of the first section** $L1 = \begin{matrix} 0.00175 \\ 0.002 \end{matrix}$

Blade Stiffness Calculations

Calculate blade widths B and B2

$B_{bl} := \frac{\frac{\pi \cdot D^2}{4}}{Th_{bl}}$ $B = \begin{matrix} 0.00097 \\ 0.00097 \end{matrix}$ $B2_{bl} := \frac{\frac{\pi \cdot D^2}{4}}{Th2_{bl}}$ $B2 = \begin{matrix} 0.00097 \\ 0.00097 \end{matrix}$

Calculate I for the round section

$I1_0 := \frac{\pi \cdot D^4}{64}$ $I1 = 4.78625 \cdot 10^{-15}$ $I1_1 := \frac{\pi \cdot Do^4 - Di^4}{64}$ $I1_1 = 1.55153 \cdot 10^{-14}$

Calculate I for flat sections

$$I2_{bl} := \frac{B_{bl} \cdot Th_{bl}^{3}}{12} \qquad I2 = \begin{matrix} 1.31853 \cdot 10^{-15} \\ 1.31853 \cdot 10^{-15} \end{matrix}$$

$$I3_{bl} := \frac{B2_{bl} \cdot \left[Th2_{(bl)}\right]^{3}}{12} \qquad I3 = \begin{matrix} 1.31853 \cdot 10^{-15} \\ 1.31853 \cdot 10^{-15} \end{matrix}$$

$F := 1$ **N**

$$yl_{bl} := \frac{F}{6 \cdot E \cdot Il_{bl}} \cdot \left[3 \cdot L3_{bl} \cdot Ll_{bl}^{2} - Ll_{bl}^{3}\right]$$

$$y2_{bl} := \frac{F}{6 \cdot E \cdot I2_{bl}} \cdot \left[3 \cdot L3_{bl} \cdot L2_{bl}^{2} - L2_{bl}^{3} - 3 \cdot L3_{bl} \cdot Ll_{bl}^{2} + Ll_{bl}^{3}\right]$$

$$y3_{bl} := \frac{F}{6 \cdot E \cdot I3_{bl}} \cdot \left[2 \cdot L3_{bl}^{3} - 3 \cdot L3_{bl} \cdot L2_{bl}^{2} + L2_{bl}^{3}\right]$$

$$y_{bl} := yl_{bl} + y2_{bl} + y3_{bl} \qquad y = \begin{matrix} 0.00091 \\ 0.00073 \end{matrix}$$

$$st_{bl} := \frac{F}{y_{bl}} \qquad st = \begin{matrix} 1095.87099 \\ 1371.74253 \end{matrix} \quad \textbf{N/m}$$

$$stif := \frac{1}{\frac{1}{st_0} + \frac{1}{st_1}}$$ **(effect of two blade spring rates added in series)** $stif = 609.19298$ **N/m**

$stif \cdot \frac{1}{9.81} = 62.09918$ **g/mm**

Generation of Pull Curves

Range of Flux assummed - generated on basis of standard flux density values to link with BH data

$Q := 0, 1 .. 33$

$FL_Q := Q \cdot 5 \cdot 10^{-2} \cdot a$ **(Wb)**

Permeance for each sector of the contact gap field (c.f. "A Practical Theory for Reed Switches")

$$Pg_{cg} := \frac{\mu \cdot b \cdot d}{g_{cg}}$$

$$Pl_{cg} := \frac{\mu \cdot 4 \cdot b}{\pi} \cdot \ln\left(1 + \frac{t}{g_{cg}}\right)$$

$$P2_{cg} := \frac{\mu \cdot 2 \cdot d}{\pi} \cdot \ln\left(1 + \frac{2 \cdot t}{g_{cg}}\right)$$

$P3_{cg} := \mu \cdot 1.04 \cdot b$

$P4 := \mu \cdot 0.52 \cdot d$

$P5_{cg} := \mu \cdot 0.308 \cdot g_{cg}$

$P6 := \mu \cdot t$

The following section derives air return path reluctance from FEA results

Counter variables and coil length, od and reed length data which FEA results correspond to

$cl := 0, 1 .. 3$ $rl := 0, 1 .. 3$ $cd := 0, 1 .. 2$

$$coil\_l := \begin{bmatrix} 8 \\ 12 \\ 16 \\ 20 \end{bmatrix} \quad reed\_l := \begin{bmatrix} 7 \\ 13.6 \\ 20.6 \\ 27.2 \end{bmatrix} \quad coil\_od := \begin{matrix} 8 \\ 12 \\ 16 \end{matrix}$$

Return path reluctance for 8mm OD coils (no gap):

$$Rr8 := \begin{bmatrix} 1.54 \cdot 10^8 & 1.80 \cdot 10^8 & 2.15 \cdot 10^8 & 2.57 \cdot 10^8 \\ 7.90 \cdot 10^7 & 8.52 \cdot 10^7 & 9.28 \cdot 10^7 & 1.02 \cdot 10^8 \\ 5.53 \cdot 10^7 & 5.82 \cdot 10^7 & 6.15 \cdot 10^7 & 6.54 \cdot 10^7 \\ 4.41 \cdot 10^7 & 4.59 \cdot 10^7 & 4.79 \cdot 10^7 & 5.01 \cdot 10^7 \end{bmatrix}$$

Return path reluctance for 12mm OD coils (no gap):

$$Rr12 := \begin{bmatrix} 1.86 \cdot 10^8 & 2.09 \cdot 10^8 & 2.40 \cdot 10^8 & 2.77 \cdot 10^8 \\ 8.90 \cdot 10^7 & 9.44 \cdot 10^7 & 1.01 \cdot 10^8 & 1.10 \cdot 10^8 \\ 6.01 \cdot 10^7 & 6.25 \cdot 10^7 & 6.55 \cdot 10^7 & 6.90 \cdot 10^7 \\ 4.71 \cdot 10^7 & 4.85 \cdot 10^7 & 5.07 \cdot 10^7 & 5.22 \cdot 10^7 \end{bmatrix}$$

Return path reluctance for 16mm OD coils (no gap):

$$Rr16 := \begin{bmatrix} 2.23 \cdot 10^8 & 2.43 \cdot 10^8 & 2.70 \cdot 10^8 & 3.03 \cdot 10^8 \\ 1.00 \cdot 10^8 & 1.05 \cdot 10^8 & 1.11 \cdot 10^8 & 1.20 \cdot 10^8 \\ 6.53 \cdot 10^7 & 6.74 \cdot 10^7 & 7.00 \cdot 10^7 & 7.32 \cdot 10^7 \\ 5.02 \cdot 10^7 & 5.14 \cdot 10^7 & 5.29 \cdot 10^7 & 5.47 \cdot 10^7 \end{bmatrix}$$

Reed and coil dimensions used in interpolation

$reed := reedlen \cdot 10^3$	**Reed length in mm**	$reed = 12.5$
$coil := coillen \cdot 10^3$	**Coil length in mm**	$coil = 10$
$od := coilOD \cdot 10^3$	**Coil OD in mm**	$od = 12$

Interpolation for 8mm OD coil

"reed" and 8mm coil

$R_{rl} := Rr8_{rl,0}$ $vs := pspline(reed\_l, R)$ $R0 := interp(vs, reed\_l, R, reed)$

"reed" and 12mm coil

$R_{rl} := Rr8_{rl,1}$ $vs := pspline(reed\_l, R)$ $R1 := interp(vs, reed\_l, R, reed)$

"reed" and 16mm coil

$R_{rl} := Rr8_{rl,2}$ $vs := pspline(reed\_l, R)$ $R2 := interp(vs, reed\_l, R, reed)$

"reed" and 20mm coil

$R_{rl} := Rr8_{rl,3}$ vs := pspline(reed_l, R) R3 := interp(vs, reed_l, R, reed)

$$Rr\_8 := \begin{bmatrix} R0 \\ R1 \\ R2 \\ R3 \end{bmatrix}$$

"reed" and "coil"

vs := lspline(coil_l, Rr_8) R8 := interp(vs, coil_l, Rr_8, coil)

Return Path Reluctance (no gap) for 8mm coil OD

$R8 = 9.11205 \cdot 10^{7}$

Interpolation for 12mm OD coil

"reed" and 8mm coil

$R_{rl} := Rr12_{rl,0}$ vs := pspline(reed_l, R) R0 := interp(vs, reed_l, R, reed)

"reed" and 12mm coil

$R_{rl} := Rr12_{rl,1}$ vs := pspline(reed_l, R) R1 := interp(vs, reed_l, R, reed)

"reed" and 16mm coil

$R_{rl} := Rr12_{rl,2}$ vs := pspline(reed_l, R) R2 := interp(vs, reed_l, R, reed)

"reed" and 20mm coil

$R_{rl} := Rr12_{rl,3}$ vs := pspline(reed_l, R) R3 := interp(vs, reed_l, R, reed)

$$Rr\_12 := \begin{bmatrix} R0 \\ R1 \\ R2 \\ R3 \end{bmatrix}$$

"reed" and "coil"

vs := lspline(coil_l, Rr_12) R12 := interp(vs, coil_l, Rr_12, coil)

Return Path Reluctance (no gap) for 12mm coil OD

$R12 = 1.02933 \cdot 10^{8}$

Interpolation for 16mm OD coil

"reed" and 8mm coil

$R_{rl} := Rr16_{rl,0}$ vs := pspline(reed_l, R) R0 := interp(vs, reed_l, R, reed)

"reed" and 12mm coil

$R_{rl} := Rr16_{rl,1}$ vs := pspline(reed_l, R) R1 := interp(vs, reed_l, R, reed)

"reed" and 16mm coil

$R_{rl} := Rr16_{rl,2}$ vs := pspline(reed_l, R) R2 := interp(vs, reed_l, R, reed)

"reed" and 20mm coil

$R_{rl} := Rr16_{rl,3}$ vs := pspline(reed_l, R) R3 := interp(vs, reed_l, R, reed)

$$Rr\_16 := \begin{bmatrix} R0 \\ R1 \\ R2 \\ R3 \end{bmatrix}$$

"reed" and "coil"

$vs := lspline(coil\_l, Rr\_16)$ $R16 := interp(vs, coil\_l, Rr\_16, coil)$

Return Path Reluctance (no gap) for 16mm coil OD

$R16 = 1.16314 \cdot 10^{8}$

Interpolate between results for 8,12 and 16mm od coils to find return path reluctance (no gap)

$$Rret := \begin{matrix} R8 \\ R12 \\ R16 \end{matrix} \qquad Rret = \begin{matrix} 9.11205 \cdot 10^{7} \\ 1.02933 \cdot 10^{8} \\ 1.16314 \cdot 10^{8} \end{matrix}$$

$vs := lspline(coil\_od, Rret)$ $Rreturn := interp(vs, coil\_od, Rret, od)$ $Rreturn = 1.02933 \cdot 10^{8}$

Function to model change in return path reluctance with working gap reluctance, Rg

$o := -4.5 \cdot 10^{-18}$

$p := \frac{1}{(reed + 13.2)} \cdot (0.275 \cdot od + 2.6) \cdot 10^{-8}$ $p = 2.29572 \cdot 10^{-9}$

$q := 1$

$$fn_{cg} := o \cdot \left(\frac{1}{Pg_{cg}}\right)^{2} + p \cdot \frac{1}{Pg_{cg}} + q$$

$R\_return_{cg} := Rreturn \cdot fn_{cg}$

The following section derives fringing (leakage) reluctance from FEA results

Fringing reluctance for 8mm OD coils (R gap=1.3e8):

$$Rfr8 := \begin{bmatrix} 2.42 \cdot 10^{8} & 2.02 \cdot 10^{8} & 1.75 \cdot 10^{8} & 1.57 \cdot 10^{8} \\ 2.28 \cdot 10^{8} & 1.92 \cdot 10^{8} & 1.66 \cdot 10^{8} & 1.49 \cdot 10^{8} \\ 2.13 \cdot 10^{8} & 1.81 \cdot 10^{8} & 1.58 \cdot 10^{8} & 1.40 \cdot 10^{8} \\ 1.99 \cdot 10^{8} & 1.70 \cdot 10^{8} & 1.49 \cdot 10^{8} & 1.32 \cdot 10^{8} \end{bmatrix}$$

Fringing reluctance for 12mm OD coils (R gap=1.3e8):

$$Rfr12 := \begin{bmatrix} 2.25 \cdot 10^{8} & 2.02 \cdot 10^{8} & 1.86 \cdot 10^{8} & 1.71 \cdot 10^{8} \\ 2.06 \cdot 10^{8} & 1.86 \cdot 10^{8} & 1.70 \cdot 10^{8} & 1.56 \cdot 10^{8} \\ 1.87 \cdot 10^{8} & 1.70 \cdot 10^{8} & 1.55 \cdot 10^{8} & 1.42 \cdot 10^{8} \\ 1.68 \cdot 10^{8} & 1.53 \cdot 10^{8} & 1.39 \cdot 10^{8} & 1.27 \cdot 10^{8} \end{bmatrix}$$

Fringing reluctance for 16mm OD coils (R gap=1.3e8):

$$Rfr16 := \begin{bmatrix} 2.26\cdot10^{8} & 2.12\cdot10^{8} & 1.98\cdot10^{8} & 1.87\cdot10^{8} \\ 2.01\cdot10^{8} & 1.89\cdot10^{8} & 1.76\cdot10^{8} & 1.66\cdot10^{8} \\ 1.75\cdot10^{8} & 1.65\cdot10^{8} & 1.54\cdot10^{8} & 1.45\cdot10^{8} \\ 1.50\cdot10^{8} & 1.41\cdot10^{8} & 1.32\cdot10^{8} & 1.24\cdot10^{8} \end{bmatrix}$$

Interpolation for 8mm OD coil

"reed" and 8mm coil

$R_{rl} := Rfr8_{rl,0}$ vs := pspline(reed_l, R) R0 := interp(vs, reed_l, R, reed)

"reed" and 12mm coil

$R_{rl} := Rfr8_{rl,1}$ vs := pspline(reed_l, R) R1 := interp(vs, reed_l, R, reed)

"reed" and 16mm coil

$R_{rl} := Rfr8_{rl,2}$ vs := pspline(reed_l, R) R2 := interp(vs, reed_l, R, reed)

"reed" and 20mm coil

$R_{rl} := Rfr8_{rl,3}$ vs := pspline(reed_l, R) R3 := interp(vs, reed_l, R, reed)

$$Rfr\_8 := \begin{bmatrix} R0 \\ R1 \\ R2 \\ R3 \end{bmatrix}$$

"reed" and "coil"

vs := lspline(coil_l, Rfr_8) Rfr8 := interp(vs, coil_l, Rfr_8, coil)

Interpolation for 12mm OD coil

"reed" and 8mm coil

$R_{rl} := Rfr12_{rl,0}$ vs := pspline(reed_l, R) R0 := interp(vs, reed_l, R, reed)

"reed" and 12mm coil

$R_{rl} := Rfr12_{rl,1}$ vs := pspline(reed_l, R) R1 := interp(vs, reed_l, R, reed)

"reed" and 16mm coil

$R_{rl} := Rfr12_{rl,2}$ vs := pspline(reed_l, R) R2 := interp(vs, reed_l, R, reed)

"reed" and 20mm coil

$R_{rl} := Rfr12_{rl,3}$ vs := pspline(reed_l, R) R3 := interp(vs, reed_l, R, reed)

$$Rfr\_12 := \begin{bmatrix} R0 \\ R1 \\ R2 \\ R3 \end{bmatrix}$$

"reed" and "coil"

vs := lspline(coil_l, Rfr_12) Rfr12 := interp(vs, coil_l, Rfr_12, coil)

Fringing reluctance for 12mm coil od(R gap=1.3e8)

$Rfr12 = 1.98411 \cdot 10^{8}$

Interpolation for 16mm OD coil

"reed" and 8mm coil

$R_{rl} := Rfr16_{rl,0}$ vs := pspline(reed_l, R) R0 := interp(vs, reed_l, R, reed)

"reed" and 12mm coil

$R_{rl} := Rfr16_{rl,1}$ vs := pspline(reed_l, R) R1 := interp(vs, reed_l, R, reed)

"reed" and 16mm coil

$R_{rl} := Rfr16_{rl,2}$ vs := pspline(reed_l, R) R2 := interp(vs, reed_l, R, reed)

"reed" and 20mm coil

$R_{rl} := Rfr16_{rl,3}$ vs := pspline(reed_l, R) R3 := interp(vs, reed_l, R, reed)

$$Rfr\_16 := \begin{bmatrix} R0 \\ R1 \\ R2 \\ R3 \end{bmatrix}$$

"reed" and "coil"

vs := lspline(coil_l, Rfr_16) Rfr16 := interp(vs, coil_l, Rfr_16, coil)

Fringing reluctance for 16mm coil od(R gap=1.3e8)

$Rfr16 = 1.99114 \cdot 10^{8}$

Interpolate between results for 8,12 and 16mm od coils to find the fringing reluctance (R gap=1.3e8)

$$Rfringe := \begin{matrix} Rfr8 \\ Rfr12 \\ Rfr16 \end{matrix} \qquad Rfringe = \begin{matrix} 2.11219 \cdot 10^{8} \\ 1.98411 \cdot 10^{8} \\ 1.99114 \cdot 10^{8} \end{matrix}$$

vs := lspline(coil_od, Rfringe) Rfr := interp(vs, coil_od, Rfringe, od) $Rfr = 1.98411 \cdot 10^{8}$

Pfr is the permeance of the fringing path around the gap which does not create any force between the blades

$u := 0.9$

$m := \dfrac{(1-u) \cdot Rfr}{1.30 \cdot 10^{8}}$ $m = 0.15262$

$c := u \cdot Rfr$ $c = 1.7857 \cdot 10^{8}$

$$Rfr_{cg} := m \cdot \frac{1}{Pg_{cg}} + c$$

$$Pfr_{cg} := \frac{1}{Rfr_{cg}}$$

Total gap permeance and reluctance

$$P\_cull_{cg} := Pg_{cg} + P1_{cg} + P2_{cg} + P3_{cg} + P4 + P5_{cg} + P6 + Pfr_{cg}$$

$$R\_gap_{cg} := \frac{1}{P\_cull_{cg}}$$

dP/dg for all non-zero components of gap permeance

$$dPg_{cg} := \frac{\mu \cdot b \cdot d}{g_{cg}^{\ 2}}$$

$$dP1_{cg} := \frac{\mu \cdot 4 \cdot b}{\pi} \cdot \frac{g_{cg}}{t + g_{cg}}$$

$$dP2_{cg} := \frac{\mu \cdot 2 \cdot d}{\pi} \cdot \frac{g_{cg}}{g_{cg} + 2 \cdot t}$$

$$dP5 := 0.308 \cdot \mu$$

$$dP\_cull_{cg} := dPg_{cg} + dP1_{cg} + dP2_{cg} + dP5$$

Nickel Iron Permeability Curve (NOT PERMEANCE !) or B-H curve

$cpc := 0, 1 .. 19$

$N_{cpc} := cpc \cdot 4.1883 \cdot 10^{-3}$

$N_{20} := 0.0875$ $N_{21} := 0.0955$ $N_{22} := 0.1273$

$N_{23} := 0.1512$ $N_{24} := 0.1910$ $N_{25} := 0.2467$ $N_{26} := 0.3024$ $N_{27} := 0.3979$ $N_{28} := 0.5013$ $N_{29} := 0.6366$

$N_{30} := 0.8157$ $N_{31} := 1.1618$ $N_{32} := 2.1088$ $N_{33} := 10^{6}$

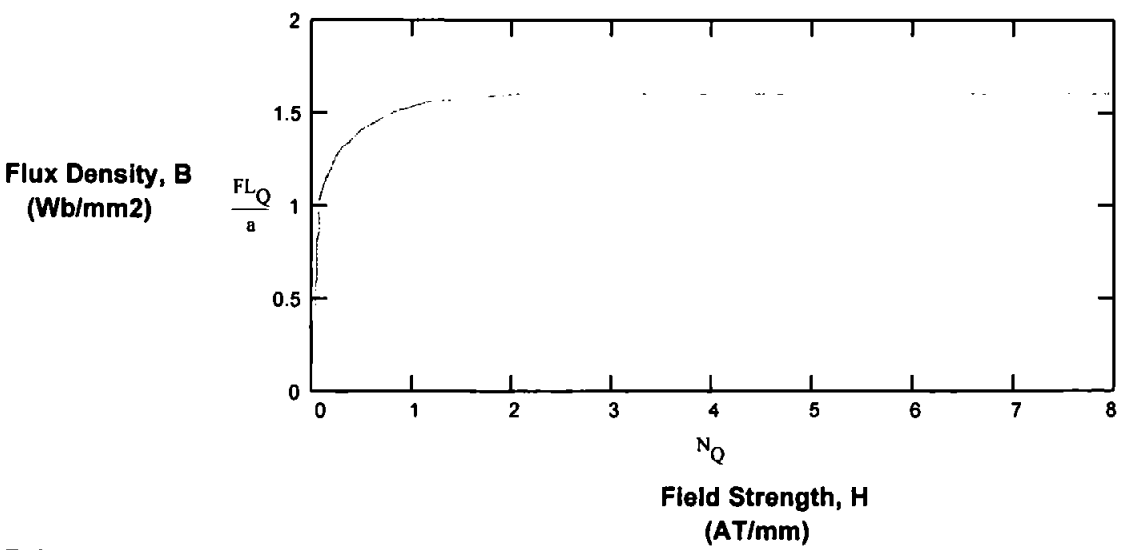

Reluctance of NiFe blades

$$R\_blades_{Q} := \frac{N_Q \cdot l \cdot 10^{3}}{FL_Q}$$

mmf across return path, reeds and contact gap

$$mmf_{cg,Q} := FL_Q \cdot R\_return_{cg} + R\_blades_Q + R\_gap_{cg}$$

Interpolation to find the flux across the contact gap corresponding to various AT applied to the whole circuit

$v_Q := mmf_{0,Q}$ $vs := pspline(v, FL)$ $Y_{cn,0} := interp\ vs, v, FL, at_{cn}$

$v_Q := mmf_{1,Q}$ $vs := pspline(v, FL)$ $Y_{cn,1} := interp\ vs, v, FL, at_{cn}$

$v_Q := mmf_{2,Q}$ $vs := pspline(v, FL)$ $Y_{cn,2} := interp\ vs, v, FL, at_{cn}$

$v_Q := mmf_{3,Q}$ $vs := pspline(v, FL)$ $Y_{cn,3} := interp\ vs, v, FL, at_{cn}$

$v_Q := mmf_{4,Q}$ $vs := pspline(v, FL)$ $Y_{cn,4} := interp\ vs, v, FL, at_{cn}$

$v_Q := mmf_{5,Q}$ $vs := pspline(v, FL)$ $Y_{cn,5} := interp\ vs, v, FL, at_{cn}$

$v_Q := mmf_{6,Q}$ $vs := pspline(v, FL)$ $Y_{cn,6} := interp\ vs, v, FL, at_{cn}$

$v_Q := mmf_{7,Q}$ $vs := pspline(v, FL)$ $Y_{cn,7} := interp\ vs, v, FL, at_{cn}$

$v_Q := mmf_{8,Q}$ $vs := pspline(v, FL)$ $Y_{cn,8} := interp\ vs, v, FL, at_{cn}$

$v_Q := mmf_{9,Q}$ $vs := pspline(v, FL)$ $Y_{cn,9} := interp\ vs, v, FL, at_{cn}$

$v_Q := mmf_{10,Q}$ $vs := pspline(v, FL)$ $Y_{cn,10} := interp\ vs, v, FL, at_{cn}$

$v_Q := mmf_{11,Q}$ $vs := pspline(v, FL)$ $Y_{cn,11} := interp\ vs, v, FL, at_{cn}$

$v_Q := mmf_{12,Q}$ $vs := pspline(v, FL)$ $Y_{cn,12} := interp\ vs, v, FL, at_{cn}$

$v_Q := mmf_{13,Q}$ $vs := pspline(v, FL)$ $Y_{cn,13} := interp\ vs, v, FL, at_{cn}$

$v_Q := mmf_{14,Q}$ $vs := pspline(v, FL)$ $Y_{cn,14} := interp\ vs, v, FL, at_{cn}$

$v_Q := mmf_{15,Q}$ $vs := pspline(v, FL)$ $Y_{cn,15} := interp\ vs, v, FL, at_{cn}$

$v_Q := mmf_{16,Q}$ $vs := pspline(v, FL)$ $Y_{cn,16} := interp\ vs, v, FL, at_{cn}$

$v_Q := mmf_{17,Q}$ $vs := pspline(v, FL)$ $Y_{cn,17} := interp\ vs, v, FL, at_{cn}$

$v_Q := mmf_{18,Q}$ $vs := pspline(v, FL)$ $Y_{cn,18} := interp\ vs, v, FL, at_{cn}$

$v_Q := mmf_{19,Q}$ $vs := pspline(v, FL)$ $Y_{cn,19} := interp\ vs, v, FL, at_{cn}$

$v_Q := mmf_{20,Q}$ $vs := pspline(v, FL)$ $Y_{cn,20} := interp\ vs, v, FL, at_{cn}$

$v_Q := mmf_{21,Q}$ $vs := pspline(v, FL)$ $Y_{cn,21} := interp\ vs, v, FL, at_{cn}$

$v_Q := mmf_{22,Q}$ $vs := pspline(v, FL)$ $Y_{cn,22} := interp\ vs, v, FL, at_{cn}$

$v_Q := mmf_{23,Q}$ $vs := pspline(v, FL)$ $Y_{cn,23} := interp\ vs, v, FL, at_{cn}$

$v_Q := mmf_{24,Q}$ $vs := pspline(v, FL)$ $Y_{cn,24} := interp\ vs, v, FL, at_{cn}$

$v_Q := mmf_{25,Q}$ $vs := pspline(v, FL)$ $Y_{cn,25} := interp\ vs, v, FL, at_{cn}$

$v_Q := mmf_{26,Q}$ $vs := pspline(v, FL)$ $Y_{cn,26} := interp\ vs, v, FL, at_{cn}$

$v_Q := mmf_{27,Q}$ $vs := pspline(v, FL)$ $Y_{cn,27} := interp\ vs, v, FL, at_{cn}$

$v_Q := mmf_{28,Q}$ $vs := pspline(v, FL)$ $Y_{cn,28} := interp\ vs, v, FL, at_{cn}$

$v_Q := mmf_{29,Q}$ $vs := pspline(v, FL)$ $Y_{cn,29} := interp\ vs, v, FL, at_{cn}$

$v_Q := mmf_{30,Q}$ $vs := pspline(v, FL)$ $Y_{cn,30} := interp\ vs, v, FL, at_{cn}$

$v_Q := mmf_{31,Q}$ $vs := pspline(v, FL)$ $Y_{cn,31} := interp\ vs, v, FL, at_{cn}$

$v_Q := mmf_{32,Q}$ $vs := pspline(v, FL)$ $Y_{cn,32} := interp\ vs, v, FL, at_{cn}$

$v_Q := mmf_{33,Q}$ $vs := pspline(v, FL)$ $Y_{cn,33} := interp\ vs, v, FL, at_{cn}$

$v_Q := mmf_{34,Q}$ $vs := pspline(v, FL)$ $Y_{cn,34} := interp\ vs, v, FL, at_{cn}$

$v_Q := mmf_{35,Q}$ $vs := pspline(v, FL)$ $Y_{cn,35} := interp\ vs, v, FL, at_{cn}$

$v_Q := mmf_{36,Q}$ $vs := pspline(v, FL)$ $Y_{cn,36} := interp\ vs, v, FL, at_{cn}$

$v_Q := mmf_{37,Q}$ $vs := pspline(v, FL)$ $Y_{cn,37} := interp\ vs, v, FL, at_{cn}$

$v_Q := mmf_{38,Q}$ $vs := pspline(v, FL)$ $Y_{cn,38} := interp\ vs, v, FL, at_{cn}$

$v_Q := mmf_{39,Q}$ $vs := pspline(v, FL)$ $Y_{cn,39} := interp\ vs, v, FL, at_{cn}$

$v_Q := mmf_{40,Q}$ $vs := pspline(v, FL)$ $Y_{cn,40} := interp\ vs, v, FL, at_{cn}$

$v_Q := mmf_{41,Q}$ $vs := pspline(v, FL)$ $Y_{cn,41} := interp\ vs, v, FL, at_{cn}$

$v_Q := mmf_{42,Q}$ $vs := pspline(v, FL)$ $Y_{cn,42} := interp\ vs, v, FL, at_{cn}$

$v_Q := mmf_{43,Q}$ $vs := pspline(v, FL)$ $Y_{cn,43} := interp\ vs, v, FL, at_{cn}$

$v_Q := mmf_{44,Q}$ $vs := pspline(v, FL)$ $Y_{cn,44} := interp\ vs, v, FL, at_{cn}$

$v_Q := mmf_{45,Q}$ $vs := pspline(v, FL)$ $Y_{cn,45} := interp\ vs, v, FL, at_{cn}$

$v_Q := mmf_{46,Q}$ $vs := pspline(v, FL)$ $Y_{cn,46} := interp\ vs, v, FL, at_{cn}$

$v_Q := mmf_{47,Q}$ $vs := pspline(v, FL)$ $Y_{cn,47} := interp\ vs, v, FL, at_{cn}$

$v_Q := mmf_{48,Q}$ $vs := pspline(v, FL)$ $Y_{cn,48} := interp\ vs, v, FL, at_{cn}$

$v_Q := mmf_{49,Q}$ $vs := pspline(v, FL)$ $Y_{cn,49} := interp\ vs, v, FL, at_{cn}$

Total attractive force between reed blades

$$F\_peek_{cn,cg} := \frac{1}{2} \cdot \left(\frac{Y_{cn,cg}}{P\_cull_{cg}}\right)^2 \cdot dP\_cull_{cg}$$

Interpolate to find magnetic force at NMG

$w_{cg} := F\_peek_{0,cg}$ $ws := lspline(g, w)$ $FM_0 := interp(ws, g, w, NMG)$

$w_{cg} := F\_peek_{1,cg}$ $ws := lspline(g, w)$ $FM_1 := interp(ws, g, w, NMG)$

$w_{cg} := F\_peek_{2,cg}$ $ws := lspline(g, w)$ $FM_2 := interp(ws, g, w, NMG)$

$w_{cg} := F\_peek_{3,cg}$ $ws := lspline(g, w)$ $FM_3 := interp(ws, g, w, NMG)$

$w_{cg} := F\_peek_{4,cg}$ $ws := lspline(g, w)$ $FM_4 := interp(ws, g, w, NMG)$

$w_{cg} := F\_peek_{5,cg}$ $ws := lspline(g, w)$ $FM_5 := interp(ws, g, w, NMG)$

$w_{cg} := F\_peek_{6,cg}$ $ws := lspline(g, w)$ $FM_6 := interp(ws, g, w, NMG)$

$w_{cg} := F\_peek_{7,cg}$ $ws := lspline(g, w)$ $FM_7 := interp(ws, g, w, NMG)$

$w_{cg} := F\_peek_{8,cg}$ $ws := lspline(g, w)$ $FM_8 := interp(ws, g, w, NMG)$

$w_{cg} := F\_peek_{9,cg}$ $ws := lspline(g, w)$ $FM_9 := interp(ws, g, w, NMG)$

$w_{cg} := F\_peek_{10,cg}$ $ws := lspline(g, w)$ $FM_{10} := interp(ws, g, w, NMG)$

$w_{cg} := F\_peek_{11,cg}$ $ws := lspline(g, w)$ $FM_{11} := interp(ws, g, w, NMG)$

$w_{cg} := F\_peek_{12,cg}$ $ws := lspline(g, w)$ $FM_{12} := interp(ws, g, w, NMG)$

$w_{cg} := F\_peek_{13,cg}$ $ws := lspline(g, w)$ $FM_{13} := interp(ws, g, w, NMG)$

$w_{cg} := F\_peek_{14,cg}$ $ws := lspline(g, w)$ $FM_{14} := interp(ws, g, w, NMG)$

$w_{cg} := F\_peek_{15,cg}$ $ws := lspline(g, w)$ $FM_{15} := interp(ws, g, w, NMG)$

$w_{cg} := F\_peek_{16,cg}$ $ws := lspline(g, w)$ $FM_{16} := interp(ws, g, w, NMG)$

$w_{cg} := F\_peek_{17,cg}$ $ws := lspline(g, w)$ $FM_{17} := interp(ws, g, w, NMG)$

$w_{cg} := F\_peek_{18,cg}$ $ws := lspline(g, w)$ $FM_{18} := interp(ws, g, w, NMG)$

$w_{cg} := F\_peek_{19,cg}$ $ws := lspline(g, w)$ $FM_{19} := interp(ws, g, w, NMG)$ $FM_{19} = 0.1116$

To find dF/dg:

$n := 0, 1 .. (last(g) - 1)$ $last(g) = 49$

$$m\_int_{cn,n} := \frac{F\_peek_{cn,n+1} - F\_peek_{cn,n}}{g_{n+1} - g_n}$$

Take average of gradients between data points to give gradients at data points

$nn := 1,2..(last(g) - 1)$

$$m_{cn,nn} := \frac{1}{2} \cdot m\_int_{cn,nn} + m\_int_{cn,nn-1}$$

Approximate first data point - assume dF/dg is proportional to 1/gap^3 for very small gaps

$$m_{cn,0} := \left(\frac{g_1}{g_0}\right)^3 \cdot m_{cn,1}$$

Approximate last data point - assume constant rate of change of gradient over last points

$$m_{cn,last(g)} := m_{cn,last(g)-1} + 2 \cdot m\_int_{cn,last(g)-1} - m_{cn,last(g)-1}$$

$$dF\_peek_{cn,cg} := -m_{cn,cg}$$

Closure condition

$$Closure_{cn,cg} := if\ dF\_peek_{cn,cg} > stif, 1, 0$$

$$cl_{cn} := \sum_{cg} Closure_{cn,cg}$$

$stif = 609.19298$

Magnetic gap for given OAT

$$gap_{cn} := g_{cl_{cn}} + \frac{F\_peek_{cn,cl_{cn}}}{stif}$$

$$gap_{cn} := if\left[g_{cl_{cn}} > NMG, g_{cl_{cn}} + \frac{F\_peek_{cn,cl_{cn}}}{stif}, NMG + \frac{FM_{cn}}{stif}\right]$$

Stiffness line corresponding to operate condition

$$STL_{cn,cg} := -stif \cdot g_{cg} + stif \cdot gap_{cn}$$

$$STL_{cn,cg} := if\ STL_{cn,cg} < 0, 0, STL_{cn,cg}$$

aa := 19 bb := 4,5..49

ba := 8

ca := 1

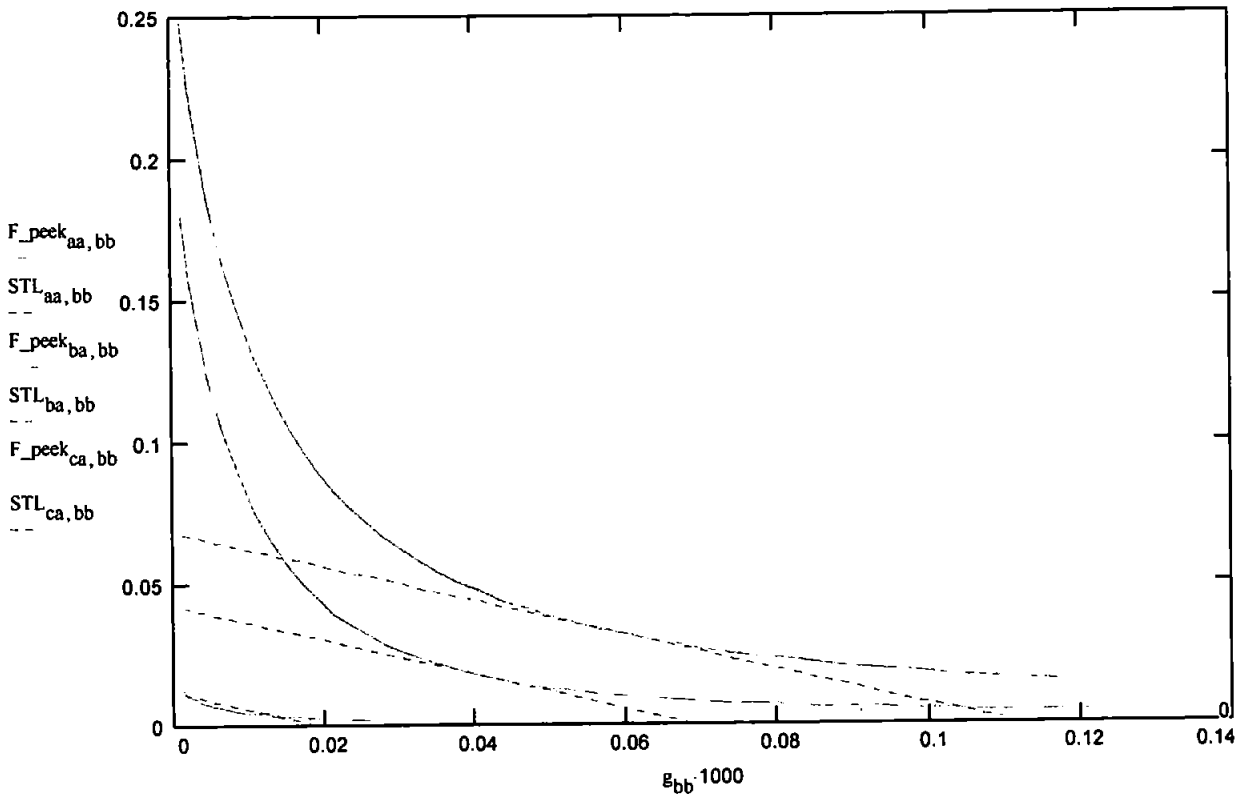

Contact gap for given OAT

$gap_{cn} := gap_{cn} - NMG$

$gap_{cn} := if\ gap_{cn} \le 0, 0, gap_{cn}$ **(prevents calculations with -ve gaps taking place)**

To calculate RAT:

$fm_{cn} := gap_{cn} \cdot stif$ **fm=magnetic force at point of release (=spring force at NMG)**

FM=magnetic force at operate condition

$spl := lspline(FM, at)$ **spline of magnetic force at operation against AT**

$RAT_{cn} := interp\ spl, FM, at, fm_{cn}$ **AT corresponding to fm**

$diff_{cn} := at_{cn} - RAT_{cn}$ **differential AT**

Contact force at OAT

$CF_{cn} := FM_{cn} - fm_{cn}$

Contact resistance data for Rhodium (figures in mOhms for 0.5g steps in CF) :

cfc := 0,1..99

$cfcr_{cfc} := 0.5 \cdot cfc \cdot \frac{9.81}{1000}$

$cr_0 := 300$ $cr_1 := 119$ $cr_2 := 53$ $cr_3 := 38$ $cr_4 := 31$ $cr_5 := 26$ $cr_6 := 22$ $cr_7 := 20$ $cr_8 := 17$ $cr_9 := 16$

$cr_{10} := 15$ $cr_{11} := 14$ $cr_{12} := 13.5$ $cr_{13} := 13.5$ $cr_{14} := 13.5$

cfd := 15..99

$cr_{cfd} := 15$

Voltage Breakdown Calculations

Intercontact capacitance (from Cullen's method of predicting permeance)

$$C\_cull_{cg} := \frac{\varepsilon}{\mu} \cdot P\_cull_{cg}$$

dC/dg

$$dC\_cull_{cg} := \frac{\varepsilon}{\mu} \cdot dP\_cull_{cg}$$

To find d2C/dg2:

$n := 0, 1 .. (last(g) - 1)$ $\quad last(g) = 49$

$$mc\_int_n := \frac{dC\_cull_{n+1} - dC\_cull_n}{g_{n+1} - g_n}$$

Take average of gradients between data points to give gradients at data points

$nn := 1, 2 .. (last(g) - 1)$

$$mc_{nn} := \frac{1}{2} \cdot \left(mc\_int_{nn} + mc\_int_{nn-1} \right)$$

Approximate first data point - assume dF/dg is proportional to 1/gap^3 for very small gaps

$$mc_0 := \left(\frac{g_1}{g_0} \right)^3 \cdot mc_1$$

Approximate last data point - assume constant rate of change of gradient over last points

$$mc_{last(g)} := mc_{last(g)-1} + 2 \cdot \left(mc\_int_{last(g)-1} - mc_{last(g)-1} \right)$$

$$d2C\_cull_{cg} := -mc_{cg}$$

$cg := 49, 48 .. 0$

$STL2_{cn,cg} := STL_{cn,cg} - stif \cdot NMG$ **convert to actual gap from magnetic gap**

$STL2_{cn,cg} := if\ STL2_{cn,cg} \le 0, 0, STL2_{cn,cg}$

Voltage breakdown criteria

$$V_{cn,cg} := \sqrt{2 \cdot STL2_{cn,cg} \cdot \frac{1}{dC\_cull_{cg}}}$$ **Voltage at which Fe=spring force for each gap considered**

$$V\_arc_{cg} := 13.4 \cdot 10^{-1} \cdot \frac{1}{\sqrt{C\_cull_{cg}}} \cdot g_{cg} \cdot 1000^{0.641}$$ **Voltage at which arcing occurs for each of the gaps considered .**

$$Fe_{cn,cg} := \frac{1}{2} \cdot V_{cn,cg}^2 \cdot dC\_cull_{cg}$$

$dFe_{cn,cg} := \frac{1}{2} \cdot V_{cn,cg}^{2} \cdot d2C\_cull_{cg}$ **dFe/dg for each of the gaps considered .**

$Closure_{cn,cg} := \text{if } dFe_{cn,cg} > stif, 1, 0$ **If dFe/dg > k then failure through closure - Closure:=1**

$Arc_{cn,cg} := \text{if } V_{cn,cg} > V\_arc_{cg}, 1, 0$ **If V > V_arc then failure through arcing - Arc:=1**

$closure_{cn} := \sum_{cg} Closure_{cn,cg}$ **The Closure flags are summed to give cg at failure (through closure)**

$arc_{cn} := \sum_{cg} Arc_{cn,cg}$ **The Arc flags are summed to give cg at failure (through arcing) condition**

$vb_{cn} := \text{if } arc_{cn} > closure_{cn}, arc_{cn}, closure_{cn}$ **vb is cg at the first failure condition to occur**

$Vat_{cn,1} := V_{cn,vb_{cn}} \cdot 10^{-3}$ $Vat_{cn,0} := at_{cn}$ **Places Vbd-AT results into a single array (in kV)**

$Vbd_{cn} := V_{cn,vb_{cn}} \cdot 10^{-3}$ **Vbd for given OAT (kV)**

Relay Characteristics

Physical constants

$\rho := 0.0178 \cdot 10^{-6}$ **Resistivity of copper**

$\mu := 4 \cdot \pi \cdot 10^{-7}$ **Permeability of free space**

$\sigma := \frac{1}{\rho}$ **Conductivity of copper**

Winding wire characteristics

f_pack := 0.785 **Packing factor for circular winding wire in rectangular winding space**

f_cu := 0.65 **Proportion of winding wire cross sectional area which is copper**

Relay operating parameters

Vnom := 12 **Nominal operating voltage**

Tmax := 180 **Max coil temperature**

Irf := 3.0 **Max RF carry current**

$f := 30 \cdot 10^{6}$ **Max frequency of RF current**

switch := 1.8 **Effective increase in RF resistance caused by switch**

Coil DC Characteristics

$MTL := \pi \cdot \frac{coilOD + coilID}{2}$ **mean turn length of coil (m)** MTL = 0.03142

$coilA := coillen \cdot \frac{coilOD - coilID}{2}$ **coil winding CSA (m^2)**

$coilAT_{cn} := \frac{234.5 + Tmax}{254.5} \cdot at_{cn}$ **coil drive reqd to operate switch at Tmax**

$Vpi := \frac{254.5}{234.5 + Tmax} \cdot Vnom$ **operate voltage at 20°C** Vpi = 7.36791

$Vdo_{cn} := \frac{RAT_{cn}}{coilAT_{cn}} \cdot Vnom$ **release voltage at 20°C**

$DCpower_{cn} := \frac{coilAT_{cn}^{2} \cdot \rho \cdot MTL}{f\_pack \cdot f\_cu \cdot coilA}$ **DC power requirement for given coil AT**

$R_{cn} := \frac{Vnom^2}{DCpower_{cn}}$ **coil resistance**

$dw_{cn} := \left(\frac{16 \cdot \rho \cdot MTL \cdot coilA \cdot f\_pack \cdot f\_cu}{R_{cn} \cdot \pi^2} \right)^{\frac{1}{4}}$ **winding wire diameter**

$wireA_{cn} := \pi \cdot \left(\frac{dw_{cn}}{2} \right)^2$ **winding wire CSA**

$T_{cn} := \frac{coilA \cdot f\_pack \cdot f\_cu}{wireA_{cn}}$ **no. of turns**

CR Characteristics for 2,4 & 6kV Devices

OAT for 2,4 & 6kV relays

sp := lspline(Vbd, at)

oat2 := interp(sp, Vbd, at, 2) oat4 := interp(sp, Vbd, at, 4) oat6 := interp(sp, Vbd, at, 6)

oat2 = 30.8298 oat4 = 47.00987 oat6 = 63.32022

Coil AT for 2,4 & 6kV relays

$coil2 := oat2 \cdot \frac{Tmax + 234.5}{254.5}$ $coil4 := oat4 \cdot \frac{Tmax + 234.5}{254.5}$ $coil6 := oat6 \cdot \frac{Tmax + 234.5}{254.5}$

coil2 = 50.212 coil4 = 76.56421 coil6 = 103.12861

RAT for 2,4 & 6kV relays

$spr := lspline(at, RAT)$

$rat2 := interp(spr, at, RAT, oat2)$ $rat4 := interp(spr, at, RAT, oat4)$ $rat6 := interp(spr, at, RAT, oat6)$

$rat2 = 26.29299$ $rat4 = 33.16654$ $rat6 = 38.15181$

Define AT range between Vnom and Vdo for each

$cz := 0, 1 .. 10$

$at2_{cz} := rat2 + \frac{coil2 - rat2}{10} \cdot cz$ $at4_{cz} := rat4 + \frac{coil4 - rat4}{10} \cdot cz$ $at6_{cz} := rat6 + \frac{coil6 - rat6}{10} \cdot cz$

Contact force over AT range for each

$spl := lspline(at, FM)$

$fm2_{cz} := interp\ spl, at, FM, at2_{cz}$ $fm4_{cz} := interp\ spl, at, FM, at4_{cz}$ $fm6_{cz} := interp\ spl, at, FM, at6_{cz}$

$f2_{cz} := fm2_{cz} - fm2_0$ $f4_{cz} := fm4_{cz} - fm4_0$ $f6_{cz} := fm6_{cz} - fm6_0$

Contact resistance over above AT ranges for each

$spl := lspline(cfcr, cr)$ $spl := lspline(cfcr, cr)$ $spl := lspline(cfcr, cr)$

$cr2_{cz} := interp\ spl, cfcr, cr, f2_{cz}$ $cr4_{cz} := interp\ spl, cfcr, cr, f4_{cz}$ $cr6_{cz} := interp\ spl, cfcr, cr, f6_{cz}$

Coil voltage corresponding to each of above AT ranges

$v2_{cz} := \frac{at2_{cz}}{coil2} \cdot Vnom$ $v4_{cz} := \frac{at4_{cz}}{coil4} \cdot Vnom$ $v6_{cz} := \frac{at6_{cz}}{coil6} \cdot Vnom$ $cy := 1, 2 .. 10$

Coil RF Characteristics

$r_{cn} := \frac{dw_{cn}}{2}$ **Radius of winding wire (m)**

$k := \sqrt{\pi \cdot f \cdot \mu \cdot \sigma}$ $k = 81570.00606$

$\delta := \frac{1}{k}$ **Skin depth (m)** $\delta = 0.00001$

$ratio_{cn} := \left[k \cdot \left[-\frac{2}{k} \cdot \exp(-k \cdot r_{cn}) + \frac{1 + \exp(-2 \cdot k \cdot r_{cn})}{k} \right] \right]^2$ **Ratio resulting from self cancelling effect of eddy currents when wire dia is not >>skin depth**

$R\_RF_{cn} := \frac{\rho}{2 \cdot \delta} \cdot \frac{1}{\frac{coilOD}{2} - \frac{coilID}{2}} \cdot \ln\left(\frac{coilOD}{coilID}\right) \cdot dw_{cn} \cdot T_{cn} \cdot switch \cdot ratio_{cn}$

$RFpower_{cn} := Irf^2 \cdot R\_RF_{cn}$

Total Power in Coil

$P_{cn} := RFpower_{cn} + DCpower_{cn}$

DC Power vs. Breakdown Voltage

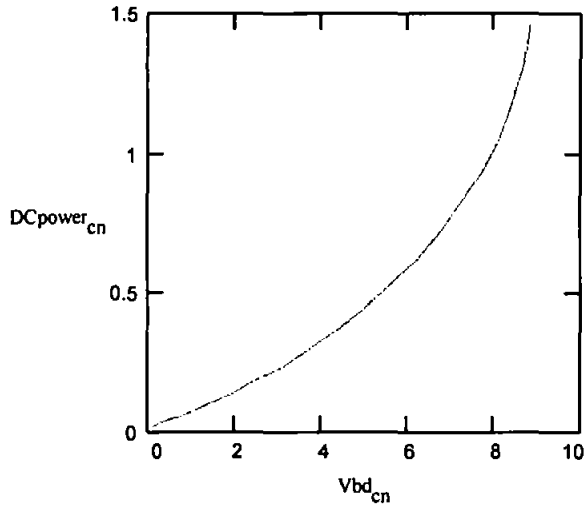

RF Power vs. Breakdown Voltage

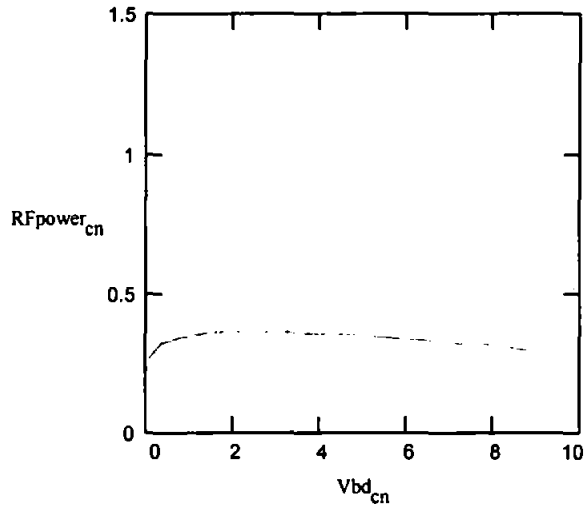

Total Coil Power (DC+RF) vs. Breakdown Voltage

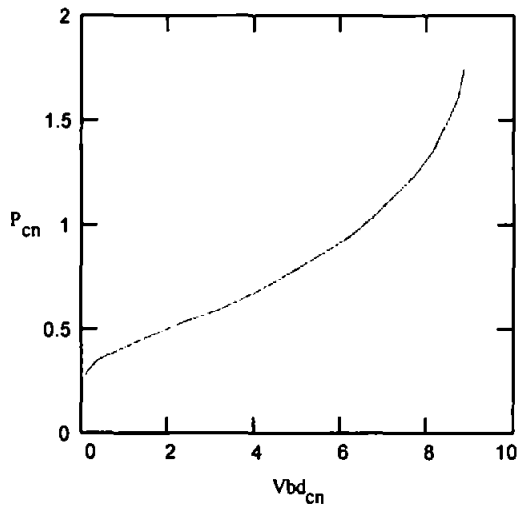

Relay Pull-In and Drop-Out Voltages vs. Vbd

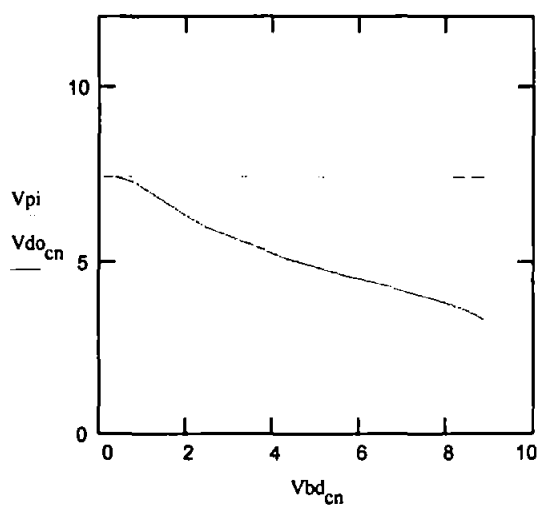

$z := 0, 1 .. 15$

Winding Wire Diameter (mm) vs. Breakdown Voltage

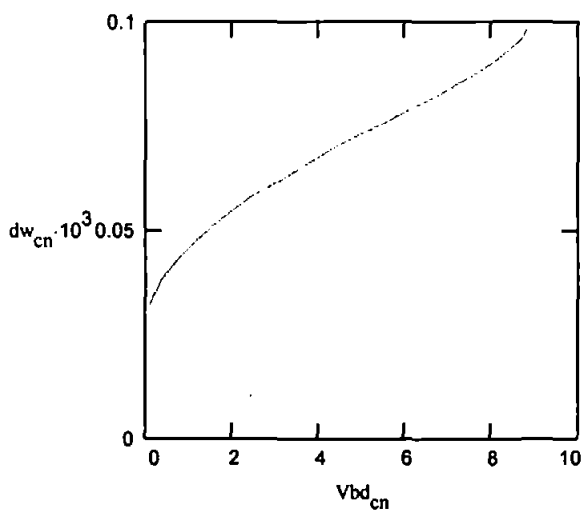

Coil Resistance vs. Breakdown Voltage

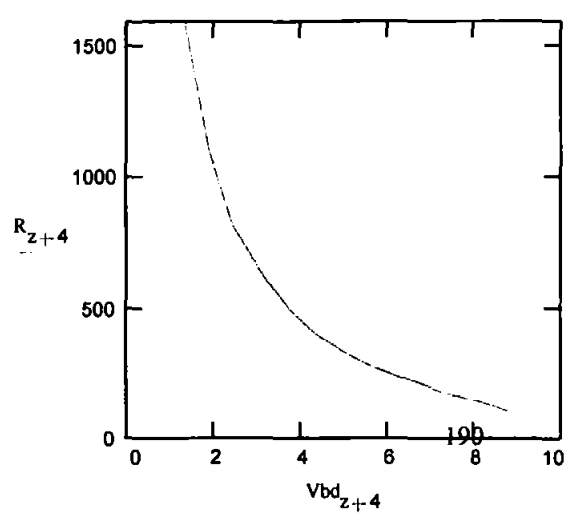

Contact Resistance vs. Coil Drive Voltage for 2kV, 4kV & 6kV Relays

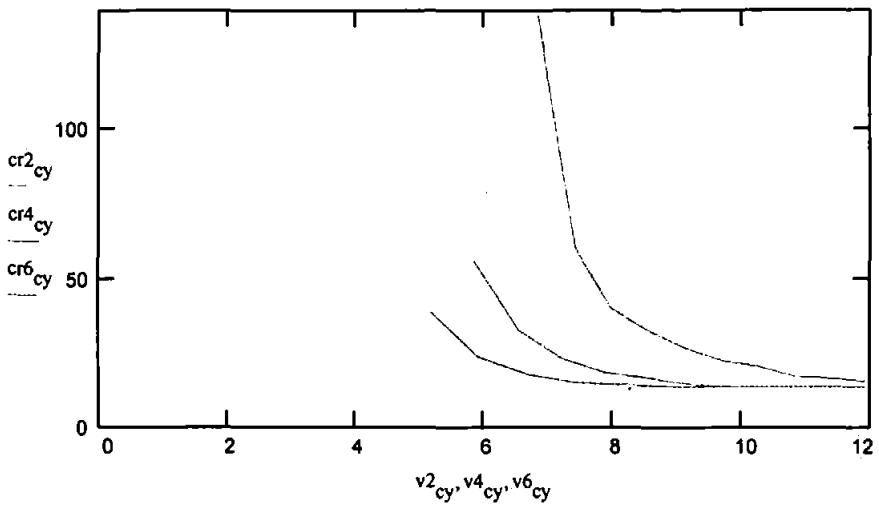

Appendix 9 - Derivation of Equations used in Section 3

Relationships derived by the author for use in the model of eddy current losses within the coil of a reed relay are as follows:

9.1 The mean value of $\frac{1}{r}$ for a coil winding, $\overline{\frac{1}{r}}$

$$\overline{\left(\frac{1}{r}\right)} = \frac{1}{r_2 - r_1}\int_{r_1}^{r_2}\frac{1}{r}\,dr$$

$$= \frac{1}{r_2 - r_1}\left[\ln(r_2) - \ln(r_1)\right]$$

$$= \frac{1}{r_2 - r_1}\ln\left(\frac{r_2}{r_1}\right) \qquad \text{(eqn 3.11)}$$

where

r_1=inside radius of the coil winding

r_2=outside radius of the coil winding

9.2 The Resultant Eddy Current when Coil Winding Wire Dia ≠<<δ

The relationship for current density, J, with depth, z, of a high frequency current in a conductor is

$$J = J_0 \cdot e^{-k \cdot z} \qquad \text{(eqn 3.12)}$$

For the case of an eddy current flowing around the circumference of a coil winding wire whose diameter is not greatly smaller than the skin depth of the current, as shown in the accompanying figure, the relationship for J is:

$$J = J_0 \cdot e^{-k \cdot z} - J_0 \cdot e^{-k(2r-z)}$$

where

J_0=current density at the surface of the conductor

$$k = \sqrt{\pi \cdot f \cdot \mu \cdot \sigma}$$

z=depth

r=radius of the winding wire about which the eddy current is flowing

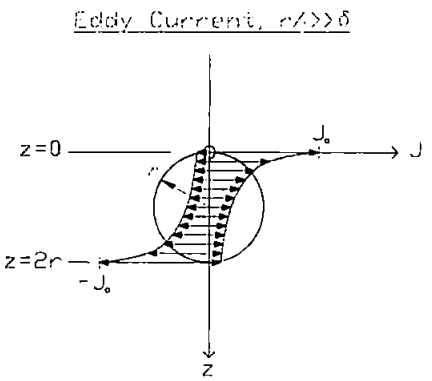

The eddy current in this instance is partly self-cancelling. The effective value of the eddy current then becomes :

$$I = I_{eddy} \cdot \frac{J_0 \int_0^r e^{-k \cdot z} - e^{-k(2r-z)} dz}{J_0 \int_0^\infty e^{-kz} dz}$$

$$= I_{eddy} \cdot \frac{\left[-\frac{2}{k} \cdot e^{-kr} + \frac{1 + e^{-2kr}}{k} \right]}{\left[\frac{1}{k} \right]}$$

$$= I_{eddy} \cdot k \cdot \left[-\frac{2}{k} \cdot e^{-kr} + \frac{1 + e^{-2kr}}{k} \right] \qquad \text{(eqn 3.13)}$$

9.3 The Influence of 3.13 on Effective Eddy Current Resistance

The self cancelling of the eddy current as described by 3.13 has the effect of reducing the power loss associated with it. As power dissipated is proportional to the square of current the effect of the self cancelling is to reduce power loss by a factor of $\left[\frac{I}{I_{eddy}}\right]^2$. It is convenient to apply this factor as an effective reduction in eddy current resistance. This factor, F_{wire}, is then:

$$F_{wire} = \left[\frac{I}{I_{eddy}}\right]^2 = \left[k \cdot \left(-\frac{2}{k} \cdot e^{-k \cdot r} - \frac{1 + e^{-2 \cdot k \cdot r}}{k}\right)\right]^2 \qquad \text{(eqn 3.14)}$$

Appendix 10 - Derivation of Equations used in Section 4

Relationships derived by the author for use in the RF Reed Relay Design Program are as follows:

10.1 The DC Power Dissipated in a Coil in terms of Magneto Motive Force

The DC power dissipated in a coil winding can be calculated if its dimensions and amp turns are known as follows:

$$W_{DC} = I^2 \cdot R$$

$$= \frac{mmf^2}{N^2} \cdot R \qquad ; \qquad R = MTL \cdot N \cdot \frac{\rho}{CSA_{wire}}$$

$$= \frac{mmf^2 \cdot MTL \cdot N \cdot \rho}{CSA_{wire} \cdot N^2} \qquad ; \qquad CSA_{wire} \cdot N = A \cdot F_{pack} \cdot F_{cu}$$

$$= \frac{mmf^2 \cdot MTL \cdot \rho}{A \cdot F_{pack} \cdot F_{cu}} \qquad \text{(eqn 4.1)}$$

where

W_{DC}=DC power

I=current

R=resistance of the coil winding

mmf=magneto motive force

MTL=mean turn length of the coil winding

N=no. of turns in the coil winding

ρ=resistivity of the coil wire

CSA_{wire}=conductive cross sectional area of the winding wire

A=cross sectional area of the coil

F_{pack}=packing factor for a round wire occupying a square space=0.785

F_{cu}=proportion of winding wire cross sectional area which is copper (typically 0.65)

10.2 Calculation of Winding Wire Diameter from Coil Dimensions and mmf Requirement

If the DC resistance, dimensions and amp turns (mmf) of a coil are known the diameter of winding wire required can be calculated as follows:

$$R = MTL \cdot N \cdot \frac{\rho}{CSA_{wire}} \quad ; \quad N = \frac{A \cdot F_{pack} \cdot F_{cu}}{CSA_{wire}}$$

$$R = MTL \cdot \frac{A \cdot F_{pack} \cdot F_{cu}}{CSA_{wire}} \cdot \frac{\rho}{CSA_{wire}}$$

$$\Rightarrow CSA_{wire}^{\ 2} = MTL \cdot \frac{A \cdot F_{pack} \cdot F_{cu} \cdot \rho}{R} \quad ; \quad CSA_{wire} = \frac{\pi \cdot d_{wire}^{\ 2}}{4}$$

$$\Rightarrow \frac{\pi^2}{16} d_{wire}^{\ 4} = \frac{MTL \cdot A \cdot F_{pack} \cdot F_{cu} \cdot \rho}{R}$$

$$\Rightarrow d_{wire} = \left[\frac{16 \cdot MTL \cdot A \cdot F_{pack} \cdot F_{cu} \cdot \rho}{\pi^2 \cdot R} \right]^{\frac{1}{4}} \qquad \text{(eqn 4.4)}$$

where

d_{wire}=diameter of winding wire

R=resistance of the coil winding

mmf=magneto motive force

MTL=mean turn length of the coil winding

N=no. of turns in the coil winding

ρ=resistivity of the coil wire

CSA_{wire}=conductive cross sectional area of the winding wire (i.e. excluding enamel)

A=cross sectional area of the coil

F_{pack}=packing factor for a round wire occupying a square space=0.785

F_{cu}=proportion of winding wire cross sectional area which is copper (typically 0.65)